

Tese de Doutorado

UM ESTUDO DA UTILIZAÇÃO DA DISTRIBUIÇÃO NÃO-EXTENSIVA NA COSMOLOGIA

Dissertação submetida

à

Universidade Federal do Rio Grande do Norte

por

Lucio Marassi de Souza Almeida

sob a orientação de

José Ademir Sales de Lima, PhD.

Como requisito parcial

para obtenção do Grau de

DOUTOR EM FÍSICA

Centro de Ciências Exatas e da Terra

Departamento de Física Teórica e Experimental

Agosto, 2006

Natal, Rio Grande do Norte

Aos meus pais, Lucio e Vanete.

Índice

Agradecimentos	xii
Resumo	xiv
Abstract	xv
1 INTRODUÇÃO	1
2 COSMOLOGIA	7
2.1 Introdução à Cosmologia do Big Bang	7
2.1.1 O Big Bang	8
2.1.2 Universos de Friedmann–Robertson–Walker	8
2.1.3 Brief thermal history of the universe	13
2.2 THE COSMOLOGICAL CONSTANT	15
2.2.1 Vacuum energy	15
2.2.2 Possible Solutions for the Cosmological Constant Problem	17
2.3 DETERMINATION OF COSMOLOGICAL PARAMETERS	20
2.3.1 The Lookback Time	20
2.3.2 The Luminosity Distance	22
2.3.3 Relation Between Distance Measures	22
2.3.4 The rate of expansion H_0	23
2.3.5 The matter content Ω_M	24
2.3.6 The cosmological constant Ω_Λ	29
2.3.7 The spatial curvature Ω_K	34

3	A FORMAÇÃO DE ESTRUTURAS EM GRANDE ESCALA	35
3.1	A Small Introduction to The Large Structure Formation	35
3.1.1	Clusters and Superclusters of Galaxies	35
3.1.2	Baryonic Matter	36
3.1.3	Non-Baryonic Dark Matter	37
3.1.4	Hot, Cold and Warm Dark Matter	37
3.1.5	Large-scale structure formation	37
3.2	The Inflationary Paradigm	42
3.2.1	Cosmological Inflation	42
3.2.2	The origin of density perturbations	42
3.2.3	Acoustic oscillations in the plasma	43
3.3	The Evolution of the Density Perturbation	44
3.3.1	Relativistic fluid flow	45
3.3.2	The transfer function	51
3.3.3	The spectrum of the density perturbation	52
3.3.4	The filtered density contrast	53
3.3.5	Linear Theory Works	55
4	MECÂNICA ESTATÍSTICA NÃO EXTENSIVA	57
4.1	INTRODUCTION	57
4.2	Central equations of nonextensive statistical mechanics	59
4.2.1	A metaphor	59
4.2.2	The nonextensive entropy S_q	60
4.2.3	A remark on other possible generalizations of the Boltzmann-Gibbs entropy	64
4.3	Applications in and out from equilibrium	64
4.4	Aplications in Astrophysics and Cosmology	65
5	O MÉTODO DE PRESS-SCHECHTER	68
5.1	Introduction	68
5.2	The Press-Schechter approach	70
5.3	PS approach with a q-Power Law	72

5.4	Some Extensions of the PS Approach and Our PL Method	75
5.5	A Study of the Normalization Problem	77
5.6	Nongaussian effects on the $\sigma_8 - \Omega_m$ plane	80
5.6.1	The Theoretical PS Model used with the HIFLUGCS Data	80
5.6.2	The Power Law Model fitting the HIFLUGCS Data	84
5.6.3	Dark Energy and Structure Formation	90
6	COSMOLOGIA NÃO-EXTENSIVA E TRATAMENTOS DE DADOS	100
6.1	Bremsstrahlung from a Nonextensive Maxwellian Gas	100
6.1.1	Maxwell-Boltzmann Thermal Bremsstrahlung Emission	102
6.1.2	Nonextensive Thermal Bremsstrahlung Emission	103
6.1.3	Averaged Gaunt Factors	105
6.1.4	Analysis	107
6.2	Nonextensivity in the Plasma Probe	111
6.2.1	Maxwellian velocity distribution	111
6.2.2	Power Law velocity distribution	112
6.2.3	The Plasma Probe - Maxwellian Case	114
6.2.4	The Plasma Probe - Power Law Case	114
6.2.5	The Density of Electrons	115
6.2.6	The Results	117
6.3	New Cosmological Constraints using Dark Energy, X-Ray Gas Mass Fractions and SNe Ia	123
6.3.1	Basic Equations	124
6.3.2	Observational Constraints	126
6.3.3	Perspectives	127
6.4	Constraining H_0 from Sunyaev-Zel'dovich effect, Galaxy Clusters X-ray data, and Baryon Oscillations	128
6.4.1	Basic Equations and Sample	130
6.5	Analysis and Results	132
6.5.1	Limits from SZE/X-ray	133
6.5.2	Joint Analysis for SZE/X-ray and BAO	134
6.5.3	Conclusions	137

7 CONCLUSÕES E PERSPECTIVAS	138
BIBLIOGRAFIA	142

Índice de Figuras

2.1	Limits from supernovae and large-scale structure data on Ω_M and the equation-of-state parameter w_X , in a flat universe dominated by matter and dark energy ⁶⁴ . Thin contours (on the left) represent limits from CMB and large-scale structure measurements, while thick contours are those from SNe observations; solid lines apply to models with constant w_X , while dashed lines apply to models of dynamical scalar fields. The constraints are combined on the right.	19
2.2	Expansion histories for different values of Ω_M and Ω_Λ . From top to bottom, the curves describe $(\Omega_M, \Omega_\Lambda) = (0.3, 0.7), (0.3, 0.0), (1.0, 0.0),$ and $(4.0, 0.0)$.	21
2.3	The rotation curve of the spiral galaxy NGC 6503, determined by radio observations of hydrogen gas in the disk ³⁶ . The dashed line shows the rotation curve expected from the disk material alone, the dot-dashed line is from the dark matter halo alone.	27
2.4	Hubble diagram for the high redshift supernovae found by the SN Cosmology Project. From Ref. ³⁹ . A similar diagram is found by the High Redshift Supernova Project ⁴⁰ . Both groups conclude that distant supernovae are fainter than expected, and this could be due to an accelerating universe. . .	31
2.5	The best-fit confidence regions (68% – 99% c.l.) in the $(\Omega_M, \Omega_\Lambda)$ plane, for the high redshift supernovae results. Present observations disfavour the Einstein-de Sitter model (circle) by several standard deviations. From Ref. ³⁹ .	32
2.6	CMB data (binned) and two theoretical curves: the model with a peak at $l \sim 200$ is a flat matter-dominated universe, while the one with a peak at $l \sim 400$ is an open matter-dominated universe. From ⁵³	33

3.1	The matter power spectrum for clusters of galaxies, from three different cluster surveys.	39
3.2	The power spectrum for cold dark matter (CDM), tilted cold dark matter (TCDM), hot dark matter (HDM), and mixed hot plus cold dark matter (MDM), normalized to COBE, for large-scale structure formation. From Ref. ²⁹	41
5.1	Fraction of critical density contributed by bound structures of mass M. The upper and lower solid curves are the corrected PS (factor 2), and the uncorrected PS curves, respectively. The long dashed, dashed and dotted curves are obtained using the PL distribution. Note that the q -parameter affects considerably the range of larger mass scales.	74
5.2	Fraction of critical density contributed by bound structures of mass M. In both panels the upper and lower solid curves are the corrected PS (factor 2), and the uncorrected PS curves, respectively. The long dashed, dashed and dotted curves in left panel are obtained using the PL distribution. In the right panel we compare the behavior using the Burr distribution (the dashed and long dashed curves) with that using the PS (solid lines) and PL (dotted line) ones.	78
5.3	HIFLUGCS mass function compared to the best fit model mass function with $\Omega_m = 0.12$ and $\sigma_8 = 0.96$ (solid line). Also shown are the best fit model mass functions for fixed $\Omega_m = 0.5$ ($\Rightarrow \sigma_8 = 0.60$, dashed line) and $\Omega_m = 1.0$ ($\Rightarrow \sigma_8 = 0.46$, dotted line).	83
5.4	Statistical confidence contours for the χ^2 procedure. The cross indicates the position of the minimum, χ^2_{\min} . Ellipses indicate the 68 %, 90 %, 95 %, and 99 % confidence levels for two interesting parameters, i.e. $\Delta\chi^2 \equiv \chi^2 - \chi^2_{\min} = 2.30, 4.61, 6.17,$ and 9.21 , respectively.	84
5.5	The $[-1 < q < 1]$ interval. We fix q and we perform a χ^2 test for $\Omega_m - \sigma_8$ parameters. As we rise the value of q , we get higher Ω_m and lower σ_8 as best-fit, until $q = 1.0$, when we obtain the same PS method result, as expected	86

5.6	The $[1 < q < 3]$ interval. We fix q and we perform a χ^2 test in the $\Omega_m - \sigma_8$ plane. We fix two different values of q , one very close to the inferior interval limit ($q = 1.03$) and the other slightly higher ($q = 1.30$). We note that a slightly variation on q produces huge variation in the two cosmological parameters. We fixed the <i>physical q interval</i> in the limit $[1.03 \leq q < 1.30]$.	87
5.7	In the upper panel, we see Reiprich results (equivalent to our method for $q \rightarrow 1$), which have Ω_m very low (comparing with recent CMB results). As we rise the value of q , we get higher Ω_m and lower σ_8 parameters as best-fit, and the bottom panel show that we can have very good cosmological parameters with the same observational data, only changing the PS method by our PL approach.	88
5.8	We fix Ω_m and we perform a χ^2 test in the $q - \sigma_8$ plane; as a result we have a transversal and almost flat statistical contour, showing a linear dependence between q and σ_8 . We will see the same behavior in the $q - \Omega_m$ plane, fixing σ_8 .	89
5.9	Another example that shows how our PL approach is powerful to constrain the cosmological parameters. We fix σ_8 and we perform a χ^2 test in the $q - \Omega_m$ plane. In the upper panel, for $\sigma_8 = 0.70$, we get $\Omega_m \sim 0.20$ as best-fit. More we increase σ_8 , more we decrease Ω_m (middle and bottom panels).	90
5.10	The triangles are the observational binned X-Ray mass function, and the lines are the mass function theoretical models (all them using the HI-FLUGCS database as points and performing a fitting procedure). The solid line is our PL method with $\sigma_8 = 0.70$ and $\Omega_m = 0.20$. The dotted line is the PS approach with the same parameters. The long dashed line is the Reiprich results : the PS method with $\Omega_m = 0.12$ and $\sigma_8 = 0.96$ (the first parameter is very lower and the second one slightly higher than the most recent WMAP CMB data).	91

5.11	Plot showing the true value of A in Eq. 5.42 as a function of w for 9 flat cosmologies with Ω_M evenly spread between 0.1 and 0.9 (grey lines). For comparison we plot the fitting formula of ¹¹⁹ (dashed line) and for Eq. 5.43 (black line).	96
5.12	Plot showing the predicted mass function calculated using the fitting formula of Sheth & Tormen ¹⁵⁸ calculated for $\Omega_M = 0.3$, $\Omega_X = 0.7$ for three different values of w , and at three epochs corresponding to $a = 1/3, 1/2, 1$. Because the power spectrum is normalized at present day, and δ_c is only weakly dependent on cosmology, then there is little difference between the predicted mass functions for $a = 1$. As we go further back in time the difference becomes more severe because of the differing linear growth factors.	97
5.13	We use the PS formalism with the HIFLUGCS X-Ray data already presented in the section 5.6.1, but with the evolution of critical density given by Eq.(5.45), so accounting for the dark energy inside the PS approach.	99
6.1	Plot from Novikov ^{184,183} , showing different regions for the Gaunt factor.	105
6.2	Thermal Bremsstrahlung emission of the “Large-Angle” and the “Large-Angle Tail” region. We obtain the solid line using the Maxwellian distribution, and the other lines using our Power Law one with different q parameters. We can easily observe the flexibility of the Power Law free q -parameter after the $\log\left(\frac{h\nu}{kT}\right) = 1$ limit.	107
6.3	Same explanation as Fig.(6.2), but for the “Small-Angle UP” region.	108
6.4	The behavior of the Thermal Bremsstrahlung Emission in the “Small-Angle Classical” region, using the Maxwellian and our PL distribution, for different $gamma2 = \left(\frac{kT}{Z^2 R_y}\right)$ values.	109
6.5	The behavior of the averaged Gaunt Factor in the “Small-Angle Classical” region, using only our PL distribution, for different q parameter values. Each curve is plotted using a different $gamma2 = \left(\frac{kT}{Z^2 R_y}\right)$ value. We can easily see that our nonextensive method presents the same averaged Gaunt Factor behavior as using the classical method; better saying, we can also use the same approximations in the Gaunt Factor, which is of the order of a unity, even for a large range of q parameter values.	110

6.6	The BG (Boltzmann-Gibbs) and the PL (Power Law, nonextensive) results for the electron density, where we fix the J_{e0} value ($J_{e0} = 0.792$ Ampères), in function of the electron temperature. In the $q > 1$ interval.	117
6.7	The BG (Boltzmann-Gibbs) and the PL (Power Law, nonextensive) results for the electron density, where we fix the J_{e0} value ($J_{e0} = 0.792$ Ampères), in function of the electron temperature. In the $1/3 < q < 1$ interval.	118
6.8	Probe outside the plasma sheath of the cathode. Region of long-range Coulombian interactions, weak chaos, plasma behavior. The PL curve with $q=1.6$ explains very well the region after the slope of the data probe (were the probe potential is overwhelmed by the plasma potential). This PL curve describes the region outside the sheath <i>of the probe</i> , where we can detect the <i>real</i> macroscopic variables of the plasma (temperature, pressure, density, etc.), and we do not need to shift the curve, as we must to do in the BG case.	120
6.9	Probe inside the plasma sheath of the cathode. Region of short-range colisional interactions, strong chaos, random kinetic behavior. The BG curve explains very well the data, specially in the bottom panel, were the probe is completely immersed in the cathode sheath region (But the shift up parameter is needed in both panels, with different values in each one).	121
6.10	The first column shows the region outside the cathode sheath. The second column shows the region inside the sheath.	122
6.11	Marginalized constraints on plane ω_0 and ω_1 from joint analysis of the Chandra $f_{\text{gas}}(z)$ and SNe Ia data shown above for models 1 (left panel) and 2 (right panel). The solid lines mark the 1, 2 and 3 σ confidence limits. See text for more details.	127
6.12	Angular diameter distance as a function of redshift for $\Omega_m = 0.3$ and some selected values of the h parameter. The data points correspond to the the SZE/X-ray distances for 25 clusters from De Filippis <i>et al.</i> ²⁰⁹ . The open diamond indicates the Abell 773 outlier cluster, which has been excluded from our statistical analysis.	132

6.13	Confidence regions (68.3%, 95.4% and 99.7%) in the (Ω_m, h) plane provided by the SZE/X-ray data from De Filippis <i>et al.</i> (2005) ²⁰⁹ . The best fit values are $h = 0.75$ and $\Omega_m = 0.15$	133
6.14	Contours in the $\Omega_m - h$ plane using the SZE/X-ray and BAO joint analysis. The contours correspond to 68.3%, 95.4% and 99.7% confidence levels. The best-fit model converges to $h = 0.74$ and $\Omega_m = 0.27$	134
6.15	Likelihood function for the h parameter in a flat Λ CDM universe, from SZE/X-ray emission. The shadow lines are cuts in the regions of 68.3% probability and 95.4%. We see that the region permitted is well constrained and in concordance with others studies ^{201,164}	136

Índice de Tabelas

5.1	Power Law Λ CDM Model Parameters and 68% Confidence Intervals. The Three Year fits in this Table assume no SZ contribution, $A_{SZ} = 0$, to allow direct comparison with the First Year results.	85
6.1	SZ/X-ray method: Limits to h from galaxy clusters (Λ CDM).	136

Agradecimentos

Durante a minha vida não foram poucas as pessoas que contribuíram, cada uma a seu modo, para que eu chegasse ao presente estágio. Quero portanto, usar este espaço para agradecer às pessoas que apoiaram e ajudaram a tornar possível este trabalho de tese. Agradeço imensamente

- Ao Prof. Dr. José Ademir Sales de Lima, pela firmeza e dedicação com que me orientou no caminho da cosmologia. Seu esforço e empenho para fazer ciência numa pátria tão difícil como a nossa é único. São raríssimos os excelentes pesquisadores com o dom de serem igualmente excelentes orientadores, e posso seguramente dizer que tive a sorte de conhecer uma dessas pessoas. Foi uma honra pessoal e um privilégio poder ter feito um doutorado com o prof. José Ademir.
- Ao Prof. Dr. Clodomiro Alves Junior, um diretor de pesquisas invejável e muito gentil, por permitir o uso de seu laboratório de tratamento de materiais a Plasma, o LabPlasma (UFRN), e colaborar, junto com sua equipe, para os resultados de meus estudos no capítulo referente à teoria do Plasma, e os artigos originados de tal estudo.
- Aos meus pais Lucio de Souza Almeida e Vanete Carmem, por toda uma vida de apoio, amor e dedicação, pela confiança em meus potenciais e o amparo amoroso nos momentos difíceis. À minha irmã Vívian e meu cunhado Marcos, pelo apoio familiar, emocional (e mesmo profissional) constante.
- À minha querida Adriana Christine e ‘a Catarina (Cacá), por aguentarem minhas manias e suavizarem meu coração, pelo seu apoio e incentivo, tão necessários nos

momentos difíceis.

- A todos os meus familiares do Rio de Janeiro: tios Roberto e Lucia, Juvenal e Nídia, primos Roberto, Rodrigo, Karin e Rafael, dentre vários outros que o pouco espaço destas linhas não permite citar, agradeço de coração. A presença amorosa dessa família me ajudou demais nos meus estágios no Rio de Janeiro.
- Aos amigos de São Paulo Cangelar e Márcia, pelo apoio constante durante as diversas viagens ao Rio e à São Paulo, necessárias à conclusão de minha tese.
- Aos amigos João Maria, João Vital, Rose Clívia e Edson, cujas críticas e sugestões por várias vezes apontaram o caminho correto. Desenvolver artigos científicos de qualidade, ainda durante a tese de doutorado, e com amigos de sala como esses, seguramente é um privilégio reservado a poucos. Espero que continuemos essa parceria em futuro bem próximo.
- Ao CNPq, pelo apoio financeiro recebido na minha tese.

UM ESTUDO DA UTILIZAÇÃO DA DISTRIBUIÇÃO NÃO-EXTENSIVA NA COSMOLOGIA

por

Lucio Marassi de Souza Almeida

Resumo

O processo de formação de estruturas foi descrito por Press e Schechter (PS) em 1974, através da função de massa dos aglomerados de galáxias. O formalismo PS pressupõe uma distribuição Gaussiana para o campo primordial das perturbações de densidade. Além de um sério problema de normalização, PS não explica os atuais dados de raio-X dos aglomerados, e está em desacordo com as modernas simulações computacionais. Realizamos um estudo da estatística desse campo primordial, já que os dados mais recentes do WMAP indicam um desvio da gaussianidade; tais desvios podem ser descritos pela estatística não extensiva de Tsallis (1988), pois ela se reduz à distribuição Gaussiana, no limite do parâmetro livre $q \rightarrow 1$, possibilitando uma comparação direta com a teoria padrão; essa distribuição proporciona melhores ajustes aos dados de raios-X dos aglomerados que a distribuição Gaussiana. Demonstramos também que a distribuição de Burr corrige o problema da normalização. As funções de massa são abordadas ainda na presença da energia escura, e obtemos limites sobre diversos parâmetros cósmicos, como a normalização do Espectro de Potência σ_8 , os parâmetros de densidade Ω_{ME} e Ω_{EE} (*matéria e energia escuras*), além do parâmetro ω da equação de estado da energia escura. A 'cosmologia não extensiva' é ainda abordada na radiação de Bremsstrahlung, a radiação primária dos aglomerados de raio-X, e também na sonda de plasma, com evidentes aplicações em astrofísica experimental. Por fim, tratamentos de dados dos atuais catálogos de galáxias permitiram análises conjuntas que limitaram melhor os principais parâmetros dos modelos, objetivando eleger o candidato mais adequado para o novo paradigma cosmológico.

A STUDY OF THE NONEXTENSIVE DISTRIBUTION ON
COSMOLOGY

by

Lucio Marassi de Souza Almeida

Abstract

Capítulo 1

INTRODUÇÃO

As novas observações astronômicas, aliadas a um arcabouço teórico em constante evolução, transformaram a cosmologia em uma das mais excitantes áreas da ciência contemporânea. Este fato se deve sobretudo às observações de SNe Ia em altos *redshifts*^{203,18}, aos novos dados de raio-X dos aglomerados de galáxias¹⁷¹, e às recentes observações da radiação cósmica de fundo (RCF) em várias escalas angulares^{163,164}.

A medida da temperatura da RCF, $T_o = 2,7$ K, permitiu recontar a história cósmica dos últimos bilhões de anos relacionando tempo com temperatura. Esse fundo de microondas é extraordinariamente isotrópico; a anisotropia de dipolo é devido ao movimento peculiar da terra e a anisotropia de quadrupolo (\sim uma parte em 10^5) tem sua origem nas perturbações gravitacionais da distribuição de matéria (anisotropia intrínseca). O espectro de corpo negro evidencia que a radiação tem estado em equilíbrio com a matéria desde o início do universo, como previsto pelo modelo do *Big Bang*. A relação entre a escala angular e o tamanho da perturbação na última superfície de espalhamento (quando os fótons interagiram pela última vez com os bárions) depende da curvatura espacial e da distância até essa superfície. A resolução e a extrema sensibilidade do *WMAP* (*Wilkinson Microwave Anisotropy Probe*) revelaram mapas completos do céu para a interação do fluido de fóton-bárion na última superfície de espalhamento, e vários parâmetros foram medidos com bastante precisão (h , $\Omega_b h^2$, $\Omega_{ME} h^2$, Ω_{Total} , n_s , σ_8 , entre outros). A posição do primeiro pico acústico no espectro de potências da RCF favoreceu um universo espacialmente plano. Em 2007 o satélite *PLANCK* deverá ser lançado, tendo este uma melhor resolução espacial e maior sensibilidade na temperatura, permitindo com isso informações ainda mais precisas que o WMAP.

Outro avanço de grande significado ocorreu no estudo de aglomerados de galáxias para investigações no campo da cosmologia. Inicialmente, importantes resultados foram obtidos através de observações em emissões de raio-X, e, mais recentemente, através do uso do efeito Sunyaev-Zel'dovich¹⁷. Os aglomerados de galáxias são os maiores sistemas virializados do Universo, bastante relaxados na região central, e devido a tais propriedades, como esperado, já começaram a fornecer limites bastante robustos em cosmologia, sendo uma das formas mais diretas de limitar a densidade de matéria do universo, Ω_m .

Dos dados da RCF sabemos que o universo é aproximadamente plano, o que está de acordo com o paradigma inflacionário¹⁶³, $\Omega_{\text{Total}} = 1,02 \pm 0,02$. Das observações dinâmicas (estudos de raio-X de estruturas em grande escala, fração de massa do gás etc.), sabemos que os modelos cosmológicos capazes de explicar os independentes estudos da idade de aglomerados globulares, precisam conter apenas cerca de 23% da densidade crítica em forma de matéria (que é gravitacionalmente atrativa). Da nucleossíntese primordial e das curvas de rotação das galáxias, sabemos que a maior parte dessa matéria é *escura*. Também sabemos hoje em dia que o universo expande aceleradamente devido aos dados atuais das supernovas SNe Ia, e para explicar tal aceleração e termos um acordo teórico com os fatos anteriormente citados, devemos ter uma outra componente de energia com pressão negativa chamada *energia escura* contribuindo com cerca de 73% para o conteúdo cósmico, cujo candidato mais antigo é a constante cosmológica.

A natureza dos dois ingredientes básicos da cosmologia contemporânea (matéria e energia escura) não foi ainda estabelecida. A matéria escura somente é percebida pelos seus efeitos gravitacionais no universo (curva de rotação das galáxias, lentes gravitacionais, estrutura de larga escala, etc.). Uma vez que a energia escura não é gravitacionalmente atrativa, a formação de praticamente todas as estruturas do universo, em pequena e grande escala, é proporcionada pela componente de matéria escura. Entender como se formam os halos de matéria escura, que abrigam todas as galáxias e aglomerados de galáxias, é essencial para se compreender o comportamento da matéria escura. Por outro lado, compreendermos o papel desempenhado pela energia escura ao longo desse processo, é igualmente importante para determinarmos a natureza desses dois componentes que respondem por 96% do universo.

As grandes estruturas do universo (aglomerados e superaglomerados de galáxias)

foram formadas pelo crescimento gravitacional de pequenas perturbações de densidade, na época do desacoplamento matéria-radiação (em um redshift $z \sim 1000$). A densidade numérica de objetos colapsados de certa massa, quantidade denominada *função de massa* dos halos de matéria escura, $F(M)$, é uma quantidade central no estudo da evolução das estruturas cósmicas.

O trabalho pioneiro descrevendo analiticamente a função de massa das galáxias foi realizado por Press & Schechter¹⁵⁴ em 1974. O chamado método Press-Schechter (PS) considera que toda região onde o contraste de densidade atingiu um valor crítico δ_c condensa, “colapsa” e torna-se um objeto auto-gravitante, destacando-se do fluxo de expansão do universo, para se transformar em um objeto “ligado”. Na aproximação de PS, o contraste de densidade, δ , é um campo aleatório descrito por uma distribuição Gaussiana¹⁵⁴.

Embora a função de massa de PS tenha tido um êxito considerável na descrição analítica da evolução dos halos, ela possui problemas graves a serem resolvidos. Em primeiro lugar a função de distribuição estatística de PS tem um problema intrínseco de normalização, ou seja, integrando sobre toda a massa M obtemos exatamente $\frac{1}{2}$, e não uma função normalizada, como deveria ser¹²¹. Para explicar tal fato, Press e Schechter consideraram que o método computa apenas metade da massa efetivamente ligada, ou seja, não contabiliza as regiões subdensas, responsáveis no futuro pelo restante da massa ligada nos halos. Além desse grave problema de normalização, notamos que o método PS está em desacordo com as mais modernas simulações de N-Corpos^{137,16}, e estudos de catálogos de halos em raio-X demonstram igualmente a inaptidão do formalismo de PS em explicar esses dados observacionais¹⁵⁶.

Os problemas inerentes ao método PS motivaram nosso estudo da função de massa dos halos, na busca de uma descrição que se adequasse melhor aos dados observacionais e, além disso, que pudesse corrigir o problema de normalização de PS sem abrir mão da simplicidade matemática desse modelo de formação de estruturas.

Vemos ainda que estudos em diversas áreas do conhecimento mostram que a estatística padrão de Boltzmann-Gibbs não se aplica a todos os sistemas físicos da natureza. Tais estudos sugerem naturalmente uma possível solução para o problema estatístico do formalismo de Press-Schechter. Conexões entre a dinâmica e a termodinâmica estão ainda longe de serem completamente compreendidas. Os últimos anos foram marcados por uma ativi-

dade teórica extraordinária nos fundamentos da termodinâmica e mecânica estatística. Todos os avanços estão de alguma forma conectados com o conceito de não-extensividade das quantidades termodinâmicas básicas. Uma importante generalização do postulado da entropia foi proposta por Tsallis em 1988⁷⁶.

Atualmente existe um grande acúmulo de evidências observacionais e argumentos teóricos sugerindo que a entropia de Tsallis fornece uma descrição estatística e uma termodinâmica convincente para vários cenários físicos, dentre os quais destacamos: comportamento de estrelas politrópicas^{107,15}, turbulências e perturbações em plasmas eletrônicos^{14,13}, difusão anômala¹², distribuições de Levy⁷⁹, o problema do neutrino solar¹⁰⁶, distribuição de velocidades peculiar de aglomerados de galáxias¹⁰⁴, ou de uma maneira geral, sistemas que apresentam interações de longo alcance ou efeitos de memória microscópica efetiva¹¹.

Como é bem conhecido, as propriedades termodinâmicas de um sistema de muitas partículas podem ser calculadas através da mecânica estatística ou da teoria cinética. A abordagem fundamental da mecânica estatística baseia-se na função de partição do sistema, a partir da qual todas as grandezas termodinâmicas podem em princípio ser calculadas (por exemplo para um gás clássico ou quântico), enquanto que a solução cinética tem como ponto de partida a função de distribuição de velocidades moleculares. Neste projeto, daremos uma ênfase especial para o ponto de vista cinético, que no caso de um gás clássico extensivo é representada pela distribuição de Maxwell.

Sabemos hoje que as interações de longo alcance, como a força gravitacional ou Coulombiana, modificam substancialmente várias propriedades termodinâmicas usuais⁹³⁻⁹⁵. Nesse sentido, depois do trabalho pioneiro de Plastino & Plastino (1993)¹⁰⁷, notamos um grande interesse na literatura por aplicações da estatística não-extensiva de Tsallis em problemas de interesse astrofísico e cosmológico, devido justamente a presença de forças gravitacionais (longo alcance) em tais sistemas físicos^{140,15}.

A formação de estruturas no universo é essencialmente provocada pela interação gravitacional dos halos de matéria escura. Desse modo parece natural aplicarmos a estatística não-extensiva para descrever esse processo auto-gravitante. Vários estudos sobre a não-gaussianidade primordial foram recentemente iniciados, como a evolução do espectro de potências da formação de estruturas em modelos não-gaussianos¹⁰ e limites da não-

gaussianidade primordial através da abundância de aglomerados em altos redshifts⁹.

Vários trabalhos ainda abordam, diretamente, a aplicação da estatística não-extensiva como uma solução da não-gaussianidade na formação de estruturas, como estudos dos limites da não-extensividade no aglomeramento de galáxias⁸, estudos do perfil de densidade da matéria escura, com comparações entre a teoria não-extensiva e as simulações de N-Corpos⁷, teorias não-extensivas da matéria escura e dos perfis de densidade dos gases⁶, e diversos estudos mostrando indícios de que as flutuações de temperatura da radiação cósmica de fundo seriam não-extensivas (veja por exemplo Bernui *et al.* 2005⁵).

Retornando ao modelo analítico padrão de formação de estruturas, ou seja, à função de massa dos halos de PS, notamos que a estatística do contraste de densidade primordial é Gaussiana. O modelo de PS, como vimos, apresenta um problema intrínseco de normalização, além de não explicar os mais recentes dados numéricos e observacionais. Em vista de tudo o que foi até agora exposto, seria natural estudarmos se o problema estaria na estatística empregada por Press & Schechter. Esse foi o início de nosso estudo da ‘cosmologia não extensiva’, onde mostramos que a estatística não extensiva é aplicável à função de massa dos halos de matéria escura, estudamos suas propriedades de normalização e provamos que ela, aplicada às observações de halos em raio-X, se adequa melhor aos atuais parâmetros cosmológicos do WMAP que a estatística Gaussiana padrão de PS. Iniciamos ainda estudos da aplicação da energia escura no processo. Por fim, ainda estudamos as aplicações da não-extensividade na radiação de Bremsstrahlung e na sonda de plasma, com evidentes aplicações para a cosmologia observacional. Mostramos ainda análises estatísticas conjuntas de catálogos atuais de galáxias, que nos permitiram uma estimativa melhor e mais atualizada dos parâmetros cosmológicos mais importantes, como os parâmetros de matéria, energia escura e a constante de Hubble.

A tese está estruturada da seguinte forma:

- No capítulo 2 procuramos mostrar uma sucinta síntese da cosmologia atual, com as suas principais definições, parâmetros e métodos de pesquisa teórica e observacional.
- No capítulo 3 apresentamos um resumo dos aspectos principais que regem o estudo da formação das grandes estruturas do universo, com um enfoque semi-relativístico da evolução temporal das perturbações de densidade.

- No capítulo 4 mostramos rapidamente os principais conceitos e equações da estatística não extensiva, que utilizaremos como base para nossos estudos.
- No capítulo 5 estão concentrados os resultados principais da tese. Mostramos os resultados de um recente trabalho¹³⁹, onde propusemos nossa função de massa dos halos baseada na estatística não-extensiva de Tsallis. Em outro recente artigo¹⁴⁶ analisamos as propriedades estatísticas, especialmente a normalização, de diversas distribuições (incluindo a não extensiva). Mostramos ainda que o nosso método se ajusta às observações do catálogo de raio-X de galáxias HIFLUGCS¹⁵⁶ (baseado no ROSAT All-Sky Survey) com parâmetros compatíveis com o WMAP, enquanto o mesmo não se processa no método PS padrão⁴. Estudamos também a influência da *energia escura* no processo de formação de estruturas.
- No capítulo 6 a cosmologia não extensiva é ainda abordada na radiação de Bremsstrahlung, a radiação primária dos aglomerados de raio-X, e também na sonda de plasma, com claras aplicações em astrofísica experimental. Por fim, tratamentos de dados dos atuais catálogos de galáxias nos permitiram análises conjuntas^{127,17} que limitaram melhor os principais parâmetros dos modelos, objetivando eleger o candidato mais adequado para o novo paradigma cosmológico.
- Finalmente, no capítulo 7 apresentamos nossas conclusões e perspectivas de trabalhos futuros.

Capítulo 2

COSMOLOGIA

2.1 Introdução à Cosmologia do Big Bang

Most of the new cosmological data can be interpreted within a coherent framework known as the standard cosmological model, based on the Big Bang theory of the universe and the inflationary paradigm.

Our present understanding of the universe is based upon the successful hot Big Bang theory. This theory rests upon four strong pillars, a theoretical framework based on general relativity, as put forward by Albert Einstein and Alexander A. Friedmann in the 1920s, and three robust observational facts: First, the expansion of the universe, discovered by Edwin P. Hubble in the 1930s, as a recession of galaxies at a speed proportional to their distance from us. Second, the relative abundance of light elements, explained by George Gamow in the 1940s, mainly that of helium, deuterium and lithium, which were cooked from the nuclear reactions that took place at around a second to a few minutes after the Big Bang, when the universe was a few times hotter than the core of the sun. Third, the cosmic microwave background (CMB), discovered in 1965 by Arno A. Penzias and Robert W. Wilson as a very isotropic blackbody radiation at a temperature of about 3 degrees Kelvin, emitted when the universe was cold enough to form neutral atoms, and photons decoupled from matter, approximately 500,000 years after the Big Bang.

According to current thinking, the history of the observable universe broadly divides into three stages. First there is an *inflationary era*, when the energy density is dominated by the potential of a scalar field. Then there is a *radiation dominated era* when the energy density is dominated by relativistic particles, which are called ‘radiation’ by cosmologists.

Finally, lasting till the present epoch, there is a *matter dominated era* when the energy density is dominated by the mass of non-relativistic particles, which are called ‘matter’.

Unless the contrary is implied by the specified units, I set $\hbar = c = k_B = 1$.

2.1.1 O Big Bang

At the present epoch the Hubble time is of order 10^{10} yr. The era when the universe is very hot and dense, and the Hubble time is only a tiny fraction of a second is popularly known as the Hot Big Bang. The beginning presumably lies at the *Planck epoch*, when the Hubble time is of order the Planck time

$$t_{\text{Pl}} = G^{1/2} = 5.39 \times 10^{-44} \text{ sec} \quad (2.1)$$

As we extrapolate back to this epoch, quantum gravity effects presumably invalidate the concept of time, which conveniently removes the need to discuss what is before the Big Bang!

2.1.2 Universos de Friedmann–Robertson–Walker

Cosmology was born as a science with the advent of general relativity and the realization that the geometry of space-time, and thus the general attraction of matter, is determined by the energy content of the universe²⁰, Einstein’s original field equations are

$$R_{\mu\nu} - \frac{1}{2}Rg_{\mu\nu} = 8\pi GT_{\mu\nu} . \quad (2.2)$$

These non-linear equations are too difficult to solve without some insight about the symmetries of the problem (the universe itself). Einstein and Friedmann speculated that the most “reasonable” symmetry for the universe at large should be *homogeneity* at all points, and thus *isotropy*. It was not until the detection, a few decades later, of the microwave background by Penzias and Wilson that this important assumption was finally put onto firm experimental ground. The most general metric satisfying homogeneity and isotropy at large scales is the Friedmann-Robertson-Walker (FRW) metric, written here in terms of the invariant geodesic distance $ds^2 = g_{\mu\nu}dx^\mu dx^\nu$ in four dimensions, $\mu = 0, 1, 2, 3$, see Ref.²⁰ (I am using $c = 1$ everywhere, unless specified).

$$ds^2 = -dt^2 + a^2(t)R_0^2 \left[\frac{dr^2}{1 - kr^2} + r^2 d\Omega^2 \right] , \quad (2.3)$$

where $d\Omega^2 = d\theta^2 + \sin^2\theta d\phi^2$ is the metric on a two-sphere. The scale factor $a(t)$ (the physical size of the universe) characterizes the relative size of the spatial sections as a function of time; we have written it in a normalized form $a(t) = R(t)/R_0$, where the subscript 0 will always refer to a quantity evaluated at the present time. The redshift z undergone by radiation from a comoving object as it travels to us today is related to the scale factor at which it was emitted by

$$a = \frac{1}{(1+z)} . \quad (2.4)$$

The spatial curvature parameter k takes on values $+1$, 0 , or -1 for positively curved, flat, and negatively curved spatial sections, respectively. Spatially open, flat and closed universes have different geometries.

Depending on the dynamics (and thus on the matter/energy content) of the universe, we will have different possible outcomes of its evolution. The universe may expand for ever, recollapse in the future or approach an asymptotic state in between.

The most general matter fluid consistent with the assumption of homogeneity and isotropy is a perfect fluid. The energy momentum tensor associated with such a fluid can be written as²⁰

$$T^{\mu\nu} = p g^{\mu\nu} + (p + \rho) U^\mu U^\nu , \quad (2.5)$$

where $p(t)$ and $\rho(t)$ are the isotropic pressure and energy density of the fluid at a given time in the expansion, and U^μ is the comoving four-velocity, satisfying $U^\mu U_\mu = -1$.

The equations of motion of such a fluid in an expanding universe can be deduced from the Einstein equations (2.2), where we substitute the FRW metric (2.3) and the perfect fluid tensor (2.5) to obtain a Robertson-Walker solution . The $\mu = \nu = 0$ component of the Einstein equations constitutes the Friedmann equation

$$H^2 \equiv \left(\frac{\dot{a}}{a}\right)^2 = \frac{8\pi G}{3}\rho - \frac{k}{a^2 R_0^2} , \quad (2.6)$$

where we have introduced the Hubble parameter $H \equiv \dot{a}/a$.

The conservation of energy ($T^{\mu\nu}{}_{;\nu} = 0$), a direct consequence of the general covariance of the theory ($G^{\mu\nu}{}_{;\nu} = 0$), can be written in terms of the FRW metric and the perfect fluid tensor (2.5) as

$$\frac{d}{dt}(\rho a^3) + p \frac{d}{dt}(a^3) = 0 , \quad (2.7)$$

where the energy density and pressure can be split into its matter and radiation components, $\rho = \rho_M + \rho_R, p = p_M + p_R$, with corresponding equations of state, $p_M = 0, p_R = \rho_R/3$. Together, the Friedmann and the energy-conservation equation give the evolution equation for the scale factor,

$$\frac{\ddot{a}}{a} = -\frac{4\pi G}{3}(\rho + 3p) . \quad (2.8)$$

Einstein was interested in finding static ($\dot{a} = 0$) solutions, both due to his hope that general relativity would embody Mach's principle that matter determines inertia, and simply to account for the astronomical data as they were understood at the time. A static universe with a positive energy density is compatible with (2.6) if the spatial curvature is positive ($k = +1$) and the density is appropriately tuned; however, (2.8) implies that \ddot{a} will never vanish in such a spacetime if the pressure p is also nonnegative (which is true for most forms of matter, and certainly for ordinary sources such as stars and gas). Einstein therefore proposed a modification of his equations, to

$$R_{\mu\nu} - \frac{1}{2}Rg_{\mu\nu} + \Lambda g_{\mu\nu} = 8\pi GT_{\mu\nu} , \quad (2.9)$$

where Λ is a new free parameter, the cosmological constant. Indeed, the left-hand side of (2.9) is the most general local, coordinate-invariant, divergenceless, symmetric, two-index tensor we can construct solely from the metric and its first and second derivatives. With this modification, the Friedmann equations become

$$H^2 = \frac{8\pi G}{3}\rho + \frac{\Lambda}{3} - \frac{k}{a^2 R_0^2} . \quad (2.10)$$

and

$$\frac{\ddot{a}}{a} = -\frac{4\pi G}{3}(\rho + 3p) + \frac{\Lambda}{3} . \quad (2.11)$$

The original cosmological constant turned out to be unnecessary when the expansion of the universe was discovered. Meanwhile, particle theorists have realized that the cosmological constant can be interpreted as a measure of the energy density of the vacuum. This energy density is the sum of a number of apparently unrelated contributions, each of magnitude much larger than the upper limits on the cosmological constant today; the question of why the observed vacuum energy is so small in comparison to the scales of particle physics has become a celebrated puzzle.

There are a number of other reviews. For astrophysical aspects, Carroll, Press and Turner⁴⁵, which should be consulted for numerous useful formulae and a discussion of several kinds of observational tests not covered here. For introductions to cosmology, see^{46,25}.

A Expansão do Universo

In 1929, Edwin P. Hubble discovered the expansion of the universe. The scale factor $a(t)$ gives *physical size* to the spatial coordinates \vec{x} , and the expansion is nothing but a change of scale (of spatial units) with time. Except for *peculiar velocities*, i.e. motion due to the local attraction of matter, galaxies do not move in coordinate space, it is the space-time fabric which is stretching between galaxies. Due to this continuous stretching, the observed wavelength of photons coming from distant objects is greater than when they were emitted by a factor precisely equal to the ratio of scale factors,

$$\frac{\lambda_{\text{obs}}}{\lambda_{\text{em}}} = \frac{a_0}{a} \equiv 1 + z, \quad (2.12)$$

where a_0 is the present value of the scale factor. Since the universe today is larger than in the past, the observed wavelengths will be shifted towards the red, or *redshifted*, by an amount characterized by z , the redshift parameter. The *Hubble parameter* is defined by $H = \dot{a}/a$.

It is convenient to set $a_0 = 1$, so that $a(t)$ is simply the size of any comoving region (one moving with the galaxies) relative to its present size. The present value of H , denoted by H_0 is called the Hubble constant. It is traditionally measured by observing the redshift $z \equiv \Delta\lambda/\lambda$ of galaxies receding from us with velocity $v \ll 1$. The velocity of such a galaxy is given by $v = Hr$, and its redshift is just the non-relativistic Doppler shift $z = v$, leading to Hubble's law

$$z(=v) = H_0 r_0 \quad (2.13)$$

Hubble's law is well established because *relative* distances are easy to establish. All one has to do is find a 'standard candle', that is a type of object (say as star of a given type) of which all examples have practically the same luminosity. Then its apparent luminosity will vary with (distance)⁻³, and so measure relative distances. On the other hand to fix H_0 which is the constant of proportionality one has to know the luminosity of

some object, which is much harder to do. Different estimates give H_0 in the range 40 to $100 \text{ km sec}^{-1} \text{ Mpc}^{-1}$, and it is usual to define a quantity h by

$$H_0 = 100h \text{ km sec}^{-1} \text{ Mpc}^{-1} \quad (2.14)$$

The parameter h has been measured to be in the range $0.4 < h < 1$ for decades, and only in the last few years has it been found to lie within 10% of $h = 0.65$.

The homogeneity and isotropy of the early universe implies that its expansion is adiabatic (no heat flow), so that entropy is conserved.

The matter and energy content of the universe

From the Friedmann equation (where henceforth we take the effects of a cosmological constant into account by including the vacuum energy density ρ_Λ into the total density ρ), for any value of the Hubble parameter H there is a critical value of the energy density such that the spatial geometry is flat ($k = 0$). One can then define a *critical* density ρ_c :

$$\rho_c \equiv \frac{3H_0^2}{8\pi G} = 1.88 h^2 10^{-29} \text{ g/cm}^3 \quad (2.15)$$

$$= 2.77 h^{-1} 10^{11} M_\odot / (h^{-1} \text{ Mpc})^3, \quad (2.16)$$

where $M_\odot = 1.989 \times 10^{33} \text{ g}$ is a solar mass unit. The critical density ρ_c corresponds to approximately 4 protons per cubic meter, certainly a very dilute fluid! In terms of the critical density it is possible to define the ratios $\Omega_i \equiv \rho_i/\rho_c$, for matter, radiation, cosmological constant and even curvature, today,

$$\Omega_M = \frac{8\pi G \rho_M}{3H_0^2} \quad \Omega_R = \frac{8\pi G \rho_R}{3H_0^2} \quad (2.17)$$

$$\Omega_\Lambda = \frac{\Lambda}{3H_0^2} \quad \Omega_K = -\frac{K}{a_0^2 H_0^2}. \quad (2.18)$$

If the individual components i have very simple equations of state of the form

$$p_i = w_i \rho_i, \quad (2.19)$$

with w_i a constant. Plugging this equation of state into the energy-momentum conservation equation $\nabla_\mu T^{\mu\nu} = 0$, we find that the energy density has a power-law dependence on the scale factor,

$$\rho_i \propto a^{-n_i}, \quad (2.20)$$

where the exponent is related to the equation of state parameter by

$$n_i = 3(1 + w_i) . \quad (2.21)$$

For massive particles (“dust” or simply “matter”) $\rho_M \propto a^{-3}$. For relativistic particles (“radiation”) $\rho_R \propto a^{-4}$. For Vacuum energy $\rho_\Lambda \propto a^0$; from (2.21) this implies a negative pressure, when the vacuum energy is positive. We can define a corresponding density parameter

$$\Omega_k = 1 - \Omega ; \quad (2.22)$$

this relation is simply (2.6) divided by H^2 . The most popular equations of state for cosmological energy sources can thus be summarized as follows:

	w_i	n_i	
matter	0	3	
radiation	1/3	4	(2.23)
“curvature”	−1/3	2	
vacuum	−1	0	

We can then write the rate of expansion H^2 in terms of its value today,

$$H^2(a) = H_0^2 \left(\Omega_R \frac{a_0^4}{a^4} + \Omega_M \frac{a_0^3}{a^3} + \Omega_\Lambda + \Omega_K \frac{a_0^2}{a^2} \right) . \quad (2.24)$$

We can safely neglect the contribution of relativistic particles to the total density of the universe today⁴⁶, which is dominated either by non-relativistic particles (baryons, dark matter or massive neutrinos) or by a cosmological constant. We can now write the Friedmann equation today, $a = a_0$, as a *cosmic sum rule*,

$$1 = \Omega_M + \Omega_\Lambda + \Omega_K , \quad (2.25)$$

where we have neglected Ω_R today.

2.1.3 Brief thermal history of the universe

According to the best accepted view, the universe must have originated at the Planck era (10^{19} GeV, 10^{-43} s) from a quantum gravity fluctuation. It is plausible that a primordial era of cosmological *inflation* originated then. Soon after, the universe may have reached

the Grand Unified Theories (GUT) era (10^{16} GeV, 10^{-35} s). Quantum fluctuations of the inflaton field most probably left their imprint then as tiny perturbations in an otherwise very homogenous patch of the universe. At the end of inflation, the huge energy density of the inflaton field was converted into particles, which soon thermalized and became the origin of the hot Big Bang as we know it. Such a process is called *reheating* of the universe. Since then, the universe became radiation dominated. It is probable that the asymmetry between matter and antimatter originated at the same time as the rest of the energy of the universe, from the decay of the inflaton. This process is known under the name of *baryogenesis* since baryons (mostly quarks at that time) must have originated then, from their annihilation with antibaryons.

After that we have the *primordial nucleosynthesis* (1 – 0.1 MeV, 1 s – 3 min), when protons and neutrons were cold enough that bound systems could form, giving rise to the lightest elements, soon after *neutrino decoupling*. The observed relative abundances of light elements are in agreement with the predictions of the hot Big Bang theory. Nowadays, Big Bang nucleosynthesis (BBN) codes compute a chain of around 30 coupled nuclear reactions, to produce all the light elements up to beryllium-7 (The rest of nuclei, up to iron (Fe), are produced in heavy stars, and beyond Fe in novae and supernovae explosions). The most important light elements are H , 4He , D , 3He , 7Li , and perhaps also 6Li , see Ref.^{23,22}. The present baryon fraction of the critical density can also be calculated as²²

$$\Omega_B h^2 = 3.6271 \times 10^{-3} \eta_{10} = 0.0190 \pm 0.0024 \quad (95\% \text{ c.l.}) \quad (2.26)$$

Clearly, this number is well below closure density, so baryons cannot account for all the matter in the universe.

Immediately afterwards, electron-positron annihilation occurs (0.5 MeV, 1 min) and all their energy goes into photons. Much later, at about (1 eV, $\sim 10^5$ yr), matter and radiation have equal energy densities. Soon after, electrons become bound to nuclei to form atoms (0.3 eV, 3×10^5 yr), in a process known as *recombination*. Immediately after, photons decouple from the plasma, travelling freely since then. Those are the photons we observe as the cosmic microwave background. Much later ($\sim 1 - 10$ Gyr), the small inhomogeneities generated during inflation have grown, via gravitational collapse, to become galaxies, clusters of galaxies, and superclusters, characterizing the epoch of

structure formation. It is the realm of long range gravitational physics, perhaps dominated by a vacuum energy in the form of a cosmological constant. Finally (3K, 13 Gyr), the Sun, the Earth, and biological life originated from previous generations of stars, and from a primordial soup of organic compounds, respectively.

I will now review some of the more robust features of the Hot Big Bang theory of which we have precise observational evidence.

The microwave background

One of the most remarkable observations ever made by mankind is the detection of the relic background of photons from the Big Bang. This background was predicted by George Gamow and collaborators in the 1940s. Penzias and Wilson had observed a weak isotropic background signal at a radio wavelength corresponding to a blackbody temperature of $T_\gamma = 3.5 \pm 1 \text{ K}$ ²⁰.

Since then many different experiments have confirmed the existence of the microwave background, as the Cosmic Background Explorer (COBE) satellite. Nowadays, the photon spectrum is confirmed to be a blackbody spectrum with a temperature given by

$$T_{\text{CMB}} = 2.725 \pm 0.002 \text{ K (systematic, 95\% c.l.)} \pm 7 \mu\text{K (1}\sigma \text{ statistical)} \quad (2.27)$$

In fact, this is the best blackbody spectrum ever measured, with spectral distortions below the level of 10 parts per million (ppm); it is an extraordinarily isotropic background.

Soon after COBE, other groups quickly confirmed the detection of temperature anisotropies at higher multipole numbers or smaller angular scales. These anisotropies play a crucial role in the understanding of the origin of structure in the universe.

2.2 THE COSMOLOGICAL CONSTANT

2.2.1 Vacuum energy

The cosmological constant Λ is a dimensionful parameter with units of $(\text{length})^{-2}$. From the point of view of particle physics the cosmological constant is a measure of the energy density of the vacuum — the state of lowest energy.

Consider a single scalar field ϕ , with potential energy $V(\phi)$. The action can be written

$$S = \int d^4x \sqrt{-g} \left[\frac{1}{2} g^{\mu\nu} \partial_\mu \phi \partial_\nu \phi - V(\phi) \right] \quad (2.28)$$

(where g is the determinant of the metric tensor $g_{\mu\nu}$), and the corresponding energy-momentum tensor is

$$T_{\mu\nu} = \frac{1}{2} \partial_\mu \phi \partial_\nu \phi + \frac{1}{2} (g^{\rho\sigma} \partial_\rho \phi \partial_\sigma \phi) g_{\mu\nu} - V(\phi) g_{\mu\nu} . \quad (2.29)$$

In this theory, the configuration with the lowest energy density (if it exists) will be one in which there is no contribution from kinetic or gradient energy, implying $\partial_\mu \phi = 0$, for which $T_{\mu\nu} = -V(\phi_0) g_{\mu\nu}$, where ϕ_0 is the value of ϕ which minimizes $V(\phi)$. There is no reason in principle why $V(\phi_0)$ should vanish. The vacuum energy-momentum tensor can thus be written

$$T_{\mu\nu}^{\text{vac}} = -\rho_{\text{vac}} g_{\mu\nu} , \quad (2.30)$$

with ρ_{vac} in this example given by $V(\phi_0)$. (This form for the vacuum energy-momentum tensor can also be argued for on the more general grounds that it is the only Lorentz-invariant form for $T_{\mu\nu}^{\text{vac}}$.) The vacuum can therefore be thought of as a perfect fluid as in (2.5), with

$$p_{\text{vac}} = -\rho_{\text{vac}} . \quad (2.31)$$

The effect of an energy-momentum tensor of the form (2.30) is equivalent to that of a cosmological constant, as can be seen by moving the $\Lambda g_{\mu\nu}$ term in (2.9) to the right-hand side and setting

$$\rho_{\text{vac}} = \rho_\Lambda \equiv \frac{\Lambda}{8\pi G} . \quad (2.32)$$

This equivalence is the origin of the identification of the cosmological constant with the energy of the vacuum.

A (free) quantum field can be thought of as a collection of an infinite number of harmonic oscillators in momentum space. Formally, the zero-point energy of such an infinite collection will be infinite (See⁴⁵ for further details). But we can apply a kind of normalization to avoid the ‘infinite’ problems.

The net cosmological constant, from this point of view, is the sum of a number of apparently disparate contributions, including potential energies from scalar fields and

zero-point fluctuations of each field theory degree of freedom, as well as a bare cosmological constant Λ_0 .

In the Weinberg-Salam electroweak model, we would naturally expect a contribution to the vacuum energy today of order

$$\rho_{\Lambda}^{\text{EW}} \sim (200 \text{ GeV})^4 \sim 3 \times 10^{47} \text{ erg/cm}^3 . \quad (2.33)$$

In the case of vacuum fluctuations, we should choose our cutoff at the energy past which we no longer trust our field theory. If we are confident that we can use ordinary quantum field theory all the way up to the Planck scale $M_{\text{Pl}} = (8\pi G)^{-1/2} \sim 10^{18} \text{ GeV}$, we expect a contribution of order

$$\rho_{\Lambda}^{\text{Pl}} \sim (10^{18} \text{ GeV})^4 \sim 2 \times 10^{110} \text{ erg/cm}^3 . \quad (2.34)$$

But cosmological observations imply

$$|\rho_{\Lambda}^{(\text{obs})}| \leq (10^{-12} \text{ GeV})^4 \sim 2 \times 10^{-10} \text{ erg/cm}^3 , \quad (2.35)$$

much smaller than any of the individual effects listed above. The ratio of (2.34) to (2.35) is the origin of the famous discrepancy of 120 orders of magnitude between the theoretical and observational values of the cosmological constant. This is the “cosmological constant problem”, one of the most significant unsolved problems in fundamental physics.

2.2.2 Possible Solutions for the Cosmological Constant Problem

Supersymmetry

Although initially investigated for other reasons, supersymmetry (SUSY) turns out to have a significant impact on the cosmological constant problem, and may even be said to solve it halfway. SUSY is a spacetime symmetry relating fermions and bosons to each other. Just as ordinary symmetries are associated with conserved charges, supersymmetry is associated with “supercharges” Q_{α} , where α is a spinor index.

Considering “globally supersymmetric” theories, which are defined in flat spacetime $Q_{\alpha}|\psi\rangle = 0$ for all α , the energy vanishes automatically, $\langle\psi|H|\psi\rangle = 0$. In the case of vacuum fluctuations, contributions from bosons are exactly canceled by equal and opposite

contributions from fermions when supersymmetry is unbroken. So the vacuum energy of a supersymmetric state in a globally supersymmetric theory will vanish.

But, in a state where SUSY was broken at an energy scale M_{SUSY} , we would expect a corresponding vacuum energy $\rho_\Lambda \sim M_{\text{SUSY}}^4$. In the real world, the fact that accelerator experiments have not discovered superpartners for the known particles of the Standard Model implies that M_{SUSY} is of order 10^3 GeV or higher. Thus, we are left with a discrepancy

$$\frac{M_{\text{SUSY}}}{M_{\text{vac}}} \geq 10^{15} . \quad (2.36)$$

So the SUSY can solve the cosmological constant problem halfway (at least on a log scale).

String theory

Unlike supergravity, string theory appears to be a consistent and well-defined theory of quantum gravity.

String theory is naturally formulated in more than four spacetime dimensions, all sub-theories, along with eleven-dimensional supergravity, composing limits of a single underlying theory, sometimes known as M-theory. To bring the theory closer to the world we observe, the extra dimensions can be compactified on a manifold whose Ricci tensor vanishes. There are a large number of possible compactifications, many of which preserve some but not all of the original supersymmetry. If enough SUSY is preserved, the vacuum energy will remain zero.

Of course, to describe our world we want to break all of the supersymmetry. Thus, the search is still on for a four-dimensional string theory vacuum with broken supersymmetry and vanishing (or very small) cosmological constant.

Other Possibilities

Although a cosmological constant is an excellent fit to the current data, the observations can also be accommodated by any form of “dark energy” which does not cluster on small scales (so as to avoid being detected by measurements of Ω_M) and redshifts away only very slowly as the universe expands (to account for the accelerated expansion).

One way to parameterize such a component X is by an effective equation of state, $p_X = w_X \rho_X$. The relevant range for w_X is between 0 (ordinary matter) and -1 (true

cosmological constant); sources with $w_X > 0$ redshift away more rapidly than ordinary matter (and therefore cause extra deceleration), while $w_X < -1$ is unphysical by the criteria of the Dominant Energy Condition (although see⁶²). Current observations of

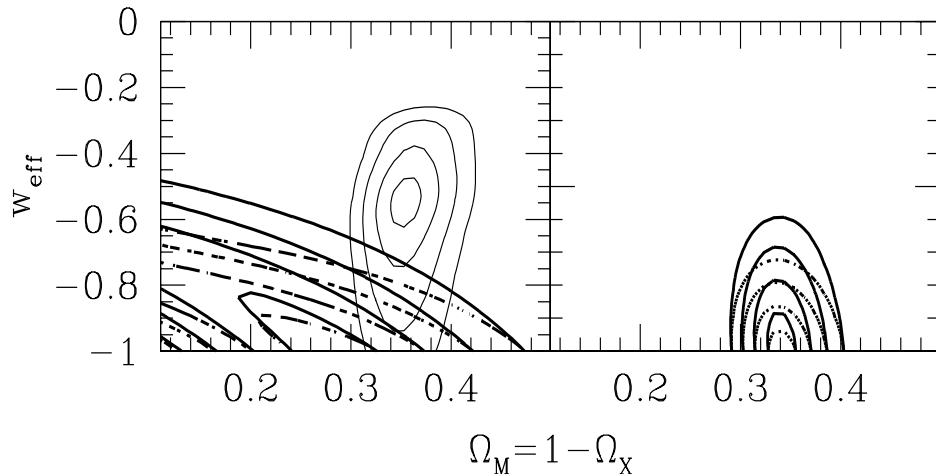


Figure 2.1: Limits from supernovae and large-scale structure data on Ω_M and the equation-of-state parameter w_X , in a flat universe dominated by matter and dark energy⁶⁴. Thin contours (on the left) represent limits from CMB and large-scale structure measurements, while thick contours are those from SNe observations; solid lines apply to models with constant w_X , while dashed lines apply to models of dynamical scalar fields. The constraints are combined on the right.

supernovae, large-scale structure, gravitational lensing, and the CMB already provide interesting limits on w_X ^{63,64}. Figure (2.1) shows an example, in this case limits from supernovae and large-scale structure on w_X and Ω_M in a universe which is assumed to be flat and dominated by X and ordinary matter. It is clear that the favored value for the equation-of-state parameter is near -1 , that of a true cosmological constant, although other values are not completely ruled out.

But the simplest physical model for an appropriate dark energy component is a single slowly-rolling scalar field, sometimes referred to as “quintessence”^{65–67}. In an expanding universe, a spatially homogeneous scalar with potential $V(\phi)$ and minimal coupling to gravity obeys

$$\ddot{\phi} + 3H\dot{\phi} + V'(\phi) = 0 , \quad (2.37)$$

where H is the Hubble parameter, overdots indicate time derivatives, and primes indicate

derivatives with respect to ϕ . The energy density is $\rho_\phi = \frac{1}{2}\dot{\phi}^2 + V(\phi)$, and the pressure is $p_\phi = \frac{1}{2}\dot{\phi}^2 - V(\phi)$, implying an equation of state parameter

$$w = \frac{p}{\rho} = \frac{\frac{1}{2}\dot{\phi}^2 - V(\phi)}{\frac{1}{2}\dot{\phi}^2 + V(\phi)}, \quad (2.38)$$

which will generally vary with time. Thus, when the field is slowly-varying and $\dot{\phi}^2 \ll V(\phi)$, we have $w \sim -1$, and the scalar field potential acts like a cosmological constant.

Replacing a constant parameter Λ with a dynamical field could allow us to avoid the fine-tuning that inevitably accompanies the cosmological constant.

There are specific particle-physics models for the quintessence field; some based on supersymmetric gauge theories, supergravity, small extra dimensions, large extra dimensions, and also the possibility that the scalar field responsible for driving inflation may also serve as quintessence⁶⁸, although this proposal has been criticized for producing unwanted relics and isocurvature fluctuations⁶⁹.

There are other models of dark energy besides those based on nearly-massless scalar fields. One scenario is “solid” dark matter, typically based on networks of tangled cosmic strings or domain walls. Strings give an effective equation-of-state parameter $w_{\text{string}} = -1/3$, and walls have $w_{\text{wall}} = -2/3$.

2.3 DETERMINATION OF COSMOLOGICAL PARAMETERS

2.3.1 The Lookback Time

The lookback time from the present day to an object at redshift z_* is given by

$$\begin{aligned} t_0 - t_* &= \int_{t_*}^{t_0} dt \\ &= \int_{1/(1+z_*)}^1 \frac{da}{aH(a)}, \end{aligned} \quad (2.39)$$

The age of the universe is obtained by taking the $z_* \rightarrow \infty$ ($t_* \rightarrow 0$) limit.

For $\Omega = \Omega_M = 1$, the behaviour $a \propto t^{2/3}$ gives the familiar answer

$$t_0 = \frac{2}{3}H_0^{-1}. \quad (2.40)$$

The age decreases as Ω_M is increased, and increases as Ω_Λ is increased. Figure (2.2) shows the expansion history of the universe for different values of these parameters and H_0 fixed; it is clear how the acceleration caused by Ω_Λ leads to an older universe. There

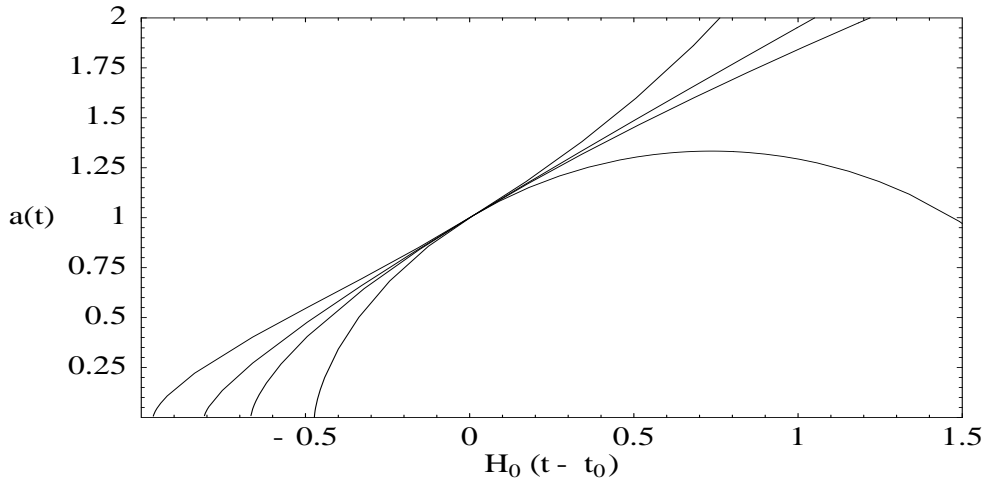


Figure 2.2: Expansion histories for different values of Ω_M and Ω_Λ . From top to bottom, the curves describe $(\Omega_M, \Omega_\Lambda) = (0.3, 0.7)$, $(0.3, 0.0)$, $(1.0, 0.0)$, and $(4.0, 0.0)$.

are analytic approximation formulas which estimate (2.39) in various regimes^{46,45}, but generally the integral is straightforward to perform numerically. We can Then use these relation as a consistency check between the cosmological observations of H_0 , Ω_M , Ω_Λ and t_0 . As an example we can estimate the Hubble parameter: using equation 2.40 we have, for $\Omega = \Omega_M = 1$

$$t_0 = \frac{2}{3}H_0^{-1} = 6.5 \times 10^9 h^{-1} \text{ yr}, \quad (2.41)$$

and the smallest conceivable value $\Omega_0 \simeq .1$ gives

$$t_0 = .9H_0^{-1} = 8.8 \times 10^9 h^{-1} \text{ yr}; \quad (2.42)$$

of course, we *cannot* measure the age of the universe directly, but only the age of its constituents; an upper limit on the age of the universe is provided by the age of the oldest stars (observed in globular clusters) which is bigger than 1.0×10^{10} years. With the favoured value $\Omega_0 = 1$ this requires $h < .65$, whereas with $\Omega_0 = .1$ the limit is $h < .88$.

2.3.2 The Luminosity Distance

The *absolute luminosity* L of a source is nothing but the energy emitted per unit time. A *standard candle* is a luminous object whose absolute luminosity is known, within certain errors. For example, Cepheid variable stars and type Ia supernovae are considered to be reasonable standard candles. The energy flux F received at the detector is the *measured* energy per unit time per unit area of the detector coming from that source. The luminosity distance d_L is then defined as the radius of the sphere centered on the source for which the absolute luminosity would give the observed flux, $F \equiv L/4\pi d_L^2$.

In a Friedmann-Robertson-Walker universe, light travels along null geodesics, $ds^2 = 0$, which determines the coordinate distance $r = r(z, H_0, \Omega_M, \Omega_\Lambda)$, as a function of redshift z and the other cosmological parameters. Now considering the effect of the universe expansion on the observed flux coming from a source at a certain redshift z from us, the total flux detected will be

$$F = \frac{L}{4\pi a_0^2 r^2(z)} \equiv \frac{L}{4\pi d_L^2}. \quad (2.43)$$

The final expression for the luminosity distance d_L as a function of redshift is thus given by⁴⁶

$$H_0 d_L = (1+z) |\Omega_K|^{-1/2} \text{sinn} \left[|\Omega_K|^{1/2} \int_0^z \frac{dz'}{\sqrt{(1+z')^2(1+z'\Omega_M) - z'(2+z')\Omega_\Lambda}} \right], \quad (2.44)$$

where $\text{sinn}(x) = x$ if $K = 0$; $\sin(x)$ if $K = +1$ and $\sinh(x)$ if $K = -1$. Expanding to second order around $z = 0$, we obtain

$$H_0 d_L = z + \frac{1}{2} \left(1 - \frac{\Omega_M}{2} + \Omega_\Lambda \right) z^2 + O(z^3). \quad (2.45)$$

The first term corresponds to the Hubble law. It is only recently that cosmological observations have gone far enough back into the early universe that we can begin to probe the second term.

2.3.3 Relation Between Distance Measures

Distance measures which can be extracted from observable quantities. These include the luminosity distance,

$$d_L \equiv \sqrt{\frac{L}{4\pi F}}, \quad (2.46)$$

where L is the intrinsic luminosity and F the measured flux; the proper-motion distance,

$$d_M \equiv \frac{u}{\dot{\theta}}, \quad (2.47)$$

where u is the transverse proper velocity and $\dot{\theta}$ the observed angular velocity; and the angular-diameter distance,

$$d_A \equiv \frac{D}{\theta}, \quad (2.48)$$

where D is the proper size of the object and θ its apparent angular size.

The three measures are related by

$$d_L = (1+z)d_M = (1+z)^2 d_A, \quad (2.49)$$

so any one can be converted to any other for sources of known redshift.

2.3.4 The rate of expansion H_0

Around 1929, Hubble measured the rate of expansion to be $H_0 = 500 \text{ km s}^{-1} \text{ Mpc}^{-1}$, which implied an age of the universe of order $t_0 \sim 2 \text{ Gyr}$, in clear conflict with the Earth age, given by geology³⁰. Hubble's data was based on Cepheid standard candles that were incorrectly calibrated. Fortunately, in the past 15 years there has been significant progress towards an accurated determination of H_0 . These improvements come from the replacement of photographic plates with CCDs (charged couple devices, i.e. solid state detectors with excellent flux sensitivity per pixel), and by the refinement of existing methods for measuring extragalactic distances (e.g. parallax, Cepheids, supernovae, etc.). Finally, with the development of completely new and independent methods to determine H_0 : a) Gravitational lensing; b) Sunyaev-Zel'dovich effect; c) Extragalactic distance scale, mainly Cepheid variability and type Ia Supernovae; d) Microwave background anisotropies. I will review here the first two.

Gravitational lensing

A measurement of the time delay and the angular separation of the different images of a variable quasar can be used to determine H_0 with great accuracy.

Assuming a flat space with $\Omega_M = 0.25$, one can determine³¹

$$H_0 = 72 \pm 7 (1\sigma \text{ statistical}) \pm 15\% (\text{systematic}) \text{ km s}^{-1} \text{ Mpc}^{-1}. \quad (2.50)$$

In the case of lensing by a cluster of galaxies, the dark matter distribution in those systems is usually unknown, associated with a complicated cluster potential. The method is just starting to give promising results and, in the near future, the prospects for measuring H_0 and lowering its uncertainty with this technique are excellent.

Sunyaev-Zel'dovich effect

The gravitational collapse of baryons onto the potential wells generated by dark matter gave rise to the reionization of the plasma, generating an X-ray halo around rich clusters of galaxies. The inverse-Compton scattering of microwave background photons off the hot electrons in the X-ray gas results in a measurable distortion of the blackbody spectrum of the microwave background, known as the Sunyaev-Zel'dovich (SZ) effect. Since photons acquire extra energy from the X-ray electrons, we expect a shift towards higher frequencies of the spectrum, $(\Delta\nu/\nu) \simeq (k_B T_{\text{gas}}/m_e c^2) \sim 10^{-2}$. This corresponds to a *decrement* of the microwave background temperature at low frequencies (Rayleigh-Jeans region) and an increment at high frequencies, see Ref.³². One can determine from this effect the distance to the cluster, and thus the Hubble rate H_0 .

The advantages of this method are that it can be applied to large distances and it is based on clear physical principles. Present measurements give the value³²

$$H_0 = 60 \pm 10 \text{ (1}\sigma \text{ statistical)} \pm 20\% \text{ (systematic)} \text{ km s}^{-1}\text{Mpc}^{-1}, \quad (2.51)$$

compatible with other determinations.

2.3.5 The matter content Ω_M

In 1970s the existence of dark matter began to be taken more seriously. At that time there was evidence that rotation curves of galaxies did not fall off with radius and that the dynamical mass was increasing with scale from that of individual galaxies up to clusters of galaxies. Since then, new possible extra sources to the matter content of the universe have been accumulating:

$$\Omega_M = \Omega_{\text{B, lum}} \quad (\text{stars in galaxies}) \quad (2.52)$$

$$+ \Omega_{\text{B, dark}} \quad (\text{MACHOs?}) \quad (2.53)$$

$$+ \Omega_{\text{CDM}} \quad (\text{weakly interacting : axion, neutralino?}) \quad (2.54)$$

$$+ \Omega_{\text{HDM}} \quad (\text{massive neutrinos?}) \quad (2.55)$$

Many cosmological tests, will constrain some combination of Ω_{M} and Ω_{Λ} . It is hard to constrain Ω_{M} alone. Almost all methods actually constrain some combination of Ω_{M} and the Hubble constant $h = H_0/(100 \text{ km/sec/Mpc})$; the HST Key Project on the extragalactic distance scale finds $h = 0.71 \pm 0.06$, which is consistent with other methods⁷, and what I will assume below.

For years, determinations of Ω_{M} based on dynamics of galaxies and clusters have yielded values between approximately 0.1 and 0.4 — noticeably larger than the density parameter in baryons as inferred from primordial nucleosynthesis, $\Omega_{\text{B}} = (0.019 \pm 0.001)h^{-2} \approx 0.04^{22}$, but noticeably smaller than the critical density. The quantitative results have remained unchanged until now, but our confidence in them has increased greatly.

The matter content of the universe can be deduced from the mass-to-light ratio of various objects in the universe; from the rotation curves of galaxies; from microlensing and the direct search of Massive Compact Halo Objects (MACHOs); from the cluster velocity dispersion with the use of the Virial theorem; from the baryon fraction in the X-ray gas of clusters; from weak gravitational lensing; from the observed matter distribution of the universe via its power spectrum; from the cluster abundance and its evolution; from direct detection of massive neutrinos; from direct detection of Weakly Interacting Massive Particles (WIMPs), and finally from microwave background anisotropies. I will briefly review just a few of them.

Luminous matter

This method of estimating Ω_{M} is performed by measuring the luminosity of stars in galaxies and then estimate the mass-to-light ratio, defined as the mass per luminosity density observed from an object, $\Upsilon = M/L$. This ratio is usually expressed in solar units, M_{\odot}/L_{\odot} , so that for the sun $\Upsilon_{\odot} = 1$. The luminosity of stars depends very sensitively on their mass and stage of evolution. The mass-to-light ratio of stars in the solar neighborhood is of order $\Upsilon \approx 3$. For globular clusters and spiral galaxies we can determine their mass and luminosity independently and this gives $\Upsilon \approx \text{few}$. For our galaxy,

$$L_{\text{gal}} = (1.0 \pm 0.3) \times 10^8 h L_{\odot} \text{Mpc}^{-3} \quad \text{and} \quad \Upsilon_{\text{gal}} = 6 \pm 3. \quad (2.56)$$

All the luminous matter in the universe, from galaxies, clusters of galaxies, etc., account for $\Upsilon \approx 10$, and thus³⁴

$$0.002 \leq \Omega_{\text{lum}} h \leq 0.006. \quad (2.57)$$

As a consequence, the luminous matter alone is far from the critical density. Moreover, comparing with the amount of baryons from Big Bang nucleosynthesis (2.26), we conclude that $\Omega_{\text{lum}} \ll \Omega_{\text{B}}$, so there must be a large fraction of baryons that are dark, perhaps in the form of very dim stars.

Studies applying the virial theorem to cluster dynamics have typically obtained values $\Omega_{\text{M}} = 0.2 \pm 0.1$ ^{55,54}. Although it is possible that the global value of M/L differs appreciably from its value in clusters, extrapolations from small scales do not seem to reach the critical density⁵⁶. New techniques to weigh the clusters, including gravitational lensing of background galaxies and temperature profiles of the X-ray gas, while not yet in perfect agreement with each other, reach essentially similar conclusions.

Rotation curves of spiral galaxies

The flat rotation curves of spiral galaxies provide the most direct evidence for the existence of large amounts of dark matter. Spiral galaxies consist of a central bulge and a very thin disk, stabilized against gravitational collapse by angular momentum conservation, and surrounded by an approximately spherical halo of dark matter. One can measure the orbital velocities of objects orbiting around the disk as a function of radius from the Doppler shifts of their spectral lines. The orbital velocity rose linearly from the center outward until it reached a typical value of 200 km/s, and then remained flat out to the largest measured radii. This was completely unexpected since the observed surface luminosity of the disk falls off exponentially with radius, $I(r) = I_0 \exp(-r/r_D)$, see Ref.³⁵. Therefore, one would expect that most of the galactic mass is concentrated within a few disk lengths r_D , such that the rotation velocity is determined as in a Keplerian orbit, $v_{\text{rot}} = (GM/r)^{1/2} \propto r^{-1/2}$. No such behaviour is observed. The measured rotation curve is shown in Fig. 2.3 together with the relative components associated with the disk, the halo and the gas.

At large radii the dark matter distribution leads to a flat rotation curve. Adding up

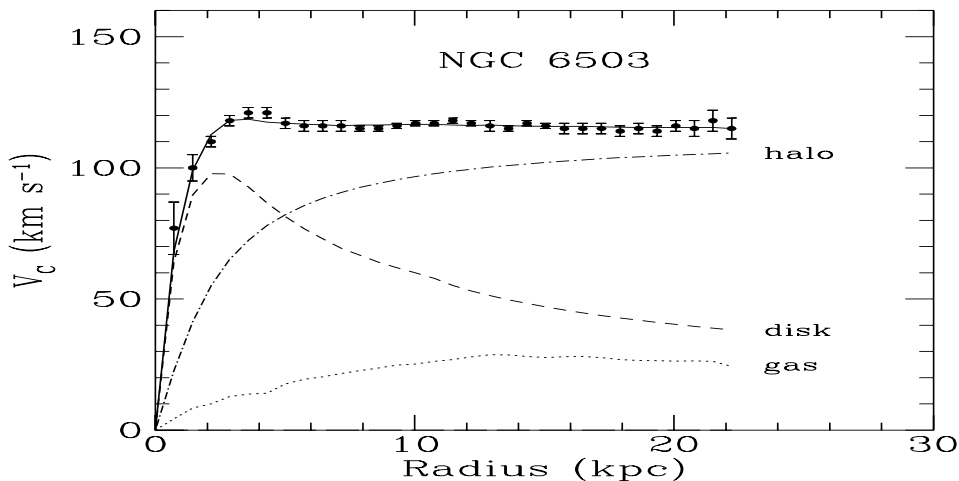


Figure 2.3: The rotation curve of the spiral galaxy NGC 6503, determined by radio observations of hydrogen gas in the disk³⁶. The dashed line shows the rotation curve expected from the disk material alone, the dot-dashed line is from the dark matter halo alone.

all the matter in galactic halos up to maximum radii, one finds $\Upsilon_{\text{halo}} \geq 30 h$, and therefore

$$\Omega_{\text{halo}} \geq 0.03 - 0.05. \quad (2.58)$$

Baryon fraction in clusters

Rather than measuring the mass relative to the luminosity density, which may be different inside and outside clusters, we can also measure it with respect to the baryon density⁵⁷, which is very likely to have the same value in clusters as elsewhere in the universe, simply because there is no way to segregate the baryons from the dark matter on such large scales. Most of the baryonic mass is in the hot intracluster gas⁵⁸. Since the 1960s, when X-ray telescopes became available, it is known that galaxy clusters are the most powerful X-ray sources in the sky³⁷. The emission extends over the whole cluster and reveals the existence of a hot plasma with temperature $T \sim 10^7 - 10^8$ K, where X-rays are produced by electron bremsstrahlung. Assuming the gas to be in hydrostatic equilibrium and applying the virial theorem one can estimate the total mass in the cluster, giving general agreement (within a factor of 2) with the virial mass estimates. From these estimates one can calculate the

baryon fraction of clusters

$$f_B h^{3/2} = 0.03 - 0.08 \quad \Rightarrow \quad \frac{\Omega_B}{\Omega_M} \approx 0.15, \quad \text{for } h = 0.65, \quad (2.59)$$

which together with (2.57) indicates that clusters contain far more baryonic matter in the form of hot gas than in the form of stars in galaxies.

In fact, the fraction f_{gas} of total mass in this form can be measured either by direct observation of X-rays from the gas⁵⁹ or by distortions of the microwave background by scattering off hot electrons (the Sunyaev-Zeldovich effect).

Assuming this fraction to be representative of the entire universe, and using the Big Bang nucleosynthesis value of $\Omega_B = 0.05 \pm 0.01$, for $h = 0.65$, we find

$$\Omega_M = 0.3 \pm 0.1 \text{ (statistical)} \pm 20\% \text{ (systematic)}. \quad (2.60)$$

This value is consistent with previous determinations of Ω_M .

Structure formation and the matter power spectrum

Finally, the matter density parameter can be extracted from measurements of the power spectrum of density fluctuations (see for example⁶⁰). One of the most important constraints on the amount of matter in the universe comes from the present distribution of galaxies. Gravitational instability increases the primordial density contrast, seen at the last scattering surface as temperature anisotropies, into the present density field responsible for the large and the small scale structure.

Since the primordial spectrum is very approximately represented by a scale-invariant *Gaussian random field*, the best way to present the results of structure formation is by working with the 2-point correlation function in Fourier space, the so-called *power spectrum*. If the reprocessed spectrum of inhomogeneities remains Gaussian, the power spectrum is all we need to describe the galaxy distribution. Non-Gaussian effects are expected to arise from the non-linear gravitational collapse of structure, and may be important at small scales²⁵.

The power spectrum measures the degree of inhomogeneity in the mass distribution on different scales. It depends upon a few basic ingredients: a) the primordial spectrum of inhomogeneities, whether they are Gaussian or non-Gaussian, whether *adiabatic* (perturbations in the energy density) or *isocurvature* (perturbations in the entropy density),

whether the primordial spectrum has *tilt* (deviations from scale-invariance), etc.; b) the recent creation of inhomogeneities, whether *cosmic strings* or some other topological defect from an early phase transition are responsible for the formation of structure today; and c) the cosmic evolution of the inhomogeneity, whether the universe has been dominated by cold or hot dark matter or by a cosmological constant since the beginning of structure formation, and also depending on the rate of expansion of the universe.

The tools used for the comparison between the observed power spectrum and the predicted one are very precise N-body numerical simulations and theoretical models that predict the *shape* but not the *amplitude* of the present power spectrum. In simple models (*e.g.*, with only cold dark matter and baryons, no massive neutrinos), the spectrum can be fit (once the amplitude is normalized) by a single “shape parameter”, which is found to be equal to $\Gamma = \Omega_M h$. Observations then yield $\Gamma \sim 0.25$, or $\Omega_M \sim 0.36$. For a more careful comparison between models and observations, see⁶¹.

The observational constraints on the power spectrum have a huge lever arm of measurements at very different scales, mainly from the observed cluster abundance, on 10 Mpc scales, to the CMB fluctuations, on 1000 Mpc scales, which determines the normalization of the spectrum. At present, deep redshift surveys are probing scales between 100 and 1000 Mpc, which should begin to see the turnover corresponding to the peak of the power spectrum at k_{eq} , see Figs. 3.1 and 3.2. The standard CDM model with $\Omega_M = 1$, normalized to the CMB fluctuations on large scales, is inconsistent with the cluster abundance. The power spectra of both a flat model with a cosmological constant or an open universe with $\Omega_M = 0.3$ (defined as Λ CDM and OCDM, respectively) can be normalized so that they agree with both the CMB and cluster observations. So, at present, these measurements suggest a low value of Ω_M , but with large uncertainties.

2.3.6 The cosmological constant Ω_Λ

It has been suspected that a cosmology with an appreciable cosmological constant is the best fit to what we know about the universe^{49,50}. However, it is only very recently that there are new observational arguments for a non-zero value. The most compelling ones are recent evidence that we live in a flat universe, from observations of CMB anisotropies, together with strong indications of a low mass density universe ($\Omega_M < 1$), from the large

scale distribution of galaxies, clusters and voids, that indicate that some kind of dark energy must make up the rest of the energy density up to critical, i.e. $\Omega_\Lambda = 1 - \Omega_M$. In addition, the discrepancy between the ages of globular clusters and the expansion age of the universe may be cleanly resolved with $\Lambda \neq 0$. Finally, there is growing evidence for an accelerating universe from observations of distant supernovae³⁸. I will now discuss the different arguments one by one.

The Expansion Age problem

This negative pressure would help accelerate the universe and reconcile the expansion age of the universe with the ages of stars in globular clusters. For the present age of the universe of $t_0 = 13 \pm 1$ Gyr, and the measured rate of expansion, $H_0 = 70 \pm 7$ km/s/Mpc, one finds $t_0 H_0 = 0.93 \pm 0.12$ (adding errors in quadrature), which corresponds to $\Omega_M = 0.05^{+0.24}_{-0.10}$ for an open universe, marginally consistent with observations of large scale structure. On the other hand, for a flat universe with a cosmological constant, $t_0 H_0 = 0.93 \pm 0.12$ corresponds to $\Omega_M = 0.34^{+0.20}_{-0.12}$, which is perfectly compatible with recent observations. These suggest that we probably live in a flat universe that is accelerating, dominated today by a vacuum energy density.

Supernovae Ia

The most direct and theory-independent way to measure the cosmological constant would be to actually determine the value of the scale factor as a function of time.

Astronomers measure distance in terms of the “distance modulus” $m - M$, where m is the apparent magnitude of the source and M its absolute magnitude. The distance modulus is related to the luminosity distance via

$$m - M = 5 \log_{10}[d_L(\text{Mpc})] + 25 . \quad (2.61)$$

Of course, it is easy to measure the apparent magnitude, but notoriously difficult to infer the absolute magnitude of a distant object. Recently, significant progress has been made by using Type Ia supernovae as “standard candles”. Supernovae are very bright and can therefore be detected at high redshifts ($z \sim 1$).

By studying the characteristic light curves, of a reasonably large statistical sample, cosmologists from two competing groups, the Supernova Cosmology Project³⁹ and the

High-redshift Supernova Project⁴⁰, are confident that they can infer from their distribution the spatial curvature and the rate of expansion of the universe. Fig. (2.4) shows the results for $m - M$ vs. z for the Supernova Cosmology Project. Under the assumption that the energy density of the universe is dominated by matter and vacuum components, these data can be converted into limits on Ω_M and Ω_Λ , as shown in Fig. (2.5).

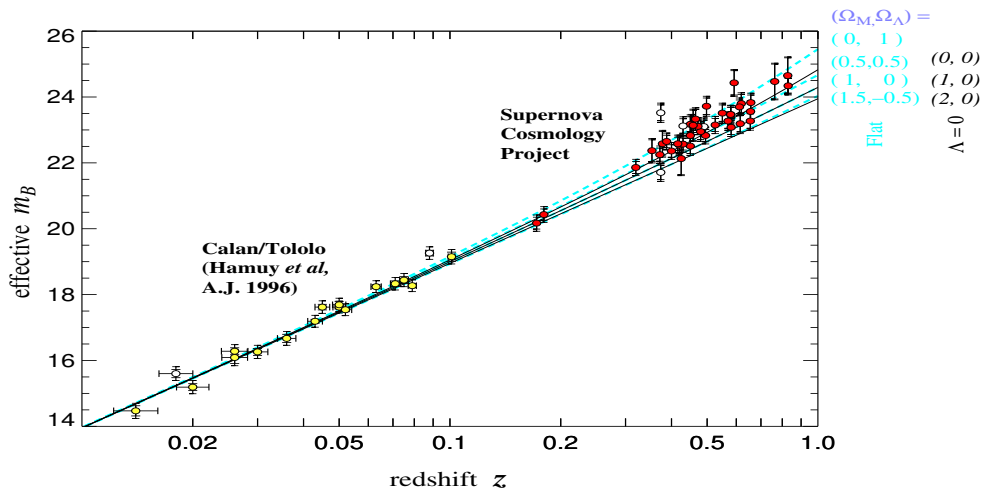


Figura 2.4: Hubble diagram for the high redshift supernovae found by the SN Cosmology Project. From Ref.³⁹. A similar diagram is found by the High Redshift Supernova Project⁴⁰. Both groups conclude that distant supernovae are fainter than expected, and this could be due to an accelerating universe.

In these observations high redshift type Ia supernovae appear fainter than expected for either an open ($\Omega_M < 1$) or a flat ($\Omega_M = 1$) universe, see Fig. 2.4. In fact, the universe appears to be accelerating instead of decelerating (as was expected from the general attraction of matter); something seems to be acting as a repulsive force on very large scales. The most natural explanation for this is the presence of a cosmological constant, a diffuse vacuum energy that permeates all space and, as explained above, gives the universe an acceleration that tends to separate gravitationally bound systems from each other. For a flat universe ($\Omega_M + \Omega_\Lambda = 1$), the best-fit values for the combined analysis of both groups^{39,40}, are

$$\Omega_M^{\text{flat}} = 0.28^{+0.09}_{-0.08} \text{ (1}\sigma \text{ statistical)} \quad ^{+0.05}_{-0.04} \text{ (identified systematics)}, \quad (2.62)$$

$$\Omega_\Lambda^{\text{flat}} = 0.72^{+0.08}_{-0.09} \text{ (1}\sigma \text{ statistical)} \quad ^{+0.04}_{-0.05} \text{ (identified systematics)}. \quad (2.63)$$

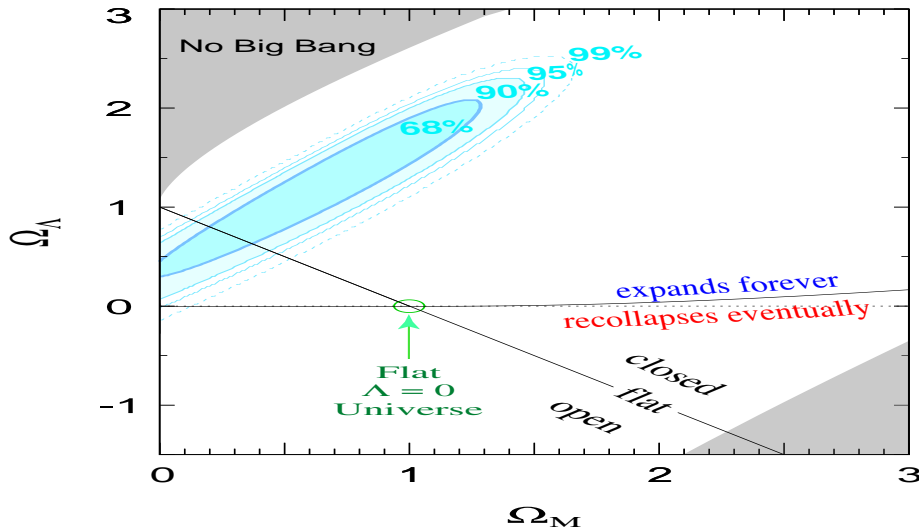


Figure 2.5: The best-fit confidence regions (68% – 99% c.l.) in the $(\Omega_M, \Omega_\Lambda)$ plane, for the high redshift supernovae results. Present observations disfavour the Einstein-de Sitter model (circle) by several standard deviations. From Ref.³⁹.

The confidence intervals in the Ω_M - Ω_Λ plane are consistent for the two groups. Both teams favor a positive cosmological constant, and strongly rule out the traditional $(\Omega_M, \Omega_\Lambda) = (1, 0)$ favorite universe. They are even inconsistent with an open universe with zero cosmological constant.

The Cosmic Microwave Background

The discovery by the COBE satellite of temperature anisotropies in the cosmic microwave background⁵¹ inaugurated a new era in the determination of cosmological parameters. To characterize the temperature fluctuations on the sky, we may decompose them into spherical harmonics,

$$\frac{\Delta T}{T} = \sum_{lm} a_{lm} Y_{lm}(\theta, \phi), \quad (2.64)$$

and express the amount of anisotropy at multipole moment l via the power spectrum,

$$C_l = \langle |a_{lm}|^2 \rangle. \quad (2.65)$$

Higher multipoles correspond to smaller angular separations on the sky, $\theta = 180^\circ/l$. Within any given family of models, C_l vs. l will depend on the parameters specifying the particular cosmology. Although the case is far from closed, evidence has been mounting in favor of a specific class of models — those based on Gaussian, adiabatic, nearly scale-free

perturbations in a universe composed of baryons, radiation, and cold dark matter. (The inflationary universe scenario typically predicts these kinds of perturbations.)

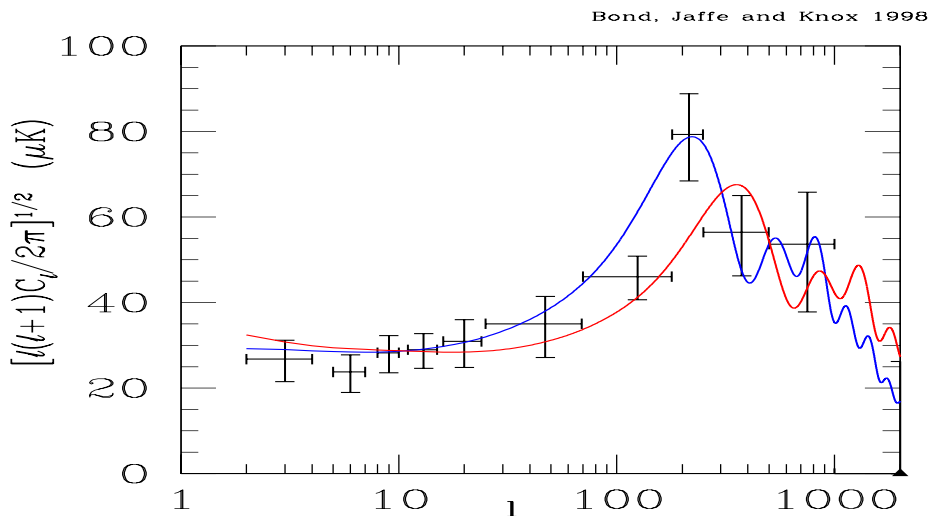


Figure 2.6: CMB data (binned) and two theoretical curves: the model with a peak at $l \sim 200$ is a flat matter-dominated universe, while the one with a peak at $l \sim 400$ is an open matter-dominated universe. From⁵³.

The location in l of the first “Doppler peak”, an increase in power due to acoustic oscillations provides one of the most direct handles on the cosmic energy density, one of the most interesting parameters. The first peak (the one at lowest l) corresponds to the angular scale subtended by the Hubble radius H_{CMB}^{-1} at the time when the CMB was formed (known variously as “decoupling” or “recombination” or “last scattering”). The angular scale at which we observe this peak is tied to the geometry of the universe: in a negatively (positively) curved universe, photon paths diverge (converge), leading to a larger (smaller) apparent angular size as compared to a flat universe. Since the scale H_{CMB}^{-1} is set mostly by microphysics, this geometrical effect is dominant, and we can relate the spatial curvature as characterized by Ω to the observed peak in the CMB spectrum via⁵²

$$l_{\text{peak}} \sim 220\Omega^{-1/2} . \quad (2.66)$$

More details about the spectrum (height of the peak, features of the secondary peaks) will depend on other cosmological quantities, such as the Hubble constant and the baryon density.

Figure 2.6 shows a summary of data as of 1998, with various experimental results

consolidated into bins, along with two theoretical models. It is clear from the figure that there is good evidence for a peak at approximately $l_{\text{peak}} \sim 200$, as predicted in a spatially-flat universe.

The CMB data provide constraints which are complementary to those obtained using supernovae; For example, the Boomerang⁴¹ and the supernovae approaches yield confidence contours which are nearly orthogonal in the Ω_M - Ω_Λ plane. The region of overlap is in the vicinity of $(\Omega_M, \Omega_\Lambda) = (0.3, 0.7)$, which is consistent with other determinations.

2.3.7 The spatial curvature Ω_K

As we said, observations of the two-point correlation function of temperature anisotropies in the CMB provide a crucial test for the spatial curvature of the universe. Even before the new WMAP data, observations made by the balloon experiment BOOMERANG suggested that the universe is indeed spatially flat ($\Omega_K = 0$) with about 10% accuracy⁴¹,

$$\Omega_0 = \Omega_M + \Omega_\Lambda = 1.0 \pm 0.1 \quad (95\% \text{ c.l.}) \quad (2.67)$$

Furthermore, with the launch in 2007 of Planck satellite⁴² we will be able to determine Ω_0 with 1% accuracy.

A FORMAÇÃO DE ESTRUTURAS EM GRANDE ESCALA

3.1 A Small Introduction to The Large Structure Formation

3.1.1 Clusters and Superclusters of Galaxies

Stars have mass in the range roughly 1 to $10M_{\odot}$. They are found only in *galaxies* may be regarded as the basic building blocks of the universe, with masses ranging from maybe $10^6 M_{\odot}$ (dwarf galaxies) to $10^{12} M_{\odot}$ (large galaxies like our own). A galaxy typically has a luminous centre containing nearly all of the stars, and a dark halo of unknown composition which extends of order 10 times as far and contains of order 10 times as much mass.

Large galaxies like our own have a size of around .1 Mpc (including the dark halo) and are of order 1 Mpc apart. Many galaxies belong to gravitationally bound clusters containing from two to ~ 1000 galaxies. Clusters of order 10 Mpc in size, are the biggest gravitationally bound objects in the universe. There do exist, though, ‘superclusters’ with size of order 100 Mpc. Presumably they will become gravitationally bound at some time in the future. On the scale of 100 Mpc there also seem to be sheetlike and filamentary structures, as well as voids containing hardly any galaxies.

On scales bigger than 100 Mpc the distribution of matter in the universe is known to be very homogeneous, both from direct observation of the galaxies and from the isotropy

of the microwave background. To be precise, if one throws down at random a sphere with radius R and measures its mass M , then the *rms* variation $\Delta M/M$ is a decreasing function of R , which is of order 1 at $R = 10$ Mpc and of order .1 at $R = 100$ Mpc

The biggest distance we can observe is of order 10^4 Mpc, the distance that light has travelled since the Big Bang. The sphere around us with this radius is thus the *observable universe*. From the fact that the microwave background anisotropy $\Delta T/T$ is of order 10^{-5} , one can deduce that $\Delta M/M \lesssim 10^{-5}$ on scales R comparable with the size of the observable universe.

From observation of the distant universe, the most important finding is that the universe is definitely evolving. The most dramatic case is that of quasars (active galactic nuclei), whose abundance per comoving volume peaks at $z \sim 3$ or so. Neither quasars nor any other objects are observed at $z \gtrsim 5$. Ordinary galaxies as well as clusters are observed out to a redshift of order 1 to 2, and they too show signs of evolution.

Ideally, high redshift observations plus an understanding of galactic evolution would give us information on the value of Ω_0 .

3.1.2 Baryonic Matter

The ordinary matter *ie* nuclei and electrons, in the context of cosmology, is usually called *baryonic matter* since the baryons (nuclei) vastly outweigh the electrons. From the nucleosynthesis calculation we know that the baryon contribution to Ω_0 is given by Eq.2.26. Thus if $\Omega_0 = 1$ there exists *non-baryonic dark matter*, whose nature I discuss later.

The luminous matter in the universe, consisting of stars and radiation-emitting gas, accounts for only $\Omega_B \sim .01$. So there is a lot of *baryonic dark matter* (that constitutes a few percent of the total amount of dark matter, as we saw before).

In a galaxy, one might expect the baryons to be concentrated more in the central, luminous part than in the dark halo. The reason is that baryons (the ordinary and luminous matter in the universe, consisting of stars and radiation-emitting gas) can emit radiation whereas non-baryonic dark matter interacts too weakly to do so (or it would not be dark). In consequence baryons can lose more energy, allowing them to settle more deeply into the galaxy centre.

3.1.3 Non-Baryonic Dark Matter

One can try to estimate the total amount of matter through its gravitational effect. The gravitational field in a bound system such as a galaxy or galaxy cluster can be deduced from the velocities of its components, as evidenced by the Doppler effect. One finds that each galaxy is surrounded by a dark halo accounting for most of its mass.

On larger scales, where the universe is almost homogeneous and isotropic, one can observe the small departure from uniform expansion. This defines a ‘peculiar velocity’ field, which is usually called the *bulk flow*. If one knew the bulk flow \mathbf{v} and the density perturbation $\delta\rho/\rho$, one could deduce Ω_0 through the relation (see ref.⁴⁶)

$$\frac{\nabla \cdot \mathbf{v}}{3H_0} = -\frac{1}{3}(\Omega_0)^6 \frac{\delta\rho}{\rho} \quad (3.1)$$

A recent study using this method⁷⁰ indicates that $\Omega_0 > .1$. From nucleosynthesis, baryonic matter contributes $\Omega_0 \simeq .01$ to $.09$. The observed total Ω_0 favoured value, from CMB, is $\Omega_0 = 1$. This means that *non-baryonic dark matter seems to be needed*.

3.1.4 Hot, Cold and Warm Dark Matter

A massive neutrino species could be a dark matter candidate. A firmer reason for wanting some neutrino species to have mass comes from the solar neutrino problem. Neutrino dark matter is called hot, because it remains relativistic until the epoch when most cosmological scales of interest have entered the horizon (come into causal contact), and therefore cannot initially undergo gravitational collapse.

Cold dark matter (CDM) is by definition non-relativistic when all cosmological interesting scales enter the horizon. Warm dark matter by definition remains relativistic until a cosmologically interesting epoch, which is however significantly earlier than the epoch for neutrino dark matter.

The dark matter candidates are known collectively as WIMPS (weakly interacting massive particles).

3.1.5 Large-scale structure formation

Although the CMB indicates that the universe in the *past* was extraordinarily homogeneous, we know that the universe *today* is not exactly homogeneous: we observe galaxies,

clusters and superclusters on large scales. These structures are expected to arise from very small primordial inhomogeneities that grow in time via gravitational instability, and that may have originated from tiny ripples in the metric, as matter fell into their troughs. Those ripples must have left some trace as temperature anisotropies in the CMB, and indeed such anisotropies were finally discovered by the COBE satellite in 1992, and they appear as perturbations in temperature of only one part in 10^5 .

If we define the density contrast as²⁵

$$\delta(\vec{x}, a) \equiv \frac{\rho(\vec{x}, a) - \bar{\rho}(a)}{\bar{\rho}(a)} = \int d^3\vec{k} \delta_k(a) e^{i\vec{k}\cdot\vec{x}}, \quad (3.2)$$

where $\bar{\rho}(a) = \rho_0 a^{-3}$ is the average cosmic density, we need a theory that will grow a density contrast with amplitude $\delta \sim 10^{-5}$ at the last scattering surface ($z = 1100$) up to density contrasts of the order of $\delta \sim 10^2$ for galaxies at redshifts $z \ll 1$, i.e. today. This is a *necessary* requirement for any consistent theory of structure formation²⁶.

Furthermore, the anisotropies observed by the COBE satellite correspond to a small-amplitude scale-invariant primordial power spectrum of inhomogeneities

$$P(k) = \langle |\delta_k|^2 \rangle \propto k^n, \quad \text{with } n = 1, \quad (3.3)$$

where the brackets $\langle \cdot \rangle$ represent integration over an ensemble of different universe realizations. These inhomogeneities are like waves in the space-time metric. When matter fell in the troughs of those waves, it created density perturbations that collapsed gravitationally to form galaxies and clusters of galaxies, with a spectrum that is also scale invariant. Such a type of spectrum was proposed in the early 1970s by Edward R. Harrison, and independently by the Russian cosmologist Yakov B. Zel'dovich, see Ref.²⁷, to explain the distribution of galaxies and clusters of galaxies on very large scales in our observable universe.

Most galaxies formed at redshifts of the order of 2 – 6; clusters of galaxies formed at redshifts of order 1, and superclusters are forming now. That is, cosmic structure formed from the bottom up: from galaxies to clusters to superclusters, and not the other way around. This fundamental difference is an indication of the type of matter that gave rise to structure. The observed power spectrum of the galaxy matter distribution from a selection of deep redshift catalogs can be seen in Fig. 3.1.

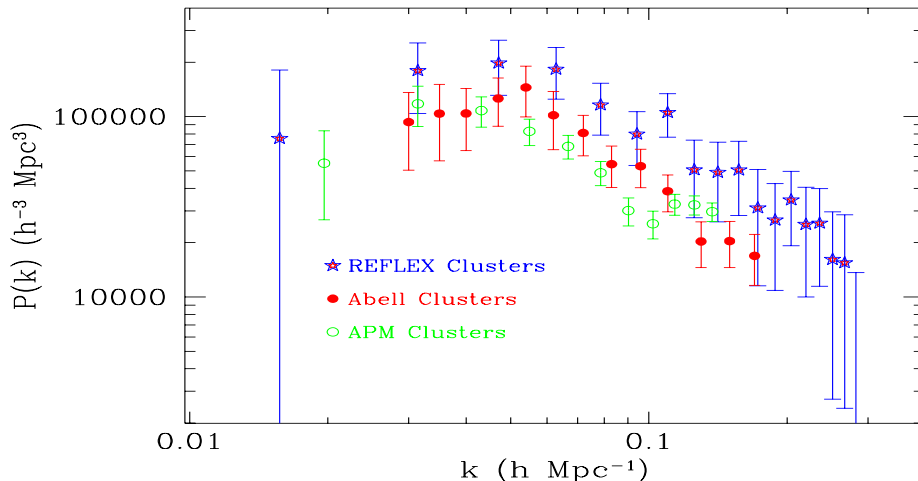


Figura 3.1: The matter power spectrum for clusters of galaxies, from three different cluster surveys.

We saw that there must be some extra matter beyond the baryonic one (dark since we don't see it) to account for its gravitational pull. Whether it is relativistic (hot) or non-relativistic (cold) could be inferred from observations: relativistic particles tend to diffuse from one concentration of matter to another, thus transferring energy among them and preventing the growth of structure on small scales. This is excluded by observations, so we conclude that most of the matter responsible for structure formation must be cold (CDM).

Nowadays, the standard theory of structure formation is a cold dark matter model with a non vanishing cosmological constant in a spatially flat universe. Gravitational collapse amplifies the density contrast initially through linear growth and later on via non-linear collapse. In the process, overdense regions decouple from the Hubble expansion to become bound systems, which start attracting each other to form larger bound structures. In fact, the largest structures, superclusters, have not yet gone non-linear.

The primordial spectrum (3.3) is reprocessed by gravitational instability after the universe becomes matter dominated and inhomogeneities can grow. Linear perturbation

theory shows that the growing mode ¹ of small density contrasts go like^{25,26}

$$\delta(a) \propto a^{1+3\omega} = \begin{cases} a^2, & a < a_{\text{eq}} \\ a, & a > a_{\text{eq}} \end{cases} \quad (3.4)$$

in the Einstein-de Sitter limit ($\omega = p/\rho = 1/3$ and 0, for radiation and matter, respectively). Since the density contrast at last scattering is of order $\delta \sim 10^{-5}$, and the scale factor has grown since then only a factor $z_{\text{dec}} \sim 10^3$, one would expect a density contrast today of order $\delta_0 \sim 10^{-2}$. Instead, we observe structures like galaxies, where $\delta \sim 10^2$. So how can this be possible? The CMB shows anisotropies due to fluctuations in the baryonic matter component only (to which photons couple, electromagnetically). If there is an additional matter component that only couples through very weak interactions, fluctuations in that component could grow as soon as it decoupled from the plasma, well before photons decoupled from baryons. The reason why baryonic inhomogeneities cannot grow is because of photon pressure: as baryons collapse towards denser regions, radiation pressure eventually halts the contraction and sets up acoustic oscillations in the plasma that prevent the growth of perturbations, until photon decoupling. On the other hand, a weakly interacting cold dark matter component could start gravitational collapse much earlier, even before matter-radiation equality, and thus reach the density contrast amplitudes observed today. The resolution of this mismatch is one of the strongest arguments for the existence of a weakly interacting cold dark matter component of the universe.

How much dark matter there is in the universe can be deduced from the actual power spectrum (the Fourier transform of the two-point correlation function of density perturbations) of the observed large scale structure. One can decompose the density contrast in Fourier components, see Eq. (3.2). This is very convenient since in linear perturbation theory individual Fourier components evolve independently. The processed power spectrum $P(k)$ will have the form:

$$P(k) \propto \begin{cases} k, & k \ll k_{\text{eq}} \\ k^{-3}, & k \gg k_{\text{eq}} \end{cases} \quad (3.5)$$

This is precisely the shape that large-scale galaxy catalogs are bound to test in the near future, see Fig. 3.2.

¹The decaying modes go like $\delta(t) \sim t^{-1}$, for all ω .

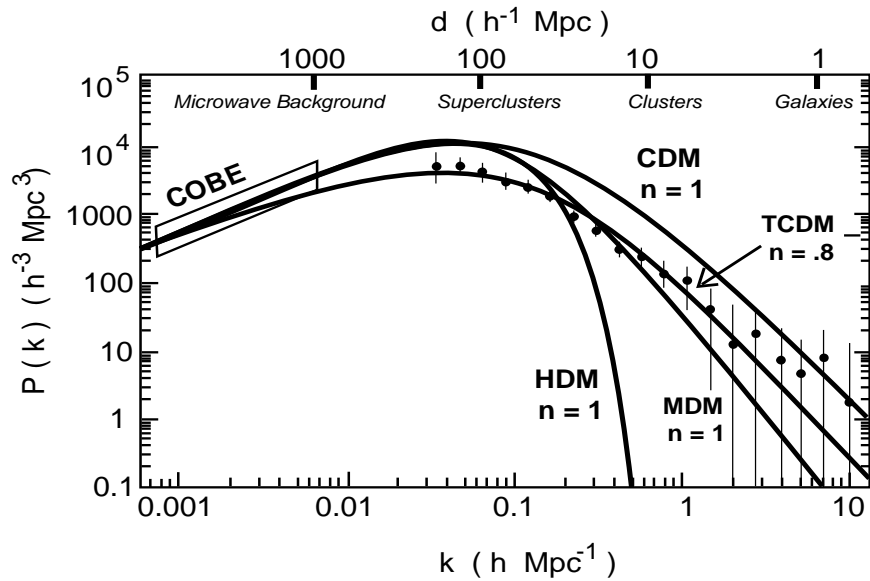


Figure 3.2: The power spectrum for cold dark matter (CDM), tilted cold dark matter (TCDM), hot dark matter (HDM), and mixed hot plus cold dark matter (MDM), normalized to COBE, for large-scale structure formation. From Ref.²⁹.

Since relativistic Hot Dark Matter (HDM) transfer energy between clumps of matter, they will wipe out small scale perturbations, and this should be seen as a distinctive signature in the matter power spectra of future galaxy catalogs. On the other hand, non-relativistic Cold Dark Matter (CDM) allow structure to form on *all* scales via gravitational collapse. The dark matter will then pull in the baryons, which will later shine and thus allow us to see the galaxies.

Naturally, when baryons start to collapse onto dark matter potential wells, they will convert a large fraction of their potential energy into kinetic energy of protons and electrons, ionizing the medium. As a consequence, we expect to see a large fraction of those baryons constituting a hot ionized gas surrounding large clusters of galaxies. This is indeed what is observed, and confirms the general picture of structure formation.

3.2 The Inflationary Paradigm

3.2.1 Cosmological Inflation

In the 1980s, a new paradigm was put forward by Alan Guth, Linde and others. According to the inflationary paradigm, the early universe went through a period of exponential expansion, driven by the approximately constant energy density of a scalar field called the inflaton, which acts like a repulsive force that makes any two points in space separate at exponentially large speeds (This does not violate the laws of causality because there is no information carried along in the expansion, it is simply the stretching of space-time).

Without inflation a given patch either collapses ($\Omega \rightarrow \infty$) or becomes practically empty ($\Omega \rightarrow 0$) within a Hubble time, unless its density parameter is very finely tuned to the value $\Omega = 1$. In contrast, inflation drives Ω towards 1 starting with an arbitrary initial value.

This superluminal expansion is capable of explaining the large scale homogeneity of our observable universe and, in particular, why the microwave background looks so isotropic: regions separated today by more than 1° in the sky were, in fact, in causal contact before inflation, but were stretched to cosmological distances by the expansion. Any inhomogeneities present before the tremendous expansion would be washed out. This explains why photons from supposedly causally disconnected regions have actually the same spectral distribution with the same temperature.

Inflation is an extremely elegant hypothesis that explains how a region much, much greater than our own observable universe could have become smooth and flat without recourse to *ad hoc* initial conditions. Furthermore, inflation dilutes away any “unwanted” relic species that could have remained from early universe phase transitions, like monopoles, cosmic strings, etc., which are predicted in grand unified theories and whose energy density could be so large that the universe would have become unstable, and collapsed, long ago.

3.2.2 The origin of density perturbations

If cosmological inflation made the universe so extremely flat and homogeneous, where did the galaxies and clusters of galaxies come from? The answer is that the quantum

fluctuation of the inflaton field, on a given comoving scale, generates a well defined inhomogeneity and anisotropy, which can be regarded as classical once the scale leaves the horizon, and can explain the perturbation the inhomogeneity and anisotropy of the observable universe¹⁹.

The quantum fluctuations of the inflaton field are stretched by the exponential expansion and generate large-scale perturbations in the metric. In the case of inflation, the inflaton fluctuations induce waves in the space-time metric that can be decomposed into different wavelengths, all with approximately the same amplitude, that is, corresponding to a **scale-invariant spectrum**.

When matter fell in the troughs of these waves, it created density perturbations that collapsed gravitationally to form galaxies, clusters and superclusters of galaxies, with a spectrum that is also scale invariant. Such a type of spectrum was proposed in the early 1970s (before inflation) by Harrison and Zel'dovich²⁷, to explain the distribution of galaxies and clusters of galaxies on very large scales in our observable universe. One should also expect to see such ripples in the metric as temperature anisotropies in the cosmic microwave background.

3.2.3 Acoustic oscillations in the plasma

The physics of the CMB anisotropies is relatively simple. The universe just before recombination is a very tightly coupled fluid, due to the large electromagnetic Thomson cross section. Photons scatter off charged particles (protons and electrons), and carry energy, so they feel the gravitational potential associated with the perturbations imprinted in the metric during inflation. An overdensity of baryons (protons and neutrons) does not collapse under the effect of gravity until it enters the causal Hubble radius. The perturbation continues to grow until radiation pressure opposes gravity and sets up acoustic oscillations in the plasma, very similar to sound waves. Since photons scatter off these baryons, the acoustic oscillations occur also in the photon field and induces a pattern of peaks in the temperature anisotropies in the sky, at different angular scales.

Metric perturbations of different wavelengths enter the horizon at different times. The largest wavelengths, of size comparable to our present horizon, are entering now. There are perturbations with wavelengths comparable to the size of the horizon at the time of

last scattering, of projected size about 1° in the sky today, which entered precisely at decoupling. And there are perturbations with wavelengths much smaller than the size of the horizon at last scattering, that entered much earlier than decoupling, all the way to the time of radiation-matter equality, which have gone through several acoustic oscillations before last scattering. All these perturbations of different wavelengths leave their imprint in the CMB anisotropies.

Since photons scatter off baryons, they will also feel the acoustic wave and create a peak in the correlation function. The height of the peak is proportional to the amount of baryons: the larger the baryon content of the universe, the higher the peak. The position of the peak in the power spectrum depends on the geometrical size of the particle horizon at last scattering (whether the universe is flat, open or closed).

Since the amplitude and position of the primary and secondary peaks are directly determined by the sound speed (and, hence, the equation of state) and by the geometry and expansion of the universe, they can be used as a powerful test of the density of baryons and dark matter, and other cosmological parameters.

The large amount of information encoded in the anisotropies of the microwave background is the reason why both NASA and the European Space Agency have decided to launch two independent satellites to measure the CMB temperature and polarization anisotropies to unprecedented accuracy. The Microwave Anisotropy Probe (WMAP) and Planck⁴² (expected in 2007).

3.3 The Evolution of the Density Perturbation

Cosmological perturbation theory develops linear equations for perturbations away from homogeneity and isotropy. Using it one can follow their growth on a given scale, until they become big enough for gravitational collapse. On scales $\gtrsim 100$ Mpc, where collapse has yet to occur, cosmological perturbation theory can be used right up to the present epoch. On smaller scales the only sure-fire way of performing calculations after perturbation theory fails is to perform numerical simulations, though analytic approximations can provide some insight.

In the Newtonian regime cosmological perturbation theory has long been recognised to

be a straightforward application of fluid flow equations. In the relativistic regime, cosmological perturbations was first discussed by Lifshitz in 1946. His formalism considers the perturbed Robertson-Walker metric. An alternative formalism, which makes no mention of the metric perturbation and works instead with relativistic fluid flow equations, was initiated by Hawking⁷¹ in 1966. This approach, which treats the Newtonian and relativistic regimes in a unified way, is becoming increasingly popular⁷²⁻⁷⁴ and is the one that I will use here.

3.3.1 Relativistic fluid flow

We populate the universe with comoving observers, who define physical quantities in their own region. By definition, the momentum density is zero with respect to a comoving observer.

A crucial concept is the *velocity gradient* u_{ij} :

$$u_{ij} \equiv \partial_j u^i \quad (3.6)$$

In the limit of homogeneity and isotropy,

$$u_{ij} = H\delta_{ij}; \quad (3.7)$$

Just as for a homogeneous isotropic universe, it is useful to consider ‘comoving hypersurfaces’, defined as those orthogonal to the fluid flow worldlines. On a given hypersurface, each quantity ρ , p and H can be split into an average plus a perturbation,

$$\rho(\mathbf{x}, t) = \bar{\rho}(t) + \delta\rho(\mathbf{x}, t) \quad (3.8)$$

$$p(\mathbf{x}, t) = \bar{p}(t) + \delta p(\mathbf{x}, t) \quad (3.9)$$

$$H(\mathbf{x}, t) = \bar{H}(t) + \delta H(\mathbf{x}, t) \quad (3.10)$$

Here t is the time coordinate labelling the hypersurfaces, and $\mathbf{x} = (\mathbf{x}^1, \mathbf{x}^2, \mathbf{x}^3)$ are space coordinates. We would like to choose the space coordinates to be comoving coordinates, related to Cartesian coordinates by $r^i = ax^i$, with a the average scale factor given by $\dot{a}/a = \bar{H}$. We consider, as a first order approximation, that all perturbations ‘live’ in flat space.

Independent scales

Each perturbation f can be written as a Fourier series, defined in a comoving box much bigger than the observable universe

$$f(\mathbf{x}, t) = \sum_{\mathbf{k}} f_{\mathbf{k}}(t) e^{i\mathbf{k}\cdot\mathbf{x}} \quad (3.11)$$

The beauty of this expansion is that each Fourier mode propagates independently. The inverse wavenumber a/k is said to define a scale, which is specified by giving its present value k^{-1} .

Now consider a small density enhancement in the early universe, which is destined to become, say, a galaxy. If its size is of order $r = xa$, it is typically made out of Fourier components with $k \sim x^{-1}$. As long as it corresponds to a small density contrast, $\delta\rho/\rho \ll 1$, it will expand with the universe so that its comoving size x remains constant. When its density contrast becomes of order 1 it will collapse and then its *physical* size will remain more or less constant. In both cases, though, the *mass* of the enhancement remains fixed. It is therefore useful to associate with each scale k the mass of matter enclosed within a sphere of comoving radius $x = k^{-1}$ (taking the universe to be practically homogeneous, corresponding to the early universe). This mass is

$$M(x) = 1.16 \times 10^{12} h^2 (x/1 \text{ Mpc})^3 M_{\odot}. \quad (3.12)$$

Horizon entry

The ratio of a given comoving scale a/k to the Hubble distance H^{-1} is equal to $aH/k = \dot{a}/k$, which decreases with time. At the epoch when this ratio falls through 1, the scale is said to *enter the horizon*.

Well after horizon entry, the scale is small compared with the Hubble distance, which means that ordinary physical effects like diffusion, free-streaming and the propagation of sound waves can operate, with the expansion of the universe playing only a minor role. Well before horizon entry, the scale is much bigger than the Hubble distance, which means that causal processes of this kind cannot operate. Instead, as we shall see, each part of the universe evolves independently.

The scale entering the horizon at a given epoch is given by

$$k^{-1} = (aH)^{-1} = \frac{a_0 H_0}{aH} H_0^{-1} \quad (3.13)$$

Except around matter-radiation equality at $z \sim 10^4$ one has

$$aH \propto a^{-1} \quad \text{radiation domination} \quad (3.14)$$

$$aH \propto a^{-1/2} \quad \text{matter domination} \quad (3.15)$$

Thus a crude estimate is that the scale entering the horizon at $z \lesssim 10^4$ is $k^{-1} \sim z^{-1/2} H_0^{-1}$, making the scale entering the horizon at matter-radiation equality $k_{\text{eq}}^{-1} \sim 10^{-2} H_0^{-1}$, and that the scale entering the horizon at $z \gtrsim 10^4$ is $k^{-1}(z) \sim 10^2 z^{-1} H_0^{-1}$. An accurate calculation shows that $k_{\text{eq}}^{-1} = 40h^{-1} \text{Mpc}$, and that the scale entering the horizon at photon decoupling is $k_{\text{dec}}^{-1} = 90h^{-1} \text{Mpc}$. The first scale is crucial for structure formation, and the second for the cmb anisotropy.

The Differential Equation

Now I derive differential equations for the perturbations. In doing so one has to remember that the comoving worldlines are not in general geodesics, because of the pressure gradient. As a result, the proper time interval $d\tau$ between a pair of comoving hypersurfaces is position dependent. Its average may be identified with the coordinate time interval dt , and one can show (using essentially the Lorentz transformation between nearby observers) that its variation with position is given by^{73,19}

$$\frac{d\tau}{dt} = \left(1 - \frac{\delta p}{\rho + p} \right) \quad (3.16)$$

Along each worldline the rate of change of ρ with respect to proper time τ is given by energy conservation and has the same form as in the unperturbed case,

$$\frac{d\rho}{d\tau} = -3H(\rho + p) \quad (3.17)$$

The rate of change of H is given by the Einstein field equation, and to first order receives just one extra term in the presence of perturbations, coming from the pressure gradient⁷³,

$$\frac{dH}{d\tau} = -H^2 - \frac{4\pi G}{3}(\rho + 3p) - \frac{1}{3} \frac{\nabla^2 \delta p}{\rho + p} \quad (3.18)$$

This equation is called the *Raychaudhuri equation*. The operator ∇^2 is the Laplacian on a comoving hypersurface, given in terms of comoving coordinates by

$$\nabla^2 = a^{-2} \delta^{ij} \frac{\partial}{\partial x^i} \frac{\partial}{\partial x^j} \quad (3.19)$$

Perturbing H , ρ and p to first order and using Eq. (3.16) gives the following equations for the Fourier components

$$(\delta\rho_{\mathbf{k}})' = -3(\rho + p)\delta H_{\mathbf{k}} - 3H\delta\rho_{\mathbf{k}} \quad (3.20)$$

$$(\delta H_{\mathbf{k}})' = -2H\delta H_{\mathbf{k}} - \frac{4\pi G}{3}\delta\rho_{\mathbf{k}} + \frac{1}{3}\left(\frac{k}{a}\right)^2 \frac{\delta p_{\mathbf{k}}}{\rho + p} \quad (3.21)$$

Eliminating $\delta H_{\mathbf{k}}$ with Eq. (3.20) gives a second order differential equation for $\rho_{\mathbf{k}}$. It is convenient to use the *density contrast* $\delta \equiv \frac{\delta\rho}{\rho}$, and the notation $w = p/\rho$ and $c_s^2 = \dot{p}/\dot{\rho}$, in terms of which the equation is (see Ref.¹⁹):

$$H^{-2}\delta_{\mathbf{k}}'' + [2 - 3(2w - c_s^2)]H^{-1}\delta_{\mathbf{k}}' - \frac{3}{2}(1 - 6c_s^2 + 8w - 3w^2)\delta_{\mathbf{k}} = -\left(\frac{k}{aH}\right)^2 \frac{\delta p_{\mathbf{k}}}{\rho} \quad (3.22)$$

Note that $c_s^2 = \dot{p}/\dot{\rho}$ is the speed of sound, because p and ρ vary adiabatically in a homogeneous isotropic universe (no heat flow).

Baryon Evolution: The Jeans Mass

Unlike the CDM density contrast, the baryon density contrast is small at the photon decoupling epoch because it has been decaying since horizon entry. After decoupling, the baryons are unaffected by the photons, but two competing forces act on them. First there is gravity, which tends to make them fall into the potential wells caused by the CDM density contrast, and second there is their own pressure gradient which tends to keep them out of the wells.

To rigorously see which effect wins one should generalize Eq. (3.22) to treat the CDM and the baryons as a pair of uncoupled fluids^{73,74}. In practice the following order of magnitude estimate is enough. Ignoring the pressure, the time taken for the baryons to fall into a well is² of order $(G\rho)^{-1/2}$. The time taken for the pressure to adjust itself to prevent the collapse is of order λ/c_s where $\lambda = 2\pi/k$ is the wavelength and c_s is the speed of sound. Collapse occurs if $\lambda/c_s \lesssim (G\rho)^{-1/2}$ because the pressure cannot act quickly enough. One concludes that collapse occurs on scales in excess of $k_J = (4\pi^2 G\rho/c_s^2)^{1/2}$. This is called the *Jeans scale* and the corresponding mass, given by Eq. (3.12), is called the *Jeans mass*.

²If a particle falls from rest towards a point mass M , its velocity at distance r is given by $mv^2 = 2GM/r$ so it falls a significant distance in a time $t \sim r/v \sim (GM/r^3)^{-1/2}$. We are replacing the point mass by a perturbation with size r and density $\rho \sim M/r^3$.

The case of zero pressure gradient

The right hand side of Eq. (3.22), which involves the pressure gradient, is negligible after matter domination because the pressure is negligible.³ It is also negligible well before horizon entry even during radiation domination, because the gradient is so small.⁴ When it is negligible, Eq. (3.22) can be reduced to a first order equation, which has a very simple interpretation⁷²

The solution hinge on the introduction of a quantity K , defined locally through the Friedmann equation. General relativity shows that K/a^2 is a measure of the curvature of the comoving hypersurfaces. When the pressure gradient is negligible K is time independent. We can say that *when the pressure gradient is negligible, each region of space evolves like a separate Friedmann universe.*

On a comoving hypersurface K can be split into an average \bar{K} plus a perturbation δK , but the average can be set equal to zero because $\Omega \simeq 1$. Perturbing the Friedmann equation therefore gives, to first order,

$$2H\delta H_{\mathbf{k}} = \frac{8\pi G}{3}\delta\rho_{\mathbf{k}} - \frac{\delta K_{\mathbf{k}}}{a^2} \quad (3.23)$$

When $\delta K_{\mathbf{k}}$ is time independent, Eqs. (3.20) and (3.23) give a *first* order differential equation for the density contrast,

$$\frac{2H^{-1}}{5+3w} \frac{d}{dt} \left[\left(\frac{aH}{k} \right)^2 \delta_{\mathbf{k}} \right] + \left(\frac{aH}{k} \right)^2 \delta_{\mathbf{k}} = \frac{2+2w}{5+3w} R_{\mathbf{k}} \quad (3.24)$$

where $w = p/\rho$ and I have introduced the useful quantity

$$R_{\mathbf{k}} = \frac{3}{2} \frac{\delta K_{\mathbf{k}}}{k^2} \quad (3.25)$$

Remembering that $\delta K/a^2$ is the curvature perturbation and that it has units of $(\text{length})^{-2}$, we see that $R_{\mathbf{k}} = (3/2)(\delta K/a^2)(a^2/k^2)$ essentially measures the curvature perturbation in units of the relevant scale a/k . Another interpretation of R is that it is essentially the Newtonian gravitational potential caused by $\delta\rho$.

³Except for the baryons on scales below the Jeans scale, and we assume that the dark matter is cold, otherwise it is modified by free-streaming.

⁴Provided that p/ρ is not extremely large, which is ensured by the adiabatic initial condition defined shortly.

During any era when w is constant, Eq. (3.24) has the solution (dropping a decaying mode)

$$\left(\frac{aH}{k}\right)^2 \delta_{\mathbf{k}} = \frac{2+2w}{5+3w} R_{\mathbf{k}} \quad (3.26)$$

In the radiation dominated era before horizon entry this becomes

$$\left(\frac{aH}{k}\right)^2 \delta_{\mathbf{k}} = \frac{4}{9} R_{\mathbf{k}}(\text{initial}) \quad (3.27)$$

and in the matter dominated era it becomes

$$\left(\frac{aH}{k}\right)^2 \delta_{\mathbf{k}} = \frac{2}{5} R_{\mathbf{k}}(\text{final}) \quad (3.28)$$

As the labels imply I am regarding the value of $R_{\mathbf{k}}$ during the first era as an ‘initial condition’, which determines its value during the ‘final’ matter dominated era.

For future reference note that during matter domination, $H \propto t^{-1} \propto a^{-3/2}$ and

$$\delta_{\mathbf{k}} \propto a \quad (\text{matter domination}) \quad (3.29)$$

The Cosmological Constant Role On Structure Formation

The introduction of a cosmological constant changes the relationship between the matter density and expansion rate in a matter-dominated universe, which in turn influences the growth of large-scale structure.

Perturbations start out very small (of order 10^{-5} at recombination, from CMB anisotropies), so linear theory is effective. The fate of the fluctuations is in the hands of two competing effects: the tendency of self-gravity to make overdense regions collapse, and the tendency of test particles in the background expansion to move apart. Essentially, the effect of vacuum energy is to contribute to expansion, thereby acting to suppress the growth of perturbations^{46,25}.

For sub-Hubble-radius perturbations in a cold dark matter component, a Newtonian analysis suffices. If the energy density in dynamical matter is dominated by CDM, the linearized Newtonian evolution equation is

$$\ddot{\delta}_{\mathbf{M}} + 2\frac{\dot{a}}{a}\dot{\delta}_{\mathbf{M}} = 4\pi G\rho_{\mathbf{M}}\delta_{\mathbf{M}}. \quad (3.30)$$

The second term represents an effective frictional force due to the expansion of the universe, characterized by a timescale $(\dot{a}/a)^{-1} = H^{-1}$, while the right hand side is a forcing

term with characteristic timescale $(4\pi G\rho_M)^{-1/2} \approx \Omega_M^{-1/2}H^{-1}$. Thus, when $\Omega_M \approx 1$, these effects are in balance and CDM perturbations gradually grow; when Ω_M dips appreciably below unity (as when curvature or vacuum energy begin to dominate), the friction term becomes more important and perturbation growth effectively ends. In fact (3.30) can be directly solved⁴⁷ to yield

$$\delta_M(a) = \frac{5}{2}H_0^2\Omega_{M0}\frac{\dot{a}}{a}\int_0^a H^{-3}(a') da' , \quad (3.31)$$

There exist analytic approximations to this formula⁴⁵, as well as analytic expressions for flat universes⁴⁸.

3.3.2 The transfer function

Since perturbations evolve after entering the horizon, the power spectrum will not remain constant. For scales entering the horizon well after matter domination ($k^{-1} \gg k_{\text{eq}}^{-1} \simeq 81 \text{ Mpc}$), the metric perturbation has not changed significantly, so that $R_k(\text{final}) = R_k(\text{initial})$. Then Eq. (3.26) determines the final density contrast in terms of the initial one. On smaller scales, there is a linear *transfer function* $T(k)$, which may be defined as

$$R_k(\text{final}) = T(k) R_k(\text{initial}) . \quad (3.32)$$

An equivalent, and more usual, definition is

$$a^{-1}\delta_{\mathbf{k}}(\text{final}) = AT(k)\delta_{\mathbf{k}}(\text{initial}) \quad (3.33)$$

where the (time dependent) right hand side is evaluated at an arbitrarily chosen time during the initial era, and the constant A is chosen so that T becomes equal to 1 on large scales.

Given the adiabatic condition, the transfer function is determined by the physical processes occurring between horizon entry and matter domination, including: neutrino free streaming around the epoch of horizon entry; the diffusion of photons around the same time; the diffusion of baryons along with the photons, and the establishment after matter domination of a common matter density contrast, as the baryons fall into the potential wells of cold dark matter. All these effects apply separately, to first order in the perturbations, to each Fourier component, so that a linear transfer function is produced.

There are several parameterizations in the literature, but the one which is more widely used is that of Ref.⁴³,

$$T(k) = \left[1 + \left(ak + (bk)^{3/2} + (ck)^2 \right)^\nu \right]^{-1/\nu}, \quad \nu = 1.13, \quad (3.34)$$

$$a = 6.4 (\Omega_M h)^{-1} h^{-1} \text{ Mpc}, \quad (3.35)$$

$$b = 3.0 (\Omega_M h)^{-1} h^{-1} \text{ Mpc}, \quad (3.36)$$

$$c = 1.7 (\Omega_M h)^{-1} h^{-1} \text{ Mpc}. \quad (3.37)$$

The transfer function, which encodes the solution to linear equations, ceases to be valid when the density contrast becomes of order 1. After that, the highly nonlinear phenomenon of gravitational collapse takes place.

3.3.3 The spectrum of the density perturbation

In order to discuss the perturbations in a given region of the universe around us, one has to perform the Fourier expansion Eq. (3.11) in a box much bigger than this region. If the box is a cube with sides of length L , the possible values of \mathbf{k} form a cubic lattice in k space is $2\pi/L$.

When discussing an isolated system, which is the usual case in physics, one can take the limit $L \rightarrow \infty$ in a straightforward way, the coefficients $f_{\mathbf{k}}$ tending to a constant limit which is a smooth function of \mathbf{k} . But cosmological perturbations do not fall off at large distances, and their Fourier coefficients are not smooth functions of \mathbf{k} . They are the spatial analogue of a signal extending over an indefinite period of time, as opposed to an isolated pulse.

Although the coefficients $f_{\mathbf{k}}$ are not smooth functions, it is reasonable to suppose that $|f_{\mathbf{k}}|^2$ is smoothly varying when smeared over a region d^3k of k space, which is large enough to contain many lattice points. I shall denote this average by $\langle |f_{\mathbf{k}}|^2 \rangle$. It depends only on $k = |\mathbf{k}|$, and up to a k dependent factor it is called the *spectrum* of f , because of the analogy with a signal. A convenient choice of the factor is to define the spectrum as

$$P_f \equiv \left(\frac{Lk}{2\pi} \right)^3 4\pi \langle |f_{\mathbf{k}}|^2 \rangle \quad (3.38)$$

The normalisation is chosen to give a simple formula for the dispersion (root mean square) of f , which I shall denote by σ_f . From the Fourier expansion one has $\sigma_f^2 = \sum |f_{\mathbf{k}}|^2$, and

since the possible values of \mathbf{k} form a cubic lattice with spacing $2\pi/L$ the transition from sum to integral is

$$\left(\frac{2\pi}{L}\right)^3 \sum_{\mathbf{k}} \longrightarrow 4\pi \int k^2 dk \quad (3.39)$$

The dispersion σ_f is therefore given by

$$\sigma_f^2 \equiv \langle f^2(\mathbf{x}) \rangle = \int_0^\infty P_f(k) \frac{dk}{k} \quad (3.40)$$

with the brackets now denoting the average over position \mathbf{x} .

For the density perturbation $f = \delta$ it is useful to define the correlation function $\xi(r)$ by

$$\xi(r) = \langle f(\mathbf{r} + \mathbf{x})f(\mathbf{r}) \rangle = \int_0^\infty P_f(k) \frac{\sin(kr)}{kr} \frac{dk}{k} \quad (3.41)$$

The analogous quantity is useful for other perturbations like the peculiar velocity components, though it is not then called the correlation function. For $r = 0$ it clearly reduces to σ_f^2 .

If the phases of the Fourier coefficients are random, f is said to be Gaussian, and then all of its stochastic properties are determined by its spectrum. In particular the probability distribution of f , evaluated at randomly chosen points, has a Gaussian profile.

From Eqs. (3.28) and (3.32), the spectrum of the density contrast after matter domination may be written

$$P_\delta(k) = \left(\frac{k}{aH}\right)^4 T^2(k) \delta_H^2(k) \quad (3.42)$$

The quantity δ_H specifies the initial spectrum. The standard assumption is that δ_H^2 is independent of k . A more general possibility is to consider a spectrum

$$\delta_H^2 \propto k^{n-1} \quad (3.43)$$

where the exponent n is called the *spectral index*. The definition of the index as $n - 1$ instead of n is a historical accident: the standard choice of $n = 1$ was first advocated by Harrison (1970) and Zel'dovich (1970) (3.3) on the ground that it is the only one making the perturbation small on all scales, at the epoch of horizon entry.

3.3.4 The filtered density contrast

At the present epoch the universe is highly inhomogeneous on small scales. In order to use linear cosmological perturbation theory one must therefore filter out the small scales, by

smearing each perturbation over a region of size $\gtrsim 100$ Mpc. The same is true at epochs in the relatively recent past, except that the comoving filtering scale goes down. Only in the truly early universe is the universe (presumably) homogeneous on all relevant scales.

The filtering is done by means of a ‘window function’ $W(R_f, r)$, which is equal to 1 at $r = 0$ and which falls off rapidly beyond some radius R_f ⁴⁶. Taking for definiteness the density contrast, the filtered quantity is

$$\delta(R_f, \mathbf{x}) = \int W(R_f, |\mathbf{x}' - \mathbf{x}|) \delta(\mathbf{x}') d^3 x' \quad (3.44)$$

and its spectrum is

$$P_\delta(R_f, k) = [\widetilde{W}(R_f, k)/V_f]^2 P_\delta(k) \quad (3.45)$$

where

$$\widetilde{W}(R_f, k) = \int e^{-i\mathbf{k}\cdot\mathbf{x}} W(R_f, r) d^3 x \quad (3.46)$$

and

$$V_f = \int W(R_f, r) d^3 x \quad (3.47)$$

The filtered dispersion is

$$\sigma^2(R_f) = \int_0^\infty [\widetilde{W}(R_f, k)/V_f]^2 P_\delta(k) \frac{dk}{k} \quad (3.48)$$

The quantity V_f is the volume ‘enclosed’ by the filter. It is convenient to define the associated mass $M = \rho_0 V_f$, where ρ_0 is the present mass density. One normally uses M instead of R_f to specify the scale, writing $\delta(M, \mathbf{x})$ and $\sigma(M)$.

The two popular choices are the Gaussian filter

$$W(R_f, r) = \exp(-r^2/2R_f^2) \quad (3.49)$$

$$V_f = (2\pi)^{3/2} R_f^3 \quad (3.50)$$

$$\widetilde{W}(R_f, k)/V_f = \exp(-k^2 R_f^2/2) \quad (3.51)$$

$$M = 4.36 \times 10^{12} h^2 (R_f/1 \text{ Mpc})^3 M_\odot \quad (3.52)$$

and the top hat filter which smears uniformly over a sphere of radius R_f

$$W(R_f, r) = \theta(r - R_f) \quad (3.53)$$

$$V_f = 4\pi R_f^3/3 \quad (3.54)$$

$$\widetilde{W}(R_f, k)/V_f = 3 \left(\frac{\sin(kR_f)}{(kR_f)^3} - \frac{\cos(kR_f)}{(kR_f)^2} \right) \quad (3.55)$$

$$M = 1.16 \times 10^{12} h^2 (R_f/1 \text{ Mpc})^3 M_\odot \quad (3.56)$$

The Gaussian filter is the most convenient for theoretical calculations, but the top hat filter is widely used to as a means of presenting data.

3.3.5 Linear Theory Works

A full comparison of theory with observation requires the use of numerical simulations, to follow the process of gravitational collapse which occurs on each scale after cosmological perturbation theory breaks down. It turns out, though, that the linear theory can be applied on a wide variety of scales, so that one can obtain powerful constraints on the parameters by considering it alone. Working from the top down, some of the most important linear constraints are explained below.

- *The large scale cmb anisotropy* The WMAP data explores scales of order the size of the observable universe, say 10^3 to 10^4 Mpc.
- *The bulk flow* Smearing the galaxy peculiar velocities over a sphere of radius tens of Mpc to get what is called the *bulk flow*, one should be in the linear regime. In principle⁷⁰ one can observe the radial component of the bulk flow, construct the corresponding potential radially, reconstruct \mathbf{v} and finally determine the density perturbation $\delta\rho(\mathbf{x})$.
- *Galaxy cluster number density* The average number density $n(> M)$ of clusters with mass bigger than $M \sim 10^{15} M_\odot$ gives information on a scale of order $10h^{-1}$ Mpc. Within linear theory one can estimate $n(> M)$ by assuming that the matter in regions of space where $\delta(M, \mathbf{x})$ exceeds some critical value δ_c of order 1 is bound into objects with mass $> M$. The fraction of space occupied by such regions is

$$f(> M) = \text{erfc} \left(\frac{\delta_c}{\sqrt{2}\sigma(M)} \right) \quad (3.57)$$

From this assumption Press and Schechter derived the formula¹⁹

$$m \frac{dn(> M)}{dM} = \frac{\langle k^2 \rangle}{12\pi^2 R_f} \nu e^{-\nu^2/2} \quad (3.58)$$

where $\nu = \delta_c/\sigma(M)$ is the number of standard deviations that δ_c represents, and

$$\langle k^2(M) \rangle = \sigma^{-2}(M) \int_0^\infty k^2 e^{-k^2 R_f^2} P_\delta(k) \frac{dk}{k} \quad (3.59)$$

(This formula includes a more or less unmotivated factor 2). An alternative prescription is to identify each peak in $\delta(M, \mathbf{x})$ higher than δ_c with an object of mass $> M$, which gives a roughly similar result. Yet another method, which in principle is superior, is to run a numerical simulation, which again gives roughly similar results.

- *The shape of the galaxy correlation function* The galaxy correlation function Eq. (3.41) can be used to probe the shape of $\sigma(M)$ on scales between those explored by the last two items, if the bias factor is taken to be scale independent.
- *Quasar number density* Given some astrophysics assumptions, the observed quasar abundance can provide a lower limit on the density contrast at high redshift.

MECÂNICA ESTATÍSTICA NÃO EXTENSIVA

4.1 INTRODUCTION

As well known, *thermodynamics* is the basic branch of physics which focuses on the generic connections between variables (temperature, pressure, volume, energy, entropy and many others) that play an important role in the description of the *macroscopic* world. Boltzmann and Gibbs provided a magnificent connection of thermodynamics with the *microscopic* world. This connection, normally referred to as *Boltzmann-Gibbs (BG) statistical mechanics* (or simply *statistical mechanics* since it was basically the only one to be formulated along more than one century), turns out to be the appropriate one for ubiquitous systems in nature.

Thermodynamics is based on two pillars: *energy* and *entropy*. The first one concerns (dynamical or mechanical) *possibilities*; the second one concerns the *probabilities* of those possibilities. The first one is more basic, and clearly depends on the *physical system* (classical, quantum, relativistic, or any other); the second one is more subtle, and reflects the *information* upon the physical system.

It was long believed that the microscopic expression of the physical entropy *had* to be universal, i.e., system-independent (but dependent of W , the total number of possibilities of the system). More precisely, it *had* to be, for *all* systems

$$S_{BG} = -k \sum_{i=1}^W p_i \ln p_i \quad (4.1)$$

with the normalization condition

$$\sum_{i=1}^W p_i = 1 . \quad (4.2)$$

Here p_i is the probability for the system to be in the i -th microstate, and k is the Boltzmann constant ($k_B = 1.38 \times 10^{-23}$ J/K). Without loss of generality one can also arbitrarily assume $k = 1$. If every microstate has the same probability $p_i = 1/W$ (*equiprobability* assumption) one obtains the famous *Boltzmann principle*

$$S_{BG}(p_i = 1/W, \forall i) = k \ln W . \quad (4.3)$$

It can be easily shown that entropy (4.1) is *nonnegative, concave, extensive* and *stable*⁷⁵ (or *experimentally robust*). If A and B are two *independent* systems in the sense that $p_{ij}^{A+B} = p_i^A p_j^B$, then we straightforwardly verify that

$$S_{BG}(A + B) = S_{BG}(A) + S_{BG}(B) . \quad (4.4)$$

One might naturally expect that the form (4.1) of S_{BG} would be rigorously *derived* from microscopic dynamics. However, the difficulty of performing such a program can be seen from the fact that still today this has not yet been accomplished from first principles. Consequently (4.1) is in practice a *postulate*. However, this widespread belief of universality appears to have no rigorous basis. Indeed, it appears nowadays that the concept of physical information, and its microscopic expression in terms of probabilities, must be adapted to each system treated.

Expressions (4.1) and (4.3) are so commonly used because most of the systems whose thermal properties are studied belong to the type involving (*strong*) chaos in its microscopic dynamics, i.e., *positive* Lyapunov exponents, known to yield quick mixing and eventually ergodicity in phase space. There is no fundamental reason for which the *same* expression should necessarily be used for systems involving say a *vanishing* Lyapunov spectrum, i.e., for systems exhibiting *weak* chaos, when the sensitivity to the initial conditions diverges *less* than exponentially. Indeed, such systems, if isolated, might have serious difficulties in satisfying the ergodic hypothesis during the observational time of physical measures.

It is clear that the above statements about the nonuniversality of the microscopic expression for the entropy are self-evident. If, however, S_{BG} is not universal, how to generalize it? The analysis of the structure of the BG theory provides us a metaphor for formulating this new statistical mechanics; but we are talking of a *generalization* of the BG theory, *and by no means an alternative to it*.

4.2 Central equations of nonextensive statistical mechanics

Nonextensive statistical mechanics and thermodynamics were introduced in 1988⁷⁶, and further developed in 1991⁷⁷ and 1998¹¹⁴, with the aim of extending the domain of applicability of statistical mechanics to systems where Boltzmann-Gibbs (BG) statistics and standard thermodynamics present serious difficulties or just plainly fail. Indeed, a rapidly increasing number of systems are pointed out in the literature for which the usual functions appearing in BG statistics appear to be violated. Some of these cases are satisfactorily handled within the formalism we are here addressing (see¹⁰³ for reviews and⁷⁸ for a regularly updated bibliography which includes crucial contributions and clarifications that many scientists have given along the years).

In this spirit, an entropy, S_q , which generalizes S_{BG} , has been proposed. The entropy S_q (with $S_1 = S_{BG}$) depends on the index q , a real number to be determined *a priori* from the microscopic dynamics. The property chosen to be generalized is extensivity, i.e., Eq. (4.4).

4.2.1 A metaphor

The simplest ordinary differential equation one might think of is

$$\frac{dy}{dx} = 0, \quad (4.5)$$

whose solution (with initial condition $y(0) = 1$) is $y = 1$. The next simplest differential equation might be thought to be

$$\frac{dy}{dx} = 1, \quad (4.6)$$

whose solution, with the same initial condition, is $y = 1 + x$. The next one in increasing complexity that we might wish to consider is

$$\frac{dy}{dx} = y, \quad (4.7)$$

whose solution is $y = e^x$. Its inverse function is

$$y = \ln x, \quad (4.8)$$

which has the same functional form of the Boltzmann-Gibbs entropy (4.3), and satisfies the well known additivity property

$$\ln(x_A x_B) = \ln x_A + \ln x_B. \quad (4.9)$$

A question that might be put is: can we unify all three cases (4.5,4.6,4.7) considered above? A trivial positive answer would be to consider $dy/dx = a + by$, and play with (a, b) . Can we unify with *only one* parameter? The answer still is positive, but this time *out of linearity*, namely with

$$\frac{dy}{dx} = y^q \quad (q \in \mathcal{R}), \quad (4.10)$$

which, for $q \rightarrow -\infty$, $q = 0$ and $q = 1$, reproduces respectively the differential equations (4.5), (4.6) and (4.7). The solution of (4.10) is given by the q -exponential function

$$y = [1 + (1 - q)x]^{\frac{1}{1-q}} \equiv e_q^x \quad (e_1^x = e^x), \quad (4.11)$$

whose inverse is the q -logarithm function

$$y = \frac{x^{1-q} - 1}{1 - q} \equiv \ln_q x \quad (\ln_1 x = \ln x). \quad (4.12)$$

This function satisfies the *pseudo-additivity* property

$$\ln_q(x_A x_B) = \ln_q x_A + \ln_q x_B + (1 - q)(\ln_q x_A)(\ln_q x_B) \quad (4.13)$$

4.2.2 The nonextensive entropy S_q

As we saw, the exponential function e^x is generalized into the q -exponential function

$$e_q^x \equiv [1 + (1 - q)x]^{\frac{1}{1-q}} \quad (q \in \mathcal{R}). \quad (4.14)$$

We can trivially verify that this (nonnegative and monotonically increasing) function (i) for $q \rightarrow 1$ yields $e_1^x = e^x$ ($\forall x$), (ii) for $q > 1$, vanishes as a power-law when $x \rightarrow -\infty$ and diverges at $x = 1/(q-1)$, and (iii) for $q < 1$, has a cutoff at $x = -1/(1-q)$, below which it is defined to be identically zero. If $x \rightarrow 0$ we have $e_q^x \sim 1+x$ ($\forall q$).

The inverse function of the q -exponential is the q -logarithm, defined as follows:

$$\ln_q x \equiv \frac{x^{1-q} - 1}{1-q} \quad (q \in \mathcal{R}). \quad (4.15)$$

Of course $\ln_1 x = \ln x$ ($\forall x$). If $x \rightarrow 1$ we have $\ln_q x \sim x-1$ ($\forall q$).

Generalization of the BG entropy

We can rewrite Eq. (4.1) in a slightly different form, namely (with $k=1$)

$$S_{BG} = - \sum_{i=1}^W p_i \ln p_i = \sum_{i=1}^W p_i \ln \frac{1}{p_i} = \left\langle \ln \frac{1}{p_i} \right\rangle, \quad (4.16)$$

where $\langle \dots \rangle \equiv \sum_{i=1}^W (\dots) p_i$. The quantity $\ln(1/p_i)$ is sometimes called *surprise* or *unexpectedness*. Indeed, $p_i = 1$ corresponds to certainty, hence zero surprise if the *expected* event does occur; on the other hand, $p_i \rightarrow 0$ corresponds to nearly impossibility, hence infinite surprise if the *unexpected* event does occur. If we introduce the q -surprise (or q -unexpectedness) as $\ln_q(1/p_i)$, it is kind of natural to define the following q -entropy

$$S_q \equiv \left\langle \ln_q \frac{1}{p_i} \right\rangle = \sum_{i=1}^W p_i \ln_q \frac{1}{p_i} = \frac{1 - \sum_{i=1}^W p_i^q}{q-1} \quad (4.17)$$

The nonextensive entropic form we postulate is

$$S_q = \frac{1 - \sum_{i=1}^W p_i^q}{q-1} \quad \left(\sum_{i=1}^W p_i = 1; q \in \mathcal{R} \right), \quad (4.18)$$

where W is the total number of microscopic configurations, whose probabilities are $\{p_i\}$.

The continuous and the quantum expressions of S_q are respectively given by

$$S_q = \frac{1 - \int dx [p(x)]^q}{q-1} \quad (4.19)$$

and

$$S_q = \frac{1 - \text{Tr} \rho^q}{q-1}, \quad (4.20)$$

where ρ is the matrix density. Unless specifically declared in what follows, we shall be using the form of Eq. (4.18). It is easy to verify that all its generic properties can be straightforwardly adapted to both the continuous and quantum cases.

Assuming equiprobability (i.e., $p_i = 1/W$) one obtains straightforwardly

$$S = \frac{W^{1-q} - 1}{1 - q} = \ln_q W. \quad (4.21)$$

which is the basis for the microcanonical ensemble. It can be shown that the nonnegative entropy S_q is concave (convex) for $q > 0$ ($q < 0$). This property implies thermodynamic stability. Such a property makes possible for two systems at different temperature to equilibrate to a common temperature.

Consequently, it is clear that S_q is a generalization of and not an alternative to the classical entropy, because if $q \rightarrow 1$, this entropy reproduces the usual Boltzmann-Gibbs-Shannon one, namely $S_1 = -\sum_{i=1}^W p_i \ln p_i$.

We may think of q as a biasing parameter: $q < 1$ privileges rare events, while $q > 1$ privileges common events. Indeed, $p < 1$ raised to a power $q < 1$ yields a value *larger* than p , and the relative increase $p^q/p = p^{q-1}$ is a *decreasing* function of p , i.e., values of p closer to 0 (rare events) are benefited. Correspondingly, for $q > 1$, values of p closer to 1 (common events) are privileged. Therefore, the BG theory (i.e., $q = 1$) is the unbiased statistics.

If A and B are two independent systems (i.e., $p_{ij}^{A+B} = p_i^A p_j^B \forall (i, j)$), then the pseudo-additivity of the q -logarithm immediately implies

$$S_q(A + B) = S_q(A) + S_q(B) + (1 - q)S_q(A)S_q(B). \quad (4.22)$$

It follows that $q = 1$, $q < 1$ and $q > 1$ respectively correspond to the *extensive*, *superextensive* and *subextensive* cases (in all cases $S_q \geq 0$). It is from this property that the corresponding generalization of the BG statistical mechanics is often referred to as *nonextensive statistical mechanics*.

The Associated Probability

To obtain the probability distribution associated with the relevant stationary state (thermal equilibrium or metaequilibrium) of our system we must optimize the entropic nonextensive form under the following constraints^{76,114}: the norm constraint given by

$$\sum_i p_i = 1,$$

and the energy constraint generalized as follows

$$\frac{\sum_i p_i^q E_i}{\sum_i p_i^q} = U_q ,$$

where $\{E_i\}$ is the set of eigenvalues of the Hamiltonian (with specific boundary conditions), and U_q is a fixed and *finite* number. This optimization yields the generalized weight

$$p_i = \frac{[1 - (1 - q)\beta_q(E_i - U_q)]^{1/(1-q)}}{Z_q} , \quad (4.23)$$

where

$$Z_q \equiv \sum_j [1 - (1 - q)\beta_q(E_j - U_q)]^{1/(1-q)} ,$$

and

$$\beta_q \equiv \frac{\beta}{\sum_j p_j^q} ,$$

β being the optimization Lagrange parameter associated with the generalized internal energy U_q .

This probability distribution corresponds to a *maximum* (*minimum*) of S_q for $q > 0$ ($q < 0$). For $q = 0$, the entropy is constant, namely $S_0 = W - 1$, and the distribution is given by $p_i = [1 - \beta_q(E_i - U_0)] / \sum_{j=1}^W [1 - \beta_q(E_j - U_0)]$ (we recall the *cutoff* of the q -exponential function for $q < 1$, i.e., the states for which $1 - \beta_q(E_i - U_0) < 0$ do *not* contribute).

Equation (4.23) can be rewritten as

$$p_i \propto [1 - (1 - q)\beta' E_i]^{1/(1-q)} \equiv e_q^{-\beta' E_i} ,$$

where β' is a renormalized inverse “temperature”, and the q -exponential function is defined as $e_q^x \equiv [1 + (1 - q)x]^{1/(1-q)} = 1/[1 - (q - 1)x]^{1/(q-1)}$ (with $e_1^x = e^x$). This function replaces, in a vast number of relations and phenomena, the usual BG factor.

Analogously, if we optimize S_q as given by Eq. (4.19) with the constraints $\int dx p(x) = 1$ and $\langle\langle x^2 \rangle\rangle_q = \sigma^2$ ($\sigma > 0$), we obtain the q -generalization of the Gaussian distribution, namely⁷⁹

$$p_q(x) = \frac{e_q^{-\bar{\beta}x^2}}{\int dy e_q^{-\bar{\beta}y^2}} \propto \frac{1}{[1 + (q - 1)\bar{\beta}x^2]^{\frac{1}{q-1}}} \quad (q < 3), \quad (4.24)$$

(fat-tailed if $q > 1$, and with a cutoff if $q < 1$) and where $\bar{\beta}$ can be straightforward and explicitly related to σ . The variance of these distributions is finite if $q < 5/3$ and diverges

if $5/3 < q < 3$. For $q = 2$ we have the Lorentzian distribution. For $q \geq 3$ the function is not normalizable, and therefore is unacceptable as a distribution of probabilities.

4.2.3 A remark on other possible generalizations of the Boltzmann-Gibbs entropy

There have been in the past other generalizations of the BG entropy. The *Renyi entropy* is one of them and is defined as follows

$$S_q^R \equiv \frac{\ln \sum_{i=1}^W p_i^q}{1-q} = \frac{\ln[1 + (1-q)S_q]}{1-q}. \quad (4.25)$$

Another entropy has been introduced by Landsberg and Vedral¹¹² and independently by Rajagopal and Abe¹¹³. It is sometimes called *normalized nonextensive entropy*, and is defined as follows

$$S_q^N \equiv S_q^{LVRA} \equiv \frac{1 - \frac{1}{\sum_{i=1}^W p_i^q}}{1-q} = \frac{S_q}{1 + (1-q)S_q}. \quad (4.26)$$

A question arises naturally: Why not using one of these entropies (or even a different one such as the so called *escort entropy* S_q^E , defined in^{114,115}), instead of S_q , for generalizing BG statistical mechanics? The answer appears to be quite straightforward. S_q^R , S_q^{LVRA} and S_q^E are not concave nor experimentally robust. Neither yield they a *finite* entropy production for unit time, in contrast with S_q . Moreover, these alternatives do not possess the suggestive structure that S_q exhibits associated with the Jackson generalized derivative. Consequently, *for thermodynamical purposes*, it seems nowadays quite natural to consider the entropy S_q as the best candidate for generalizing the Boltzmann-Gibbs entropy.

4.3 Applications in and out from equilibrium

A considerable amount of applications and connections have been advanced in the literature using, in a variety of manners, the nonextensive formalism. They concern physics, astrophysics, geophysics, chemistry, biology, mathematics, economics, linguistics, engineering, medicine, physiology, cognitive psychology, sports and others⁷⁸. The fact that

the range of applications is so wide probably is deeply related to and reflects the ubiquity of self-organized criticality⁸⁰, fractal structures and, ultimately, power laws in nature.

Examples that have been analyzed include re-association in folded proteins⁸¹, fluxes of cosmic rays⁸², finance and economics⁸³, electron-positron annihilation⁸⁴, quark-gluon plasma⁹⁶, kinetic theory⁹⁷, classical chaos⁹⁸, quantum chaos⁹⁹, quantum entanglement¹⁰⁰, anomalous diffusion¹⁰¹, long-range-interacting many-body classical Hamiltonian systems (¹⁰² and references therein), epilepsy⁸⁵, linguistics⁸⁶, nuclear physics⁸⁷, astrophysics, distributions in music⁸⁸, urban agglomerations⁸⁹, internet phenomena⁹⁰, and others are known nowadays which in no trivial way accommodate within BG statistical mechanical concepts. Systems like these have been handled with the functions and concepts which naturally emerge within nonextensive statistical mechanics^{76,114,103}.

4.4 Applications in Astrophysics and Cosmology

Connections between dynamics and thermodynamics are far from being completely clarified. For instance, long-range interactions are expected to substantially modify various usual thermodynamical properties. Enrico Fermi addressed such question in his famous book *Thermodynamics* (1936)⁹¹.

Laszlo Tisza says in 1961⁹²:

From the molecular point of view, additivity and homogeneity can be expected to be reasonable approximations for systems containing many particles, provided that the intramolecular forces have a short range character.

Finally, from Peter T. Landsberg (1978)⁹³:

The presence of long-range forces causes important amendments to thermodynamics, some of which are not fully investigated as yet.

In recent papers, also E.G.D. Cohen⁹⁴ and M. Baranger⁹⁵ have addressed this question too. If we put all this together, as well as many other similar statements available in the literature, we may conclude that physical entropies different from the BG one could exist which would be the appropriate ones for anomalous systems. Among the anomalies that we may focus on we include (i) metaequilibrium (metastable) states in large systems involving long range forces between particles, (ii) metaequilibrium states in small systems,

i.e., whose number of particles is relatively small, say up to 100-200 particles, (iii) glassy systems, (iv) some classes of dissipative systems, (v) mesoscopic systems with nonmarkovian memory, and others which, in one way or another, might violate the usual simple ergodicity. Such systems might have a multifractal, scale-free or hierarchical structure in their phase space.

Let us now cite recent applications of the ideas associated with nonextensive statistical mechanics to phenomena in astronomy and astrophysics, namely the solar neutrino deficit¹⁰⁶, self-gravitating polytropic systems^{107–109}, peculiar velocities of galaxy clusters¹⁰⁴, the flux of cosmic rays⁸², and some cosmological effects¹⁰⁵.

Polytropic Equilibrium Solutions to the Vlasov-Poisson Equations:

The first physical application of the non-extensive thermostatistical formalism was related to the study of maximum entropy solutions to the Vlasov-Poisson equations describing self gravitating N -body systems like galaxies^{107,108}. The maximization of the standard Boltzmann-Gibbs entropy under the constraints imposed by mass and energy conservation lead to the isothermal sphere distribution, which has *infinite* mass and energy¹¹⁰. In^{107,108}, it was shown that the extremalization of the nonextensive q -entropy under the same constraints leads to the stellar polytropic sphere distributions which, for a certain range of the q parameter, are endowed with *finite* mass and energy, as physically expected. This constituted the first clue suggesting that the generalized thermostatistical formalism based on S_q may be of some relevance for the study of systems exhibiting non extensive thermodynamical properties due to long range interactions.

Peculiar velocities of galaxy clusters

The COBE (Cosmic Background Explorer) satellite measured the peculiar velocities (difference of velocity with regard to the average expansion of the universe) of some clusters of spiral galaxies. A distribution was found which exhibits a cutoff around 500 Km/s . The Princeton astrophysical group¹¹¹ analyzed the distribution of velocities within four different cosmological models. None of those attempts succeeded in reproducing the observed cutoff, although each of those models involved several free parameters (that were fixed through a variety of arguments). By assuming within nonextensive statistical mechanics, an extremely simplified model as an ideal classical gas, the empirical velocity distribution was quite satisfactorily matched¹⁰⁴. Only two fitting parameters were used,

namely the scale of velocities and $q \simeq 0.23$. In spite of the extreme simplicity of the model, the fact that the statistics was allowed to change proved its high efficiency.

Cosmology:

Nonextensive statistical mechanics has also been applied to a variety of cosmological and general relativity problems including the cosmic background radiation in a Robertson-Walker universe, the dynamics of inflationary cosmologies, the universal density profile of dark halos, early universe phenomena (e.g., the primordial ${}^4\text{He}$ formation), among others¹⁰⁵.

O MÉTODO DE PRESS-SCHECHTER

5.1 Introduction

It is widely believed that the structure of the universe observed nowadays, like the clusters and superclusters of galaxies, has been formed from the gravitational growth of small amplitude density perturbations in the epoch of matter-radiation decoupling (at redshift $z \sim 1000$).

An important theoretical question in cosmology is how to determine the fraction of matter in the universe that has formed bounded structures, and what is its distribution in mass at any given redshift after recombination. The number density of collapsed objects for a given mass, named the *mass function*, is a central quantity in analysis of cosmic structures such clusters of galaxies. The mass function can distinguish easily different galaxy formation theories, including whether the initial perturbations were Gaussian or not¹⁴³. The mass function is applied in a wide range of cosmological problems, like measures of volumes (eg. galaxy lensing), or determining the normalization of the power spectrum.

The pioneering work in describing analytically the mass function was done by Press & Schechter¹⁵⁴ (hereafter PS). The PS formalism is simple and presents a good fit to the observational data¹²⁹ and numerical simulations results^{137,169}. Nowadays, the PS formalism is largely adopted to derive the mass function, $F_{(M)}$, of bounded objects in the observed Universe.

In their statistical approach PS assume that the initial density field is Gaussian. We take the initial density field, at a very early time, and smooth it on the scale R . The evolution of the density field δ in each point is linear, and when this evolved density gets as large as a threshold $\delta_c \sim 1$, then the density at that region becomes non-linear, better saying, that region becomes gravitationally unstable, and we consider it as a collapsed (bound) region. The fraction of the bound particles at the mass M , the mass function $F_{(M)}$, is the probability that the linear density is larger than the threshold δ_c in the PS formalism.

The usefulness of the spherical model was emphasised when Press & Schechter considered smoothing the initial density field to determine the relative abundances of perturbations on different scales¹⁵⁴. When combined with the critical overdensity for collapse this provided a statistical model for the formation of structure in the Universe: smoothing the fluctuations leads to the masses of collapsed objects, while the spherical perturbation model gives the epoch of collapse for those perturbations that are sufficiently dense.

Although considering its importance, the PS approach is endowed with a fundamental difficulty, namely: the mass function has only a half of the correct normalization (there is a fudge factor 2). In order to correct that, the authors argued that only half of the bounded mass was counted on their formalism because the under density regions were not taken correctly into account, and they simply put by hand a factor of 2 in the expression of $F_{(M)}$. Actually, there are some proposals appearing in the literature accounting for the fudge factor 2. However, the majority of them, like the peak ansatz and the various cloud-in-cloud solutions^{121,151} lacks the analytical simplicity of the original PS formalism.

Some recent development of massive high resolution N-body simulations are suggesting that the PS approach does not provide an accurate description to the structure formation problem¹³⁷. Obviously such a simple model will fail in detail, particularly given the known complexities of asymmetrical gravitational collapse, and numerical simulations have now quantified these problems^{158,135}. However PS theory has been successful and still provides key insight into the processes at work in structure formation.

More recently, inspired by the so-called Tsallis q -nonextensive statistics^{76,159,140,160,138,189}, we have proposed a simple extension of the PS analytical formalism¹³⁹, in order to present better fits to the most recent observational and numerical data of structure formation.

The basic modification is the adoption of a power law Tsallis distribution for describing the fluctuations of the density field instead of the Gaussian function assumed by the standard PS approach. An attractive feature of this new distribution is that the models are analytically tractable in such a way that a detailed comparison with the PS approach is immediate. The extended formalism recovers the PS treatment as a special case, and presents the same simplicity of the standard PS method.

5.2 The Press-Schechter approach

To determine the mass function analytically we need both dynamics and statistics. In the dynamic *ansatz*, PS adopted the top-hat spherical model, in which all the cosmological dependence is contained within the rms density fluctuation, $\sigma_{(M)}$, smoothed with a top-hat filter on a scale $R^3 = 3M/4\pi\bar{\rho}$. In their statistical approach PS assume that the initial density field is Gaussian. The PS approach take the initial density field, at a very early time, and smooth it on the scale R . The evolution of the density field δ in each point is linear, and when this evolved density gets as large as a threshold $\delta_c \sim 1$, then the density at that region becomes non-linear, better saying, that region becomes gravitationally unstable, and we consider that these high density regions will condense out as collapsed (bound) objects of mass M at time t . The fraction of the bound particles at the mass M , $F_{(M)}$, is the probability that the linearly evolved density is larger than the threshold δ_c in the PS formalism. The comoving density of bound particles at each mass scale, say the comoving mass function $N_{(M)}$, is directly related with that fraction $F_{(M)}$.

Considering now the statistical view of the PS approach, we consider that the primordial density perturbations are Gaussian fluctuations. Thus the phases of the waves of the density distribution will be random, and the amplitudes of the perturbations can be described by a gaussian function

$$P(\delta) = \frac{1}{\sqrt{2\pi}\sigma_{(M)}} \exp\left(-\frac{\delta^2}{2\sigma_{(M)}^2}\right), \quad (5.1)$$

where $\sigma_{(M)}^2 \equiv \langle \delta_M^2 \rangle$ is the mean squared fluctuation. By definition, bounded objects are those whose amplitudes of the density contrast became greater than a critical value (δ_c) and, as such, their fraction $F_{(M)}$ at a given cosmological time can be written as¹⁴²

$$F_{(M)} = \int_{\delta_c}^{\infty} P(\delta) d\delta = \frac{1}{\sqrt{2\pi}\sigma_{(M)}} \int_{\delta_c}^{\infty} \exp\left(-\frac{\delta^2}{2\sigma_{(M)}^2}\right) d\delta, \quad (5.2)$$

and from that it is straightforward to derive the distribution of bound objects with masses between M and $M + dM$:

$$\frac{dF_{(M)}}{dM} = +\frac{1}{\sqrt{2\pi}} \frac{\delta_c}{\sigma_{(M)}^2} \left(\frac{\partial\sigma_{(M)}}{\partial M}\right) \exp\left(-\frac{\delta_c^2}{2\sigma_{(M)}^2}\right). \quad (5.3)$$

In the linear regime, the mass of the perturbation is $M = \bar{\rho} \cdot V$ where $\bar{\rho}$ is the mean density of the background model. If we divide the mass function of Eq.(5.3) by this volume V , we obtain finally the spatial density, or *comoving number density* $N_{(M)}dM$ at a time t

$$\begin{aligned} N_{(M)}dM &= \frac{\frac{dF_{(M)}}{dM} dM}{V} = +\frac{\bar{\rho}}{M} \frac{1}{\sqrt{2\pi}} \frac{\delta_c}{\sigma_{(M)}^2} \left(\frac{\partial\sigma_{(M)}}{\partial M}\right) \\ &\quad \cdot \exp\left(-\frac{\delta_c^2}{2\sigma_{(M)}^2}\right) dM \end{aligned} \quad (5.4)$$

Now we can see the weaknesses of the PS formalism: the “incomplete” normalization condition. The quantity dF , integrated over all mass M should give the unity, however, the result reads

$$\int_0^{\infty} dF = \frac{1}{2}. \quad (5.5)$$

In other words, the PS formalism counts only half of the total bound particles in the system. As widely known, PS argued that their formalism does not treat the underdense regions properly (cloud-in-cloud problem). In order to correct that they simply multiply the resulting expression by two, without any physical reason.

For further reference, we also note that by introducing a new variable, $\nu = \delta_c/\sigma_{(M)}$, into Eq.(5.3) multiplied by the mass M and the correcting factor 2, one may obtain a simple expression to the fraction of the critical density contributed by bound structures of mass M :

$$\Omega_{(M)PS} = \frac{dF_{(M)}}{d(\ln M)} = \sqrt{\frac{2}{\pi}} \cdot \left| \frac{\partial(\ln \sigma_{(M)})}{\partial(\ln M)} \right| \nu \exp\left(-\frac{\nu^2}{2}\right). \quad (5.6)$$

5.3 PS approach with a q-Power Law

Now, instead of Gaussian initial fluctuations, let us consider that the amplitudes are described by a class of q-parameterized power law distributions^{76,159,140,160,138}

$$P(\delta)_{PL} = \frac{B_q}{\sqrt{2\pi}\sigma_{(M)}} \left[1 - (1-q) \cdot \left(\frac{\delta}{\sqrt{2}\sigma_{(M)}} \right)^2 \right]^{\frac{1}{(1-q)}}, \quad (5.7)$$

where PL denotes the q-nonextensive ‘‘Power Law’’ in order to distinguish from the PS approach. The factor B_q is the one-dimensional normalization constant which may assume the following forms:

$$\text{a) } B_q = (1-q)^{\frac{1}{2}} \left(\frac{3-q}{2} \right) \frac{\Gamma\left(\frac{1}{2} + \frac{1}{(1-q)}\right)}{\Gamma\left(\frac{1}{(1-q)}\right)}, \quad (\text{if } 0 < q \leq 1)$$

$$\text{b) } B_q = (q-1)^{\frac{1}{2}} \frac{\Gamma\left(\frac{1}{(q-1)}\right)}{\Gamma\left(\frac{1}{(q-1)} - \frac{1}{2}\right)}, \quad (\text{if } 1 \leq q < 2)$$

For all values of q , $\lim_{q \rightarrow 1} B_q = 1$; knowing this information and using a simple mathematical definition¹¹⁶

$$\lim_{d \rightarrow 0} (1 + d \cdot y)^{\frac{1}{d}} = \exp y \quad (5.8)$$

we can easily see that

$$\lim_{q \rightarrow 1} P(\delta)_{PL} = \frac{1}{\sqrt{2\pi}\sigma_{(M)}} \exp\left(-\frac{\delta^2}{2\sigma_{(M)}^2}\right) = P(\delta)_{PS}. \quad (5.9)$$

Then we conclude that our approach is reduced to the PS formalism if $q \rightarrow 1$.

The fraction $F_{(M)}$ of bound objects (where $\delta > \delta_c$) of a given mass M at a particular time t will be, in the interval $0 < q \leq 1$,

$$F_{(M)_{PL}} = \frac{B_q}{\sqrt{2\pi}\sigma_{(M)}} \cdot \int_{\delta_c}^{\delta_{\max}} \left[1 - (1-q) \cdot \left(\frac{\delta}{\sqrt{2}\sigma_{(M)}} \right)^2 \right]^{\frac{1}{(1-q)}} d\delta \quad (5.10)$$

where the limit $\delta_{\max} = \sqrt{2}\sigma_M / \sqrt{(1-q)}$ is defined by the argument of Eq.(5.7). In the case $q \geq 1$, this cutoff is absent, and we have $\delta_{\max} \equiv \infty$.

Regardless of the values of q the bound objects with masses between M and $M + dM$ reads:

$$\frac{dF_{(M)_{PL}}}{dM} = + \frac{B_q}{\sqrt{2\pi}\sigma_{(M)}^2} \frac{\delta_c}{\left(\frac{\partial\sigma_{(M)}}{\partial M}\right)} \cdot \left[1 - (1-q) \cdot \left(\frac{\delta_c}{\sqrt{2}\sigma_{(M)}} \right)^2 \right]^{\frac{1}{(1-q)}}. \quad (5.11)$$

The *comoving number density* $N_{(M)PL} dM$ at a time t will be

$$\begin{aligned}
N_{(M)PL} dM &= \frac{dF_{(M)PL}}{dM} dM \\
&= + \frac{\bar{\rho}}{M} \frac{B_q}{\sqrt{2\pi}} \frac{\delta_c}{\sigma_{(M)}^2} \left(\frac{\partial \sigma_{(M)}}{\partial M} \right) \cdot \\
&\quad \left[1 - (1 - q) \cdot \left(\frac{\delta_c}{\sqrt{2}\sigma_{(M)}} \right)^2 \right]^{\frac{1}{(1-q)}} dM. \tag{5.12}
\end{aligned}$$

We must to point out that the above functions are also reduced to the PS formalism if $q \rightarrow 1$.

Now we use Eq.(5.11), multiplied by the mass M , with the corrected factor of 2, and defining $\nu = \delta_c/\sigma_{(M)}$, we find that the fraction of critical density contributed by bound structures of mass M reads:

$$\Omega_{(M)PL} = \frac{dF_{(M)}}{d(\ln M)} = B_q \sqrt{\frac{2}{\pi}} \left| \frac{\partial (\ln \sigma_{(M)})}{\partial (\ln M)} \right| \nu \left[1 - (1 - q) \cdot \frac{\nu^2}{2} \right]^{\frac{1}{(1-q)}}. \tag{5.13}$$

As $\sigma_{(M)} \sim M^{-\frac{(3+n)}{6}}$, and considering the power spectrum index $n = 1$, we plot in Fig.(5.1) the curves of the equations (5.6) and (5.13). Note that since $\frac{dF_{(M)}}{d(\ln M)} = M \frac{dF_{(M)}}{dM} = \frac{M^2 N_{(M)}}{\bar{\rho}}$, these plots are identical in shape to the multiplicity function. The upper and bottom solid lines are, respectively, the PS curves with correct normalization (the PS original result multiplied by 2), and the original PS curve (with the wrong normalization). All other curves are PL curves with different q -parameters. Note that for $\log(\nu) > 1$ we present different behaviors for the “end-tail curves”, for different values of the free parameter (q), in our PL approach, which contrast to the fixed PS curve; that flexibility makes the PL approach more suitable to fix nowadays mass-function data¹³⁹

Note also that for small mass scales ($M \leq M_*$), in $q \sim \frac{1}{3}$ the multiplicity function is always larger than the PS at a constant linear correlation. But as $F_{(M)}$ is unchanged, to cancel the increase of $\frac{dF_{(M)}}{dM}$ at smaller scales, $\frac{dF_{(M)}}{dM}$ decreases faster at larger scales ($M \geq M_*$); Our $q = \frac{1}{3}$ curve horizontally moves to smaller mass scale compared with the PS mass function. We see that for $q = 0.5$, soon we reach $M \sim M_*$ the curve begins to “fall”, for the same reason that the $q = \frac{1}{3}$ curve mentioned above; but here $\frac{dF_{(M)}}{dM}$ decreases slower than in the $q = \frac{1}{3}$ case, so at larger scales the $q = 0.5$ curve reaches a greater scale than the first one. Here our $q = 0.5$ curve moves horizontally to larger

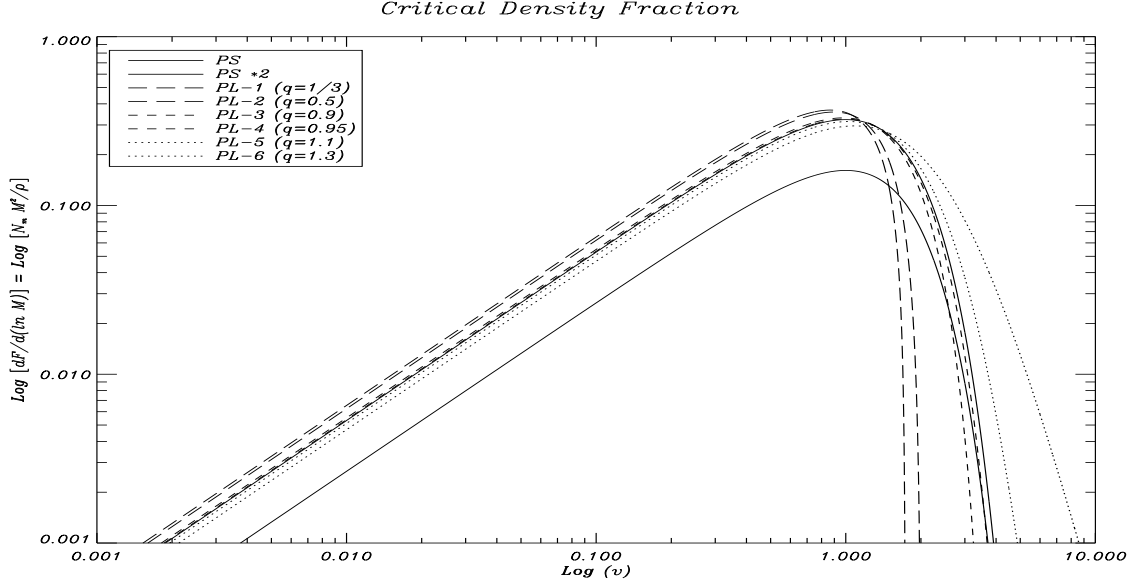


Figure 5.1: Fraction of critical density contributed by bound structures of mass M . The upper and lower solid curves are the corrected PS (factor 2), and the uncorrected PS curves, respectively. The long dashed, dashed and dotted curves are obtained using the PL distribution. Note that the q -parameter affects considerably the range of larger mass scales.

mass scales compared with the $q = \frac{1}{3}$ curve, but the general amplitude of the multiplicity function is lower. More we increase the q value, lower the amplitude becomes and more shifted to larger mass the curve is. As we reach the limit $q \rightarrow 1$, at smaller mass scales ($M \leq M_*$), the PL curve tends to lower down its amplitude (always in parallel with other curves, as expected by our power law behavior) until reach the PS curve (with the corrected normalization); and at larger scales ($M \geq M_*$) the curve tends to shift to larger masses until also reaches the PS result, as expected in our analytical analysis. The two dashed lines with $q = 0.9$ and $q = 0.95$ show this behavior in detail. Again more we increase q , more we lower the amplitude and shift the curve to larger masses, as well showed by the dotted curves with $q = 1.1$ and $q = 1.3$.

5.4 Some Extensions of the PS Approach and Our PL Method

We saw that the PS method has an intrinsic problem of normalization. Integrating over all masses M , the quantity $dF_{(M)}$ is equal to $\frac{1}{2}$ instead of 1. PS argued that in this formalism we have not taken into account the underdense regions correctly, and underdense regions at a time t may become a part of a bound region at a posterior time $t + dt$, reaching half of the total mass using the Gaussian statistics. To correct this, PS simply multiply the result by two, without any physical reason. The correct treatment of the underdense regions to solve the mystery of the “fudge factor” 2 was named *cloud-in-cloud* problem.

The PS argument for the “cloud-in-cloud problem” was taken into account by many authors: the solution of the normalization problem would be obtained taking the underdense regions in the calculation. Peacock & Heavens¹⁵¹ (hereafter PH90) and Bond et al.¹²¹ (hereafter Bond) approached the cloud-in-cloud problem in a rigorous way. In this treatment small structures can be included into larger collapsing ones, even if their density has not reached the threshold, and it increases the total collapsed mass fraction. It is important to note that this treatment rises the value of collapsed objects if we use different filter functions, but only in the special case of the sharp k-space filter the correct “fudge factor” of 2 is really recovered by Bond “without needing to cheat”¹⁵¹. This type of formalism also gives a different shape of the mass function (comparing to the PS mass function): we have much more low-mass objects than the original PS formula¹⁵¹. We must also note the lack of simplicity in the PH90 formalism compared to the easy PS one.

In the important work of Bond, the space is continuously filtered by several sharp low pass filters in k space, and with that assumption the density at any point in space obeys a random walk as the filtering scale is decreased. We can then use a diffusion equation to derive the probability $P(\delta, \sigma^2)$ that a trajectory lies between δ and $\delta + d\delta$ when the variance of the density field is σ^2 (see¹²¹):

$$\frac{\partial P}{\partial \sigma^2} = \frac{1}{2} \frac{\partial^2 P}{\partial \delta^2}$$

Calculating the probability distribution of trajectories that reach (δ, σ) without exceeding a critical value δ_c at smaller σ , will exclude all non-linear systems more massive

than M_n , whose trajectories crosses δ_c over a filtering scale k_n . The cloud-in-cloud solution will be well implemented, solving the diffusion equation above at $\delta = \delta_c$:

$$P = \frac{1}{\sqrt{2\pi}\sigma} \left[\exp\left(-\frac{\delta^2}{2\sigma^2}\right) - \exp\left(-\frac{(\delta - 2\delta_c)^2}{2\sigma^2}\right) \right]$$

Integrating the above equation, the mass fraction that collapses into non-linear objects naturally reaches the same form of the PS solution multiplied by the factor of 2, thus given the correct normalization. The diffusion solution proposed in Bond also obtain a very good fit on comparisons with numerical simulations. Unfortunately, that approach works only for sharp filters in k space. Any other filter will present correlation between steps in the $\delta - \sigma^2$ trajectories, and the system evolution will only be solved numerically.

Yano, Nagashima & Gouda¹⁷⁰ (hereafter YNG) show that the complete cloud-in-cloud problem was not be considered by PH90 and Bond, because they considered only the probability for the density fluctuations at one point in the space and neglected the spatial correlation of the density fluctuations; YNG shows that this spatial correlation effect alters the PS formalism, even using the sharp k -space filter. Jedamzik¹³⁴ approached the cloud-in-cloud problem using the integral equation of the mass function, but again without using the spatial correlation in his treatment. YNG corrected the Jedamzik work, deriving the same results as PH90 and Bond for the sharp k -space filter (always without the spatial correlation) and, using the Jedamzik corrected method and including the effect of spatial correlation - but only on the sharp k -space filter, YNG derives the new mass function. Unfortunately, it is very complicated to derive numerically the mass function with this new formula. This lack of simplicity puts a severe restriction on the YNG formalism, instead of its completeness.

We saw that the cloud-in-cloud solution doesn't bring us a simple model to replace the PS formalism, which is still easy to use and have good fits with a lot of cosmological problems. Our PL method, however, is as simple as the PS one, with two great advantages: first, it presents strong theoretical connection with the nonextensive entropy (which treats long-range interaction systems, and that is the case of the gravitational forces involved in the structure formation; better saying, we consider the "correlation effect" mentioned by YNG in a simple analytical way); second, we have a q free-parameter, which grants malleability to fit the nowadays mass function data. Essentially we have a

better parametrization than the PS curves, with a physical motivated distribution function, which reduces to the original PS case when q tends to 1.

But the mean goal of all cloud-in-cloud solution was to correct the normalization problem of the PS method. We must to accomplish a complete study of the mass function normalization to verify if our distribution presents the same problem of the PS method, and if it does, try to understand why, and yet, what is the dependence of the normalization condition to the statistical distribution of the primordial density field?

5.5 A Study of the Normalization Problem

Let us now consider the normalization problem in this PL approach. In principle, the quantity dF , from Eq.(5.11), integrated over all mass M should give the unity. However, it is easy to check that the integration results

$$\int_{\tau}^{\infty} dF = \frac{1}{2}. \quad (5.14)$$

where $\tau = 0$ in the range $1 \leq q < 2$; but in the range $0 < q \leq 1$ we have a cut-off value in our function when $(1 - q) \cdot \left(\frac{\delta_c}{\sqrt{2}\sigma_{(M)}}\right)^2 = 1$, so that $\tau = \sigma_{\min}$. The intriguing aspect here is that the same value of the Gaussian PS approach is obtained.

By analyzing more closely the normalization condition of our approach, we have concluded that the nonextensive distribution does not solve the problem of incomplete normalization present in the Gaussian PS formalism, namely: only half of the mass is also taken into account when the calculated mass function is normalized. This simple but intriguing coincidence is the leitmotiv of our study of the normalization problem¹⁴⁶. Basically, we would like to know whether the fudge factor 2 has some degree of universality within the PS formalism. Due to the generality of the q -statistics (it also includes the Lorentzian distribution as a particular case), one should be tempted to think that the normalization problem in the PS approach might be independent of the statistical distribution describing the primordial density fluctuations.

In what follows, by considering some explicit examples, we show that the normalization of the resulting mass function depends heavily on the initial distribution. In particular, we found that the mass function is normalized if one assumes that the initial perturbations

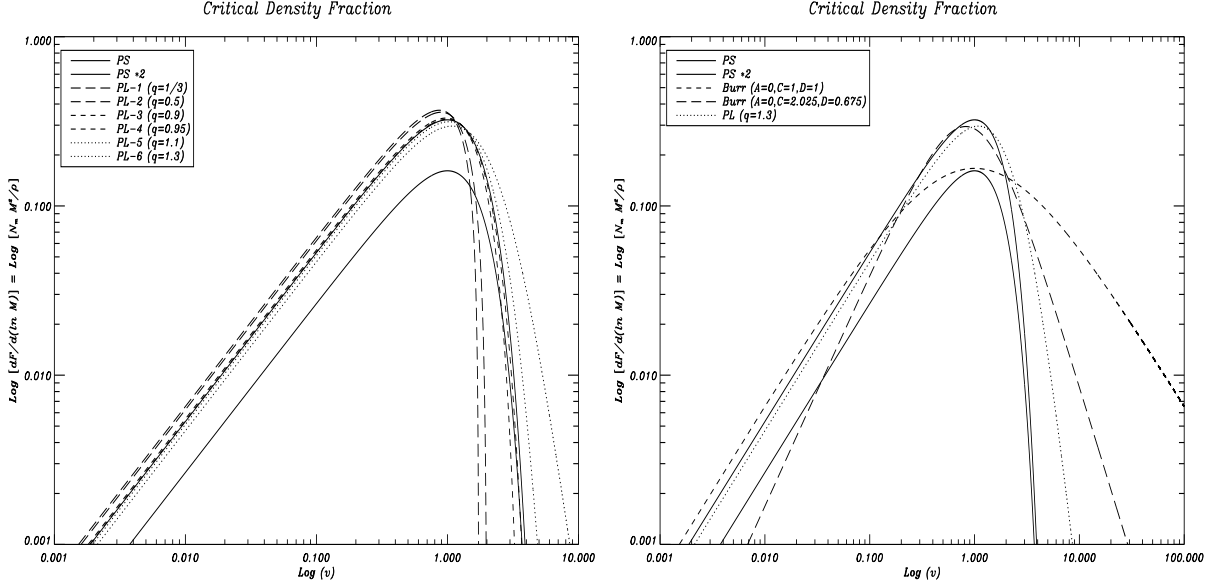


Figure 5.2: Fraction of critical density contributed by bound structures of mass M . In both panels the upper and lower solid curves are the corrected PS (factor 2), and the uncorrected PS curves, respectively. The long dashed, dashed and dotted curves in left panel are obtained using the PL distribution. In the right panel we compare the behavior using the Burr distribution (the dashed and long dashed curves) with that using the PS (solid lines) and PL (dotted line) ones.

are described by the so-called Burr distribution regardless of the values assumed by the arbitrary free parameters.

By working some specific examples, we show that the PS normalization problem depends, in general, on the adopted class of distribution functions describing the primeval density perturbations. We focus our attention to the Log-normal and Burr distributions.

The general normalized Log-Normal distribution is defined by:

$$p(\delta) = \frac{1}{\delta \cdot B \sqrt{2\pi}} \exp\left(-\frac{1}{2} \left[\frac{\log \delta - A}{B}\right]^2\right). \quad (5.15)$$

In the above expression the B parameter is a function of the mass. In addition, in order to simplify all the computations the shift parameter A is chosen to be zero. As one may check, the mass function now assumes the form

$$\frac{dF_{(M)Log-Normal}}{dM} = + \frac{1}{\sqrt{2\pi}} \frac{\log \delta_c}{B^2} \left(\frac{\partial B}{\partial M}\right) \cdot \exp\left(-\frac{1}{\sqrt{2}} \frac{\log \delta_c}{B}\right) \quad (5.16)$$

with $\int_0^\infty dF = \frac{1}{\sqrt{\pi}}$ which is different from $1/2$. This means that the normalization problem in the PS approach depends on the initial distribution. For some particular classes the

correcting factor may be 2. This happens, for instance, with the nonextensive PL and Laplace distributions (if we only consider overdense instead of underdense regions; actually this later result was not discussed here). Let us now discuss the intriguing behavior of the normalized Burr distribution

$$p_{(\delta)} = \left(\frac{CD}{B} \left(\frac{\delta - A}{B} \right)^{-C-1} \left[1 + \left(\frac{\delta - A}{B} \right)^{-C} \right] \right)^{-D-1}, \quad (5.17)$$

where $0 < C, D \leq 100$ (see Ref.¹⁶⁶). By taking again $A = 0$, $B = B(M)$, and the parameters C and D constants we find

$$\frac{dF_{(M)Burr}}{dM} = + \frac{CD}{B} \left(\frac{\delta_c}{B} \right)^{-C} \left(\frac{\partial B}{\partial M} \right) \cdot \left[1 + \left(\frac{\delta_c}{B} \right)^{-C} \right]^{-D-1}. \quad (5.18)$$

In this case, it is easy to check that¹⁴⁶

$$\int_0^\infty dF = 1, \quad (5.19)$$

regardless of the values assumed by the constants C and D (they cancel out in the integration process). Note that although presenting more free parameters than the others distributions considered before, the resulting PS approach based on the Burr distribution satisfies the normalization condition. This unexpected property suggests that the Burr distribution may provide a convenient description of the physics behind the structure formation process. In this case, the fraction of the critical density reads

$$\Omega_{(M)Burr} = \frac{dF_{(M)}}{d(\ln M)} = CD \left| \frac{\partial (\ln B)}{\partial (\ln M)} \right| \nu^{-c} \left[1 + \nu^{-c} \right]^{-D-1}. \quad (5.20)$$

In Fig.(5.2) we show the fraction of critical density contributed by bound structures of mass M . In both panels the upper and lower solid curves are the corrected PS (factor 2), and the uncorrected PS curves, respectively. The long dashed, dashed and dotted curves in left panel are obtained using the PL distribution. In the right panel we compare the behavior using the Burr distribution (the dashed and long dashed curves) with that using the PS (solid lines) and PL (dotted line) ones. We see clearly that the Burr distribution is a possible viable function to describe the primordial density field, having the great advantage of the correct normalization¹⁴⁶.

A more detailed study involving physical applications of the Burr distribution, as a possible non-Gaussian distribution describing the initial density fluctuations, is still

lacking. Here we limit ourselves to point out its powerful mathematical appeal concerning the normalization of the dF derived function. Some additional consequences will be discussed elsewhere.

5.6 Nongaussian effects on the σ_8 - Ω_m plane

In the last years, the original PS approach starts to fail in fitting very well the new massive N-body simulation results and the most recent observational data. Particularly in the case of an x-ray flux-limited sample of galaxy clusters, based on the ROSAT All-Sky Survey (hereafter HIFLUGCS), referenced in the paper of Reiprich & Boehringer¹⁵⁶ (hereafter Reiprich), we note that using the PS approach with this data we get as best-fit mass parameter an Ω_m equals to 0.12 (which is very low compared with the nowadays independent CMB results of around 0.27^{120,163,164}), and we have also a σ_8 parameter of 0.96, which is very high based in the most up to date WMAP data¹⁶⁴.

We already proposed¹³⁹ an alternative approach to compute the mass function of galaxy clusters, consisting on a power law distribution (hereafter PL, for “Power Law”), which parameterizes the PS formalism; simple as PS and having a free parameter q which could be used to better fit the recent numerical simulated data. We also proposed an study of the normalization problem¹⁴⁶ showing that it depends of the distribution chosen (as the Gaussian or our PL one).

We will show that our PL formalism fits very well the HIFLUGCS data allowing at the same time cosmological parameters compatible with all other independent measurements in the literature, even taking account of dark energy models¹²⁷. We will also show that our PL approach can be useful to constrain cosmological parameters as well.

5.6.1 The Theoretical PS Model used with the HIFLUGCS Data

A new X-ray selected and X-ray flux-limited galaxy cluster sample is presented. Based on the ROSAT All-Sky Survey the 63 brightest clusters have been compiled. Gravitational masses have been determined utilizing intracluster gas density profiles, derived mainly from ROSAT PSPC pointed observations, and gas temperatures, as published mainly

from ASCA observations, assuming hydrostatic equilibrium. This sample and an extended sample of 106 galaxy clusters is used to establish the X-ray luminosity–gravitational mass relation. From the complete sample the galaxy cluster mass function is determined and used to constrain the mean cosmic matter density and the amplitude of mass fluctuations.

Having determined the integrated mass as a function of radius, a physically meaningful fiducial radius for the mass measurement has to be defined. The radii commonly used are either the Abell radius, r_{200} , or r_{500} . The Abell radius is fixed at $r_A \equiv 3 h_{50}^{-1}$ Mpc. The radius r_{200} (r_{500}) is the radius within which the mean gravitational mass density $\langle \rho_{\text{tot}} \rangle = 200$ (500) ρ_c . The critical cosmic matter density is defined as $\rho_c \equiv 3 H^2 / (8 \pi G)$, where $H^2 = H_0^2 E(z)^2$ and $E(z) = [\Omega_m(1+z)^3 + \Omega_k(1+z)^2 + \Omega_\Lambda]^{1/2}$. It has been shown that a correction for redshift is not necessary for the nearby clusters included in HIFLUGCS¹²⁸ and we use the zero redshift value for all calculations, i.e. $\rho_c = 4.6975 \times 10^{-30} \text{ g cm}^{-3}$, unless noted otherwise.

In order to treat clusters of different size in a homogeneous way we determine the cluster mass at a characteristic density but also give the mass determined formally at a fixed radius for comparison. Spherical collapse models predict a cluster virial density $\langle \rho_{\text{vir}} \rangle \approx 178 \rho_c$ for $(\Omega_m = 1, \Omega_\Lambda = 0)$, so a pragmatic approximation to the virial mass is to use r_{200} as the outer boundary. The most accurate results are expected for $M_{\text{tot}}(< r_{500}) \equiv M_{500}$, but for a comparison to predicted mass functions M_{200} is the more appropriate value¹⁵⁶.

We use the standard formalism based on the Press–Schechter (PS) prescription to predict cluster mass functions for given cosmological models (see, e.g.,¹²²). The mass function is then given by^{154,121}(see, e.g.,¹⁵⁷ for a compilation of published extensions of the PS mass function)

$$\frac{dn(M)}{dM} = \sqrt{\frac{2}{\pi}} \frac{\bar{\rho}_0}{M} \frac{\delta_c(z)}{\sigma(M)^2} \left| \frac{d\sigma(M)}{dM} \right| \exp \left(-\frac{\delta_c(z)^2}{2\sigma(M)^2} \right). \quad (5.21)$$

Here M represents the halo (cluster) virial mass and $\bar{\rho}_0 = 2.7755 \times 10^{11} \Omega_m h_{100}^2 M_\odot \text{ Mpc}^{-3}$ is the present day mean matter density. The linear overdensity computed at present $\delta_c(z) = \delta_c v(z) D(0) D(z)^{-1}$, where the linear overdensity at the time of virialization, $\delta_c v(z)$, is computed using the spherical collapse model summarized in¹³⁶, for $\Omega_m = 1$ using (A2) and for $\Omega_m < 1 \wedge \Omega_k = 0$ using (A6,7); the linear growth factor $D(z) = 2.5 \Omega_m E(z) \int_z^\infty (1+z') E(z')^{-3} dz'$ and $E(z)$ has been defined above. As mentioned earlier

due to the low redshift range spanned by HIFLUGCS, the effect of a redshift correction is very small and we therefore set $z = 0$ for all calculations, unless noted otherwise. The variance of the cosmic mass density fluctuations is

$$\sigma(M)^2 = \sigma_8^2 \frac{\int_0^\infty k^{2+n} T(k)^2 |W(k R(M))|^2 dk}{\int_0^\infty k^{2+n} T(k)^2 |W(k 8 h_{100}^{-1} \text{Mpc})|^2 dk}, \quad (5.22)$$

where σ_8 represents the amplitude of density fluctuations in spheres of radius $8 h_{100}^{-1}$ Mpc. Recent measurements of the cosmic microwave background (CMB) anisotropies indicate that the primordial power spectral index, n , has a value close to $1^{117,133}$ and is therefore set to 1, unless noted otherwise. For the transfer function we use the fitting formula for Cold Dark Matter (CDM) cosmologies provided by¹¹⁸ for $q(k) = k/(\Gamma h_{100} \text{Mpc}^{-1})$

$$T(k) \equiv T(q(k)) = \ln(1 + 2.34q)/(2.34q) \\ \times [1 + 3.89q + (16.1q)^2 + (5.46q)^3 + (6.71q)^4]^{-1/4}, \quad (5.23)$$

where the shape parameter is given by (modified to account for a small normalized baryon density $\Omega_b > 0$,¹⁶⁵)

$$\Gamma = \Omega_m h_{100} \left(\frac{2.7 \text{K}}{T_0} \right)^2 \exp \left(-\Omega_b - \sqrt{\frac{h_{100}}{0.5}} \frac{\Omega_b}{\Omega_m} \right). \quad (5.24)$$

The temperature of the CMB $T_0 = 2.726 \text{K}^{147}$ and $\Omega_b h_{100}^2 = 0.0193^{123}$, for the latter equation and (5.24) $h_{100} = 0.71$ has been used¹⁴⁹. The comoving filter radius $R(M) = [3M/(4\pi\bar{\rho}_0)]^{1/3}$ for the top hat filter function $W(x) = 3(\sin x - x \cos x)/x^3$ is adopted in this analysis, because the HIFLUGCS masses have been determined with a top hat filter, too. Since the PS recipe as outlined above assumes virial masses based on the spherical collapse model we use M_{200} as approximation to the virial mass.

For the modeling to be independent of the precise knowledge of the L_X - M_{tot} relation the quantitative comparison has been performed using a standard χ^2 procedure on the differential binned mass function given in Fig. 5.3 (rather than using a maximum likelihood approach on the mass distribution). After identifying the crude position where χ^2 is minimal in a large Ω_m - σ_8 parameter space region the χ^2 values have been calculated in a fine grid of 200 by 200 Ω_m - σ_8 values in the range $0.05 \leq \Omega_m \leq 0.26$ and $0.65 \leq \sigma_8 \leq 1.30$. A flat cosmic geometry has been assumed, i.e. $\Omega_m + \Omega_\Lambda = 1$. The cosmological constant enters the calculation only through δ_c , however, and therefore has

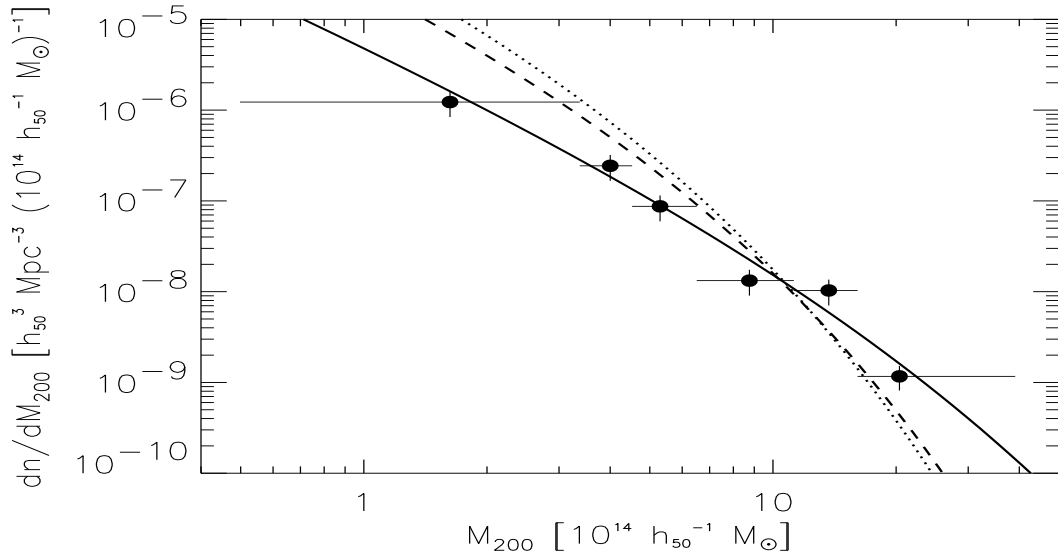


Figure 5.3: HIFLUGCS mass function compared to the best fit model mass function with $\Omega_m = 0.12$ and $\sigma_8 = 0.96$ (solid line). Also shown are the best fit model mass functions for fixed $\Omega_m = 0.5$ ($\Rightarrow \sigma_8 = 0.60$, dashed line) and $\Omega_m = 1.0$ ($\Rightarrow \sigma_8 = 0.46$, dotted line).

a negligible influence here. The minimum and statistical error ellipses for some standard confidence levels (c.l.) are given in Fig. 5.4. The tight constraints obtained show that with HIFLUGCS we can go beyond determining an Ω_m - σ_8 relation and put limits on Ω_m and σ_8 individually. It is found that

$$\Omega_m = 0.12_{-0.04}^{+0.06} \quad \text{and} \quad \sigma_8 = 0.96_{-0.12}^{+0.15} \quad (5.25)$$

(90% c.l. statistical uncertainty for two interesting parameters), indicating a relatively low value for the density parameter. In Fig. 5.3 we also plot the best fit model mass functions for given $\Omega_m = 0.5$ and $\Omega_m = 1.0$ and one notes immediately that these value pairs give a poorer description of the shape of the mass function.

We have also tested whether or not the recently found deviations of the PS formalism compared to large N -body simulations^{130,135} have a significant influence on the results obtained here. We have compared the best fit PS model ($\Omega_m = 0.12$, $\sigma_8 = 0.96$) to the model obtained using the ‘universal’ mass function (fit to N -body simulations,¹³⁵) for the same parameter values. These two models agree well for $M \leq 10^{15} h_{50}^{-1} M_{\odot}$. The differences become larger than the size of the Poissonian error bars (Fig. 5.3) for

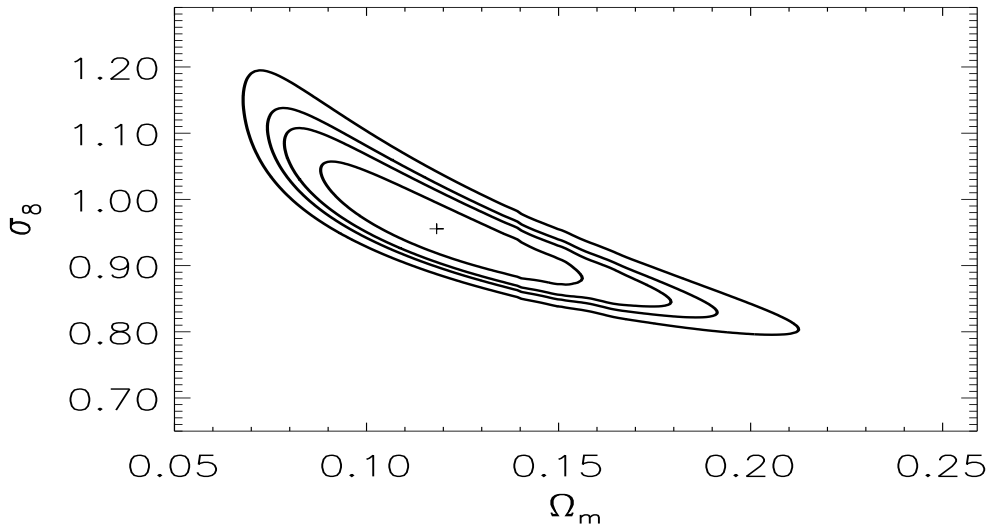


Figure 5.4: Statistical confidence contours for the χ^2 procedure. The cross indicates the position of the minimum, χ^2_{\min} . Ellipses indicate the 68 %, 90 %, 95 %, and 99 % confidence levels for two interesting parameters, i.e. $\Delta\chi^2 \equiv \chi^2 - \chi^2_{\min} = 2.30, 4.61, 6.17,$ and $9.21,$ respectively.

$M \geq 2 \times 10^{15} h_{50}^{-1} M_{\odot}$, in the sense that the Jenkins mass function¹³⁵ predicts higher cluster abundances than PS. For larger values of Ω_m the differences become comparable to the size of the error bars at lower masses, e.g., for $\Omega_m = \sigma_8 = 0.5$ around $M \sim 5 \times 10^{14} h_{50}^{-1} M_{\odot}$. To estimate the influence of these differences on the best fit values derived using the PS mass function, we adjusted the parameter values of the Jenkins model to reproduce the PS mass function, finding $\Omega_m = 0.15$ and $\sigma_8 = 0.86$. The value for Ω_m becomes slightly larger but the combination of both values is still contained within the 90 % error ellipse. We therefore conclude that the differences between the model mass functions do not significantly affect the interpretation of the HIFLUGCS mass function. Moreover we regard this test as confirmation of the validity of the PS mass function for the accuracy needed here.

5.6.2 The Power Law Model fitting the HIFLUGCS Data

In Reiprich¹⁵⁶ a compilation of the HIFLUGCS data (an x-ray flux limited galaxy cluster sample based on the ROSAT data, as described before) is accomplished. The mass func-

tion from this observational data was compared with that of the theoretical PS approach. Reiprich performs then a standard χ^2 procedure and finds the best fit parameters

$$\Omega_m = 0.12^{+0.06}_{-0.04} \quad \text{and} \quad \sigma_8 = 0.96^{+0.15}_{-0.12} \quad (5.26)$$

We see that Ω_m is very low, completely out of range, compared with the nowadays independent CMB results^{120,163,164}, and the σ_8 is very high, also out of the limit, based in the most up to date WMAP data¹⁶⁴,

$$\Omega_m = 0.234^{+0.035}_{-0.035} \quad \text{and} \quad \sigma_8 = 0.76^{+0.05}_{-0.05} \quad (5.27)$$

Tabela 5.1: Power Law Λ CDM Model Parameters and 68% Confidence Intervals. The Three Year fits in this Table assume no SZ contribution, $A_{SZ} = 0$, to allow direct comparison with the First Year results.

Parameter	First Year	WMAPext	Three Year	First Year	WMAPext	Three Year
	Mean	Mean	Mean	ML	ML	ML
$100\Omega_b h^2$	$2.38^{+0.13}_{-0.12}$	$2.32^{+0.12}_{-0.11}$	2.23 ± 0.08	2.30	2.21	2.23
$\Omega_m h^2$	$0.144^{+0.016}_{-0.016}$	$0.134^{+0.006}_{-0.006}$	0.126 ± 0.009	0.145	0.138	0.128
H_0	72^{+5}_{-5}	73^{+3}_{-3}	74^{+3}_{-3}	68	71	73
τ	$0.17^{+0.08}_{-0.07}$	$0.15^{+0.07}_{-0.07}$	0.093 ± 0.029	0.10	0.10	0.092
n_s	$0.99^{+0.04}_{-0.04}$	$0.98^{+0.03}_{-0.03}$	0.961 ± 0.017	0.97	0.96	0.958
Ω_m	$0.29^{+0.07}_{-0.07}$	$0.25^{+0.03}_{-0.03}$	0.234 ± 0.035	0.32	0.27	0.24
σ_8	$0.92^{+0.1}_{-0.1}$	$0.84^{+0.06}_{-0.06}$	0.76 ± 0.05	0.88	0.82	0.77

The new WMAP estimations above can be summarized, with other cosmological parameters, in the table 5.1, from Ref.¹⁶⁴.

We perform exactly the same Reiprich χ^2 procedure, following the same conditions and general theoretical framework, but instead of using the PS mass function equation we use our PL approach (Equation (5.12), were in the term $\frac{\rho}{M}$, ρ is the present-day mean matter density and M is the halo virial mass). Reiprich uses the PS mass function multiplied by

2 (to correct the normalization), and so we do the same with our PL mass function. As we have two intervals in our approach ($[-1 < q < 1]$ and $[1 < q < 3]$), the results will be presented related to each one.

In the $[-1 < q < 1]$ interval, when we fix $q = 0.93$ and we perform the χ^2 test for $\Omega_m - \sigma_8$ parameters we find as best-fit $\Omega_m = 0.109$ (even lower than using the PS method) and $\sigma_8 = 1.058$, which is higher than the nowadays expected value from CMB data (top of figure 6.9). As we rise the value of q , we get higher Ω_m and lower σ_8 as best-fit parameters (the first 3 panels from top to bottom of fig.6.9), until the maximum interval limit of $q = 1.0$, when we obtain the same PS method parameters, as expected (fig.6.9, bottom panel). As conclusion, the $[-1 < q < 1]$ interval presents even worse cosmological parameters than using the standard PS method.

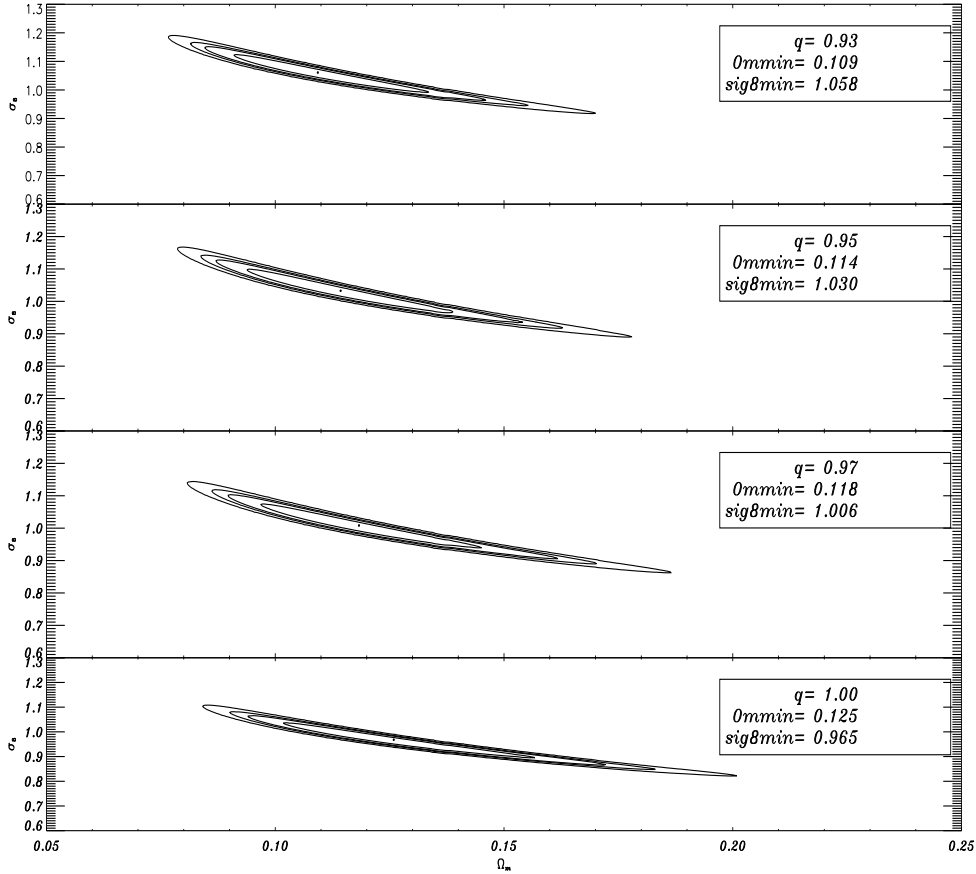


Figure 5.5: The $[-1 < q < 1]$ interval. We fix q and we perform a χ^2 test for $\Omega_m - \sigma_8$ parameters. As we rise the value of q , we get higher Ω_m and lower σ_8 as best-fit, until $q = 1.0$, when we obtain the same PS method result, as expected

Now we analyze the $[1 < q < 3]$ interval. In the figure 6.10 we fix two different values of q , one very close to the inferior interval limit ($q = 1.03$) and the other slightly higher ($q = 1.30$), and we perform the χ^2 test for the $\Omega_m - \sigma_8$ parameters. We note that a slightly variation on q produces huges variation in the two cosmological parameters, and more than that, we fixed the *physical q interval* in the limit $[1.03 \leq q < 1.30]$. In the figure 5.7 we show why our PL method is better than the PS one: in the upper panel, we see Reiprich results (equivalent to our method for $q \rightarrow 1$), and we note that Ω_m is very low here (comparing with independent recent CMB results, as discussed before). As we rise the value of q , we get higher Ω_m and lower σ_8 parameters as best-fit, and the bottom panel show that we can have very good cosmological parameters with the same observational data, only changing the PS method by our PL approach.

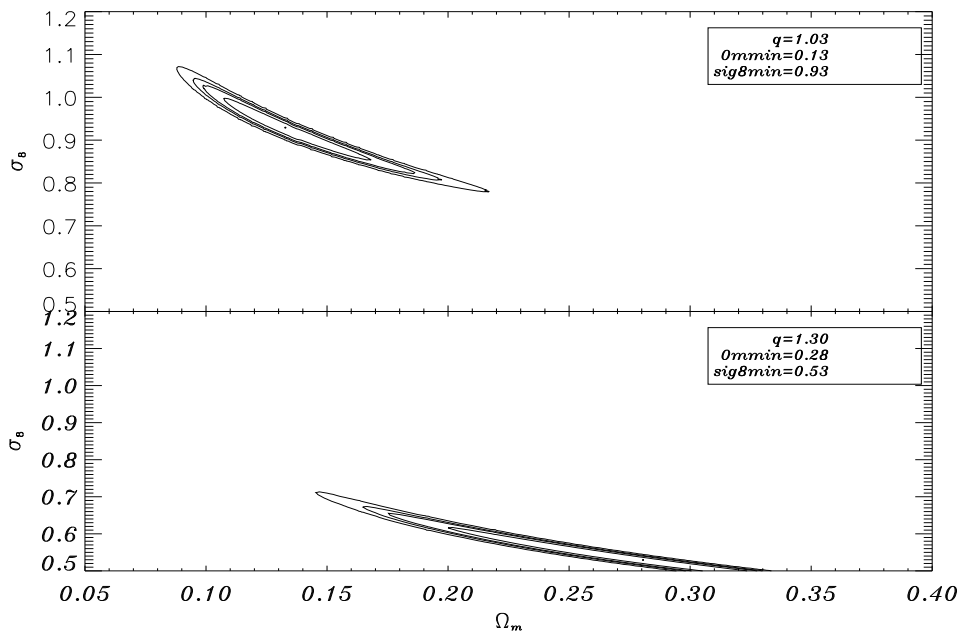


Figure 5.6: The $[1 < q < 3]$ interval. We fix q and we perform a χ^2 test in the $\Omega_m - \sigma_8$ plane. We fix two different values of q , one very close to the inferior interval limit ($q = 1.03$) and the other slightly higher ($q = 1.30$). We note that a slightly variation on q produces huges variation in the two cosmological parameters. We fixed the *physical q interval* in the limit $[1.03 \leq q < 1.30]$.

In the figure 5.8; we fix $\Omega_m = 0.20$ and we perform a χ^2 test in the $q - \sigma_8$ plane; as a result we have a transversal and almost flat statistical contour, showing a linear

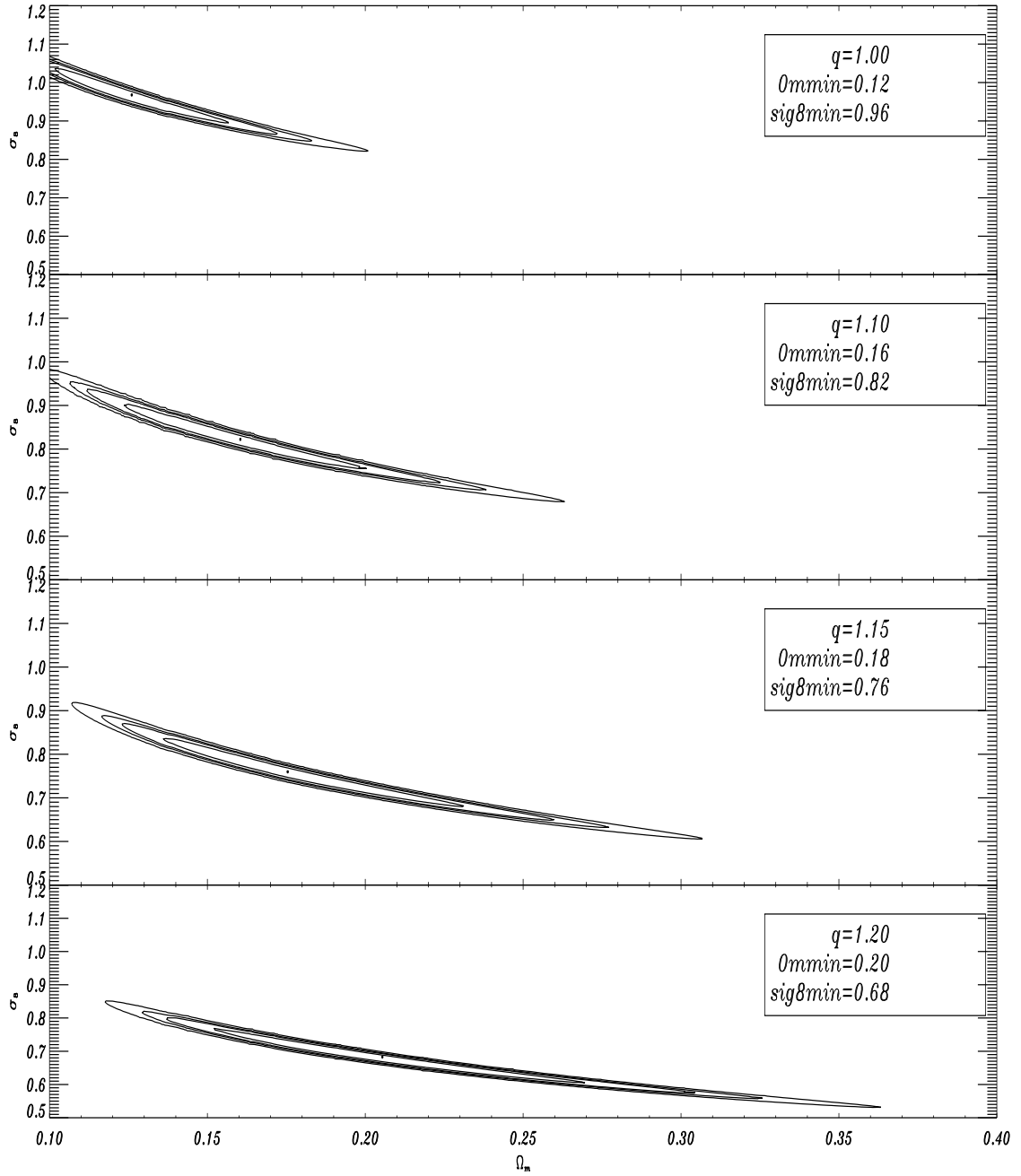


Figure 5.7: In the upper panel, we see Reiprich results (equivalent to our method for $q \rightarrow 1$), which have Ω_m very low (comparing with recent CMB results). As we rise the value of q , we get higher Ω_m and lower σ_8 parameters as best-fit, and the bottom panel show that we can have very good cosmological parameters with the same observational data, only changing the PS method by our PL approach.

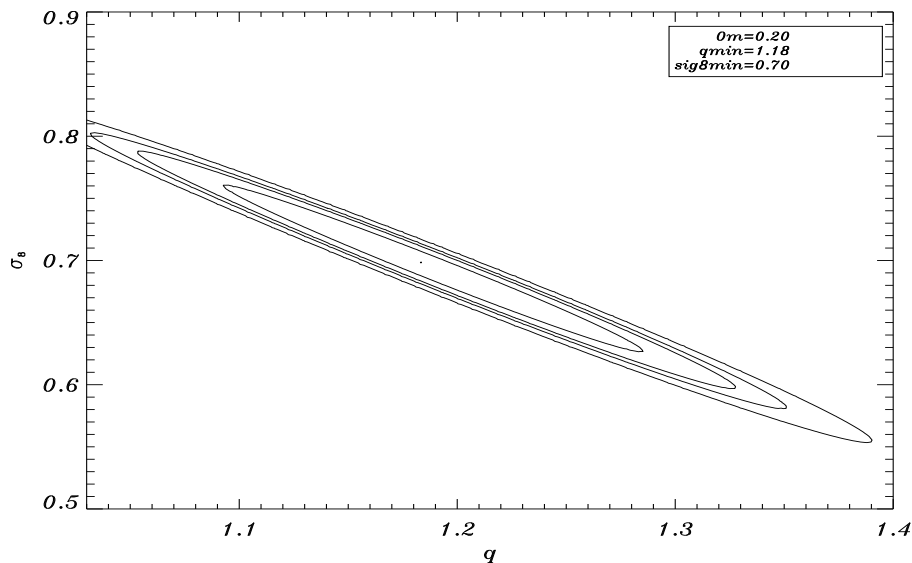


Figure 5.8: We fix Ω_m and we perform a χ^2 test in the $q - \sigma_8$ plane; as a result we have a transversal and almost flat statistical contour, showing a linear dependence between q and σ_8 . We will see the same behavior in the $q - \Omega_m$ plane, fixing σ_8 .

dependence between q and σ_8 . We will see the same behavior in the $q - \Omega_m$ plane, fixing σ_8 .

As another example that shows how our PL approach is powerful to constrain the parameters is given in the figure 5.9; we fix σ_8 and we perform a χ^2 test in the $q - \Omega_m$ plane. In the upper panel, for $\sigma_8 = 0.70$, we get $\Omega_m \sim 0.20$ as best-fit. More we increase σ_8 , more we decrease Ω_m (middle and bottom panels). Only $\sigma_8 \leq 0.70$ gives $\Omega_m \geq 0.20$ (which is a good value accepted nowadays in independent X-Ray or optical mass measurements, and also compatible with CMB data).

When we perform a χ^2 test over all parameters in our model (q , Ω_m and σ_8), we find that with $q = 1.1$, $\Omega_m = 0.16$ and $\sigma_8 = 0.82$ we have the excellent fit to HIFLUGCS data. We can see the $\Omega_m - \sigma_8$ plane of these best-fit parameters in the second pannel (from top to bottom) of figure 5.7, and the approximated $q - \Omega_m$ plane can be seen at the middle pannel of figure 5.9.

In figure 5.9 we fixed $\sigma_8 = 0.70$ and we obtain $\Omega_m = 0.20$ and $q = 0.19$ as best-fit parameters. Only to show how good is this fit applying directly on the HIFLUGCS data, we show figure 5.10. The triangles are the observational binned X-Ray mass function,

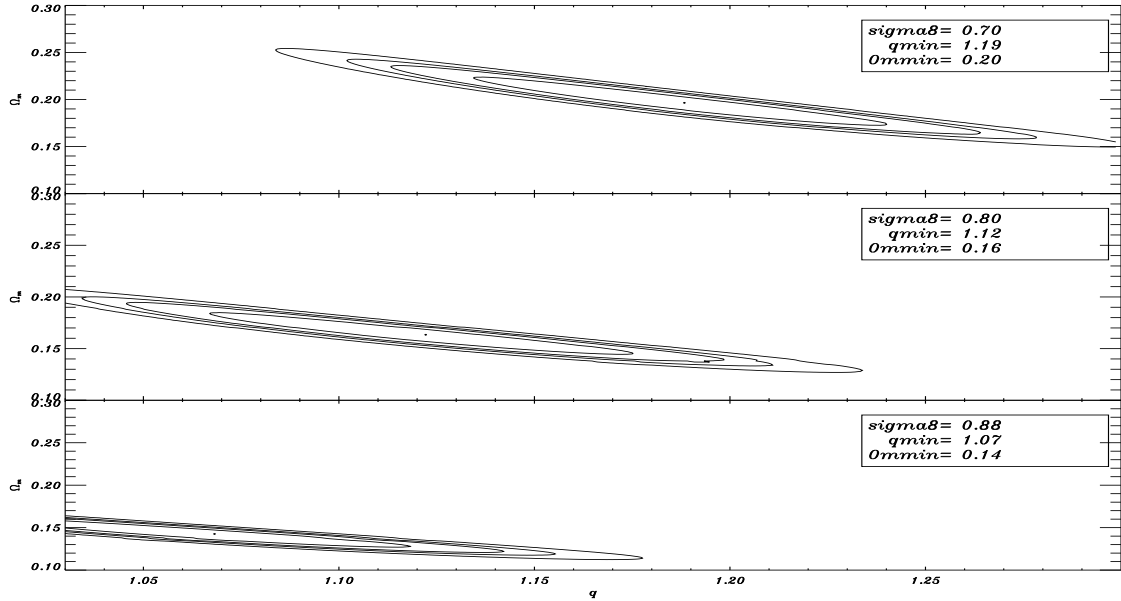


Figure 5.9: Another example that shows how our PL approach is powerful to constrain the cosmological parameters. We fix σ_8 and we perform a χ^2 test in the $q - \Omega_m$ plane. In the upper panel, for $\sigma_8 = 0.70$, we get $\Omega_m \sim 0.20$ as best-fit. More we increase σ_8 , more we decrease Ω_m (middle and bottom panels).

and the lines are the mass function theoretical models (all them using the HIFLUGCS database as points and performing a fitting procedure). The solid line is our PL method with the parameters cited above. The long dashed line is the Reiprich PS procedure with $\Omega_m = 0.12$ and $\sigma_8 = 0.96$ (and we already discussed that the first parameter is very lower and the second one slightly higher than the most recent WMAP CMB data). Only for curiosity, we present the Reiprich PS procedure using our PL best cosmological parameters, which is seen by the dotted line. We easily see here how our PL method is flexible regarding the old PS one.

5.6.3 Dark Energy and Structure Formation

Analysis of the distance-redshift relation using high redshift Type Ia supernovae has led to the discovery that the expansion of the Universe is currently accelerating. This suggests that the dominant contribution to the present-day energy budget is a component with equation of state $w < -1/3$, called “dark energy”. Combining measurements of CMB fluctuations with measurements of the clustering of present day galaxies favour a flat

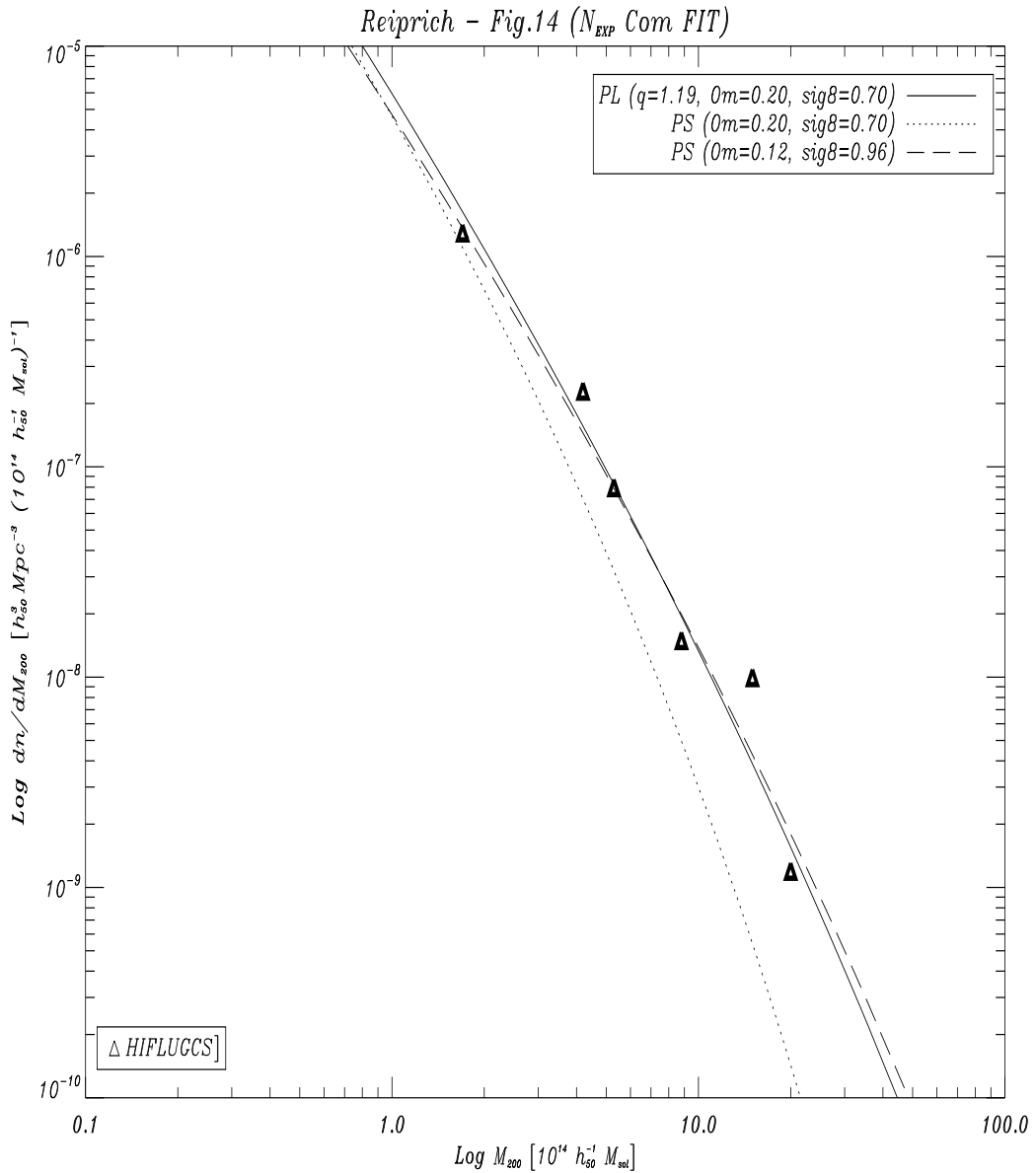


Figura 5.10: The triangles are the observational binned X-Ray mass function, and the lines are the mass function theoretical models (all them using the HIFLUGCS database as points and performing a fitting procedure). The solid line is our PL method with $\sigma_8 = 0.70$ and $\Omega_m = 0.20$. The dotted line is the PS approach with the same parameters. The long dashed line is the Reiprich results : the PS method with $\Omega_m = 0.12$ and $\sigma_8 = 0.96$ (the first parameter is very lower and the second one slightly higher than the most recent WMAP CMB data).

Universe with $\Omega_M \simeq 0.3$, with the remaining contribution made up of dark energy.

The nature of the dark energy is the source of much debate. Perhaps the most straightforward candidate is a positive cosmological constant Λ with equation of state parameter $w = -1$. This simple picture forms a special case in a broader class of models where the dark energy is the manifestation of a scalar field slowly rolling down its potential. In the limit of a completely flat potential, these models lead to $w = -1$ ¹⁵⁵.

If the dark energy equation of state only varies slowly with time, then observational predictions are well approximated by treating $w(a) = w$ as a constant¹⁶⁸.

The equation of state for the dark energy does not uniquely define the behaviour of this component. The formation of structure is also dependent on the sound speed of the dark energy which limits its clustering properties. In the original formalism for quintessence^{125,126}, the dark energy component has a high sound speed which means that it can cluster on the largest scales, but does not cluster on the scales of galaxy clusters and below.

Consequently, the dark energy only affects the matter power spectrum and the CMB anisotropies on very large scales. For the special case of a cosmological constant, $w = -1$, the clustering of the dark energy is not an issue as the energy density in perturbations always remains at the background level. Obviously, for $w \neq -1$, the clustering properties of the dark energy strongly affect the build-up of structure in the Universe. In particular for spherical perturbations, the linear growth rate, critical overdensity for collapse, and details of subsequent behaviour and virialisation are all dependent on this property. In this section we follow the majority of current literature and only consider a non-clustering dark energy component. However, we do note that models in which the dark energy clusters on small scales are being discussed with increasing frequency^{132,145}.

For the variables used in this section, if no dependence is quoted for a given quantity (e.g. Ω_M), it should be assumed to be calculated at present day. If instead explicit dependence is given (e.g. $\Omega_M(a)$), the quantity is assumed to vary with epoch. We additionally assume that $w(a) = w$ is constant in time.

It is assumed that the dark energy has an equation of state relating its pressure p_X and density ρ_X given by $p_X = w(a)\rho_X$. For general $w(a)$, the dynamical expansion of the

Universe is specified by the Friedmann equation

$$E^2(a) = \frac{H^2(a)}{H_0^2} = \Omega_M a^{-3} + \Omega_K a^{-2} + \Omega_X a^{f(a)}, \quad (5.28)$$

where $\Omega_K \equiv (1 - \Omega_M - \Omega_X)$ is the curvature constant, $H(a) \equiv \dot{a}/a$ is the Hubble parameter with present day value H_0 . $f(a)$ is calculated by solving the conservation of energy equation for the dark energy $d(\rho_X a^3)/da = -3p_X a^2$ (Ref.¹²⁶), giving $\rho_X \propto a^{f(a)}$, where

$$f(a) = \frac{-3}{\ln a} \int_0^{\ln a} [1 + w(a')] d \ln a'. \quad (5.29)$$

For constant w , $f(a) = -3(1 + w)$. The evolution of the matter density $\Omega_M(a)$ and dark energy density $\Omega_X(a)$ are given by

$$\Omega_M(a) = \frac{\Omega_M a^{-3}}{E^2(a)}, \quad \Omega_X(a) = \frac{\Omega_X a^{f(a)}}{E^2(a)}. \quad (5.30)$$

Considering the behaviour of homogeneous spherical perturbations provides one of the most simple models for the formation of structure in the Universe. The behaviour of an homogeneous sphere of uniform density can itself be modelled using the same equations discussed until now. One of the important applications of the spherical perturbation model is the derivation of the linear growth rate. The application proceeds as follows: We consider two spheres containing equal amounts of material, one of background material with radius a , and one of radius a_p with a homogeneous change in overdensity. Henceforth quantities with a subscript p refer to the perturbation, while no subscript relates to the background. The densities within the spheres are related to their radii, with

$$\rho_p a_p^3 = \rho a^3, \quad \delta \equiv \rho_p / \rho - 1, \quad (5.31)$$

giving, to first order in δ ,

$$a_p = a(1 - \delta/3). \quad (5.32)$$

The cosmological equation for both the spherical perturbation and the background is¹⁵²

$$\frac{1}{a} \frac{d^2 a}{dt^2} = -\frac{H_0^2}{2} \left[\Omega_M a^{-3} + [1 + 3w(a)] \Omega_X a^{f(a)} \right], \quad (5.33)$$

where a should be replaced by a_p in the matter density term for the perturbation. The dark energy density $\rho_X \propto a^{f(a)}$, is the same for both the perturbation and the background

if the dark energy does not cluster. Because of this, substituting Eqns(5.31) & (5.32) into this equation gives, to first order in δ ,

$$\frac{3}{2}\Omega_M H_0^2 a^{-3} \delta = \frac{d^2 \delta}{dt^2} + \frac{2}{a} \frac{da}{dt} \frac{d\delta}{dt}. \quad (5.34)$$

Changing variables from t to a gives

$$\begin{aligned} \frac{3}{2}\Omega_M a^{-3} \delta &= \frac{d^2 \delta}{da^2} E^2(a) a^2 + \frac{d\delta}{da} \left\{ 2a E^2(a) \right. \\ &\quad \left. - \frac{a}{2} \left[\Omega_M a^{-3} + [3w(a) + 1] \Omega_X a^{f(a)} \right] \right\}, \end{aligned} \quad (5.35)$$

which can be further simplified to give

$$\begin{aligned} \frac{3}{2}\Omega_M(a) &= \frac{d^2 \ln \delta}{d \ln a^2} + \left(\frac{d \ln \delta}{d \ln a} \right)^2 + \frac{d \ln \delta}{d \ln a} \left\{ 1 \right. \\ &\quad \left. - \frac{1}{2} \left[\Omega_M(a) + [3w(a) + 1] \Omega_X(a) \right] \right\}. \end{aligned} \quad (5.36)$$

This is the generalisation of Equation B7 in Ref.¹⁶⁷ to non-flat cosmologies, and is valid for general $w(a)$.

Eq.(5.36) can easily be solved by numerical integration. For Λ cosmologies, the growing mode solution to this equation is⁴⁷

$$D(a) = \frac{5\Omega_M}{2} E(a) \int_0^a \frac{da'}{[a' E(a')]^3}, \quad (5.37)$$

where $E(a)$ is given by Eq.(5.28). Although this integral can be easily solved numerically, it is common to use the approximation of Carrol *et al.*⁴⁵,

$$\begin{aligned} D(a) &\simeq \frac{5\Omega_M(a)a}{2} \left[\Omega_M(a)^{4/7} - \Omega_\Lambda(a) \right. \\ &\quad \left. + \left(1 + \frac{\Omega_M(a)}{2} \right) \left(1 + \frac{\Omega_\Lambda(a)}{70} \right) \right]^{-1}. \end{aligned} \quad (5.38)$$

A general solution for the growing mode solution in dark energy cosmologies, equivalent to Eq.(5.37), has yet to be found. However, for flat cosmological models, with constant w , the solution can be written in terms of the hypergeometric function ${}_2F_1$ ¹⁶¹

$$D(a) = a {}_2F_1 \left[-\frac{1}{3w}, \frac{w-1}{2w}, 1 - \frac{5}{6w}, -a^{-3w} \frac{1 - \Omega_M}{\Omega_M} \right]. \quad (5.39)$$

Writing the growth index as

$$\frac{d \ln \delta}{d \ln a} = \Omega_M^\alpha(a), \quad (5.40)$$

Wang and Steinhardt¹⁶⁷ use Eq.(5.36) for the special case of flat cosmologies to give

$$\alpha \simeq \frac{3}{5 - w/(1 - w)} + \frac{3}{125} \frac{(1 - w)(1 - 3w/2)}{(1 - 6w/5)^3} [1 - \Omega_M(a)]. \quad (5.41)$$

This led Basilakos¹¹⁹ to extend the approximation of Carrol *et al.*⁴⁵ given by Eq.(5.38) to the case of $w \neq -1$

$$D(a) \simeq \frac{5\Omega_M(a)a}{2} [\Omega_M(a)^\alpha - \Omega_X(a) + \left(1 + \frac{\Omega_M(a)}{2}\right) (1 + A\Omega_X(a))]^{-1}, \quad (5.42)$$

with α given by Eq.(5.41), and $A \simeq 1.742 + 3.343w + 1.615w^2$. In Fig. 5.11 we plot the A values required to match Eq.(5.42) to the true linear growth factor (given by Eq.(5.39)), for flat cosmological models with $0.1 < \Omega_M < 0.9$ as a function of w (grey lines). The fit of Basilakos¹¹⁹ is shown by the dashed line. This is a poor fit for $w < -1$, so instead, Percival¹⁵² propose

$$A = \frac{-0.28}{w + 0.08} - 0.3, \quad (5.43)$$

shown by the black line in Fig. 5.11.

Eq.(5.43) has been determined by fitting to flat cosmological models with $0.1 < \Omega_M < 0.9$. For non-flat models, the approximation of Eq.(5.42) remains a good fit. The fitting formula fails for $\Omega_M \ll 0.1$, but for $\Omega_M > 0.1$, the maximum error (with $0 < \Omega_X < 1$) is 3.8% for $w = -4/3$, 2.6% for $w = -1$ and 5.1% for $w = -2/3$. For comparison, the fitting formula of Carrol *et al.*⁴⁵ given by Eq.(5.38) is accurate to 2.1% for $w = -1$ over this range of Ω_M .

We now will show the critical overdensity for collapse of homogeneous spherical perturbations at present day in a homogeneous dark energy background. The method adopted is a development of that in Ref.¹⁵³, where the critical overdensity in Λ cosmologies was calculated. Solution schemes for an Einstein-de Sitter cosmology, for open cosmologies and for flat Λ cosmologies were summarised in Ref.¹³⁶.

We consider again two spheres containing equal amounts of material: one of background material with radius a , and one of radius a_p with a homogeneous change in overdensity.

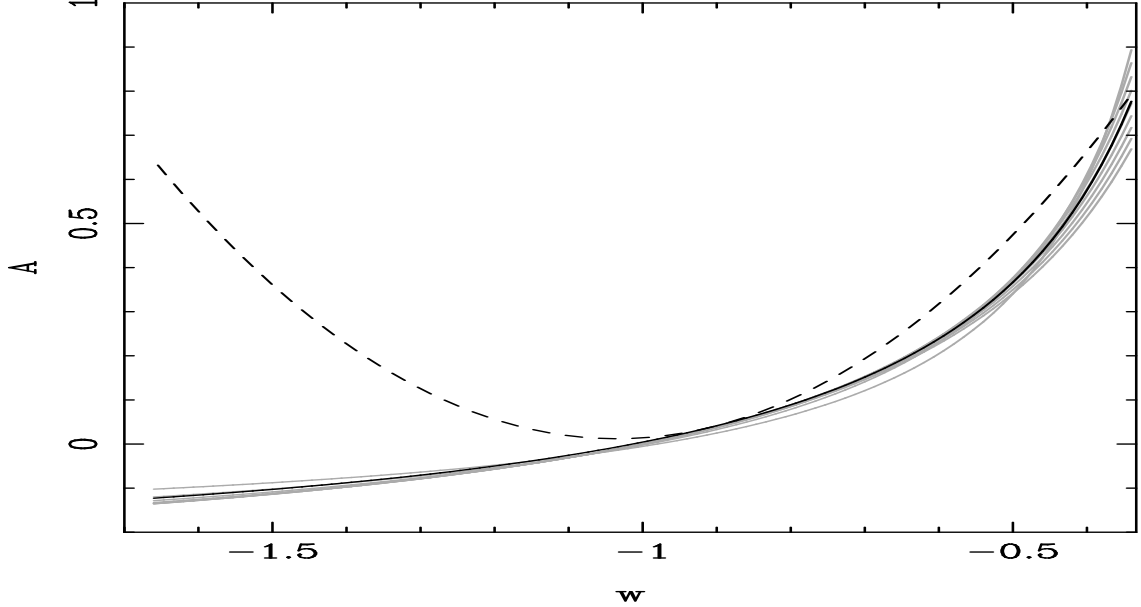


Figure 5.11: Plot showing the true value of A in Eq. 5.42 as a function of w for 9 flat cosmologies with Ω_M evenly spread between 0.1 and 0.9 (grey lines). For comparison we plot the fitting formula of¹¹⁹ (dashed line) and for Eq. 5.43 (black line).

If $\Omega_\Lambda = 0$, for an Einstein-de Sitter cosmology, the critical overdensity for collapse at present day reduces to

$$\delta_{\text{EdS}} \equiv \frac{3}{20}(12\pi)^{2/3} \simeq 1.686, \quad (5.44)$$

which was first derived by¹³¹.

The evolution of the critical overdensity for collapse $\delta_c(a)$, is usually defined as follows: for a cosmological model with parameters Ω_M & Ω_X , $\delta_c(a)$ gives the overdensity for a perturbation that collapses at scale factor a , normalised at present day. For example if we had a density field (and associated power spectrum) normalised at present day, then $\delta_c(a)$ (where a does not necessarily equal 1) relates to spherical perturbations in this density field that collapse at scale factor a . δ_c is the particular case for perturbations that collapse at present day: perturbations that collapse earlier obviously have to be significantly more overdense.

The rather weak evolution of the critical overdensity as a function of cosmological model, means that the linear growth factor can be used to approximate $\delta_c(a)$: If δ_c is constant along a particular cosmological track then the evolution of $\delta_c(a)$ is purely driven by $D(a)^{-1}$ (Ref.¹⁵²). The only change in $\delta_c(a)$ between two collapse times is caused by the

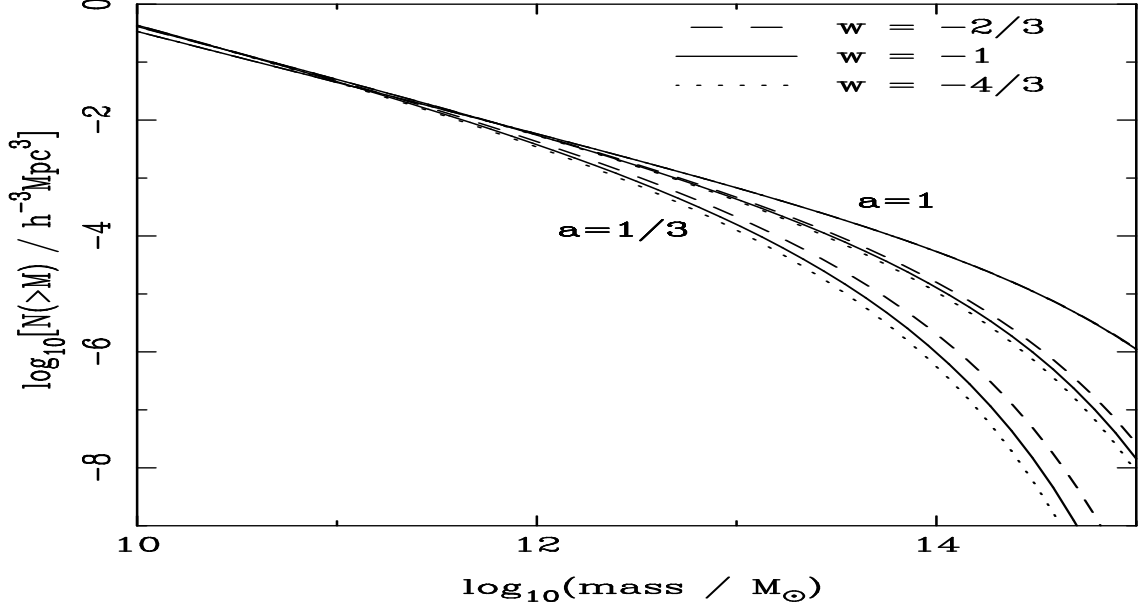


Figure 5.12: Plot showing the predicted mass function calculated using the fitting formula of Sheth & Tormen¹⁵⁸ calculated for $\Omega_M = 0.3$, $\Omega_X = 0.7$ for three different values of w , and at three epochs corresponding to $a = 1/3, 1/2, 1$. Because the power spectrum is normalized at present day, and δ_c is only weakly dependent on cosmology, then there is little difference between the predicted mass functions for $a = 1$. As we go further back in time the difference becomes more severe because of the differing linear growth factors.

change in overall normalisation of the field. The most obvious choice for the normalisation is δ_{EdS} , so the approximation will be correct in the limit as $a \rightarrow 0$, given¹⁵²

$$\delta_c(a) \simeq \frac{D_0}{D(a)} \delta_{\text{EdS}}. \quad (5.45)$$

The error in using the Einstein-de Sitter critical overdensity is of the same order as the error in the approximation of using the fitting formula of Eq.(5.42).

Ma *et al.*¹⁴⁴ considered the effect of quintessence on the mass transfer function. They provided fitting formulae for the ratio between the quintessence and Λ cosmologies. However, if the dark energy only clusters on very large scales, the transfer function is only altered on these scales. If the power spectrum is normalized to σ_8 (the rms density fluctuation on scales of $8 h \text{ Mpc}^{-1}$), then the scales usually of interest are not affected¹⁴¹.

To demonstrate the effect of the dark energy equation of state on the mass function, Percival¹⁵² plotted the cumulative mass function $N(> M)$, calculated using the numerical fit of Sheth & Tormen¹⁵⁸ for 3 different cosmologies and 3 different epochs in Fig. 5.12.

The critical overdensity for collapse for $w = -2/3, -1$ & $-4/3$ and $\Omega_X = 0.7$ was then calculated for $a = 1/3, 1/2, 1$, corresponding to redshifts $z = 2, 1, 0$. As expected, because the critical overdensity for collapse is only weakly dependent on cosmological parameters, at $a = 1$ (the epoch at which the power spectrum is normalized) we see very little difference in the predicted mass functions for different cosmologies. If the normalization of the power spectrum had been constrained at a different epoch (for example by CMB fluctuations), then this would not be correct. The evolution of the mass function is strongly dependent on w because of the effect on the evolution of $\delta_c(a)$ through the linear growth factor. Consequently, determining the mass function at redshifts other than that used to normalize the power spectrum offers a stronger possibility of measuring $w(a)$.

We expect to study the dark energy in the structure formation applying observational data in the process. We use then the same PS formalism using the HIFLUGCS X-Ray data already presented in the section 5.6.1, but with the evolution of critical density given by Eq.(5.45), so accounting for the dark energy inside the PS approach. We summarize our results in Fig. 5.13.

One of our goals in the near future is to accomplish a meaningful and detailed analysis of the dark energy in the structure formation process, using the Eq.(5.45) for the evolution of critical density, and applying a PS method with our PL distribution on the observational data of the HIFLUGCS X-Ray catalog, as showed in the section 5.6.2. The intrinsic problem of this procedure is the high number of free parameters, as the w in the dark energy equation of state and the q parameter of our PL distribution. But a detailed and comparative study could broke the possible degenerencies in the cosmological parameters.

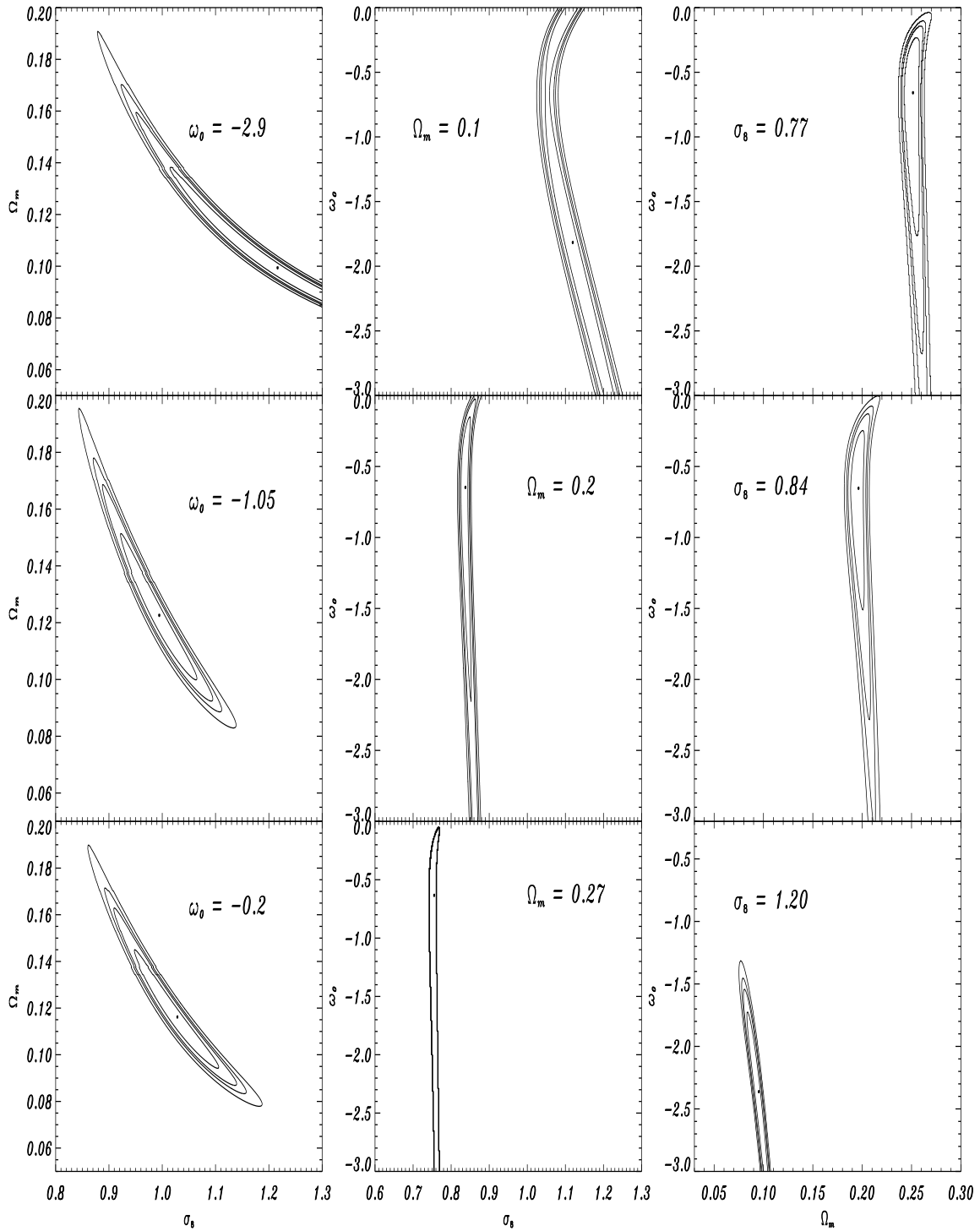


Figure 5.13: We use the PS formalism with the HIFLUGCS X-Ray data already presented in the section 5.6.1, but with the evolution of critical density given by Eq.(5.45), so accounting for the dark energy inside the PS approach.

COSMOLOGIA NÃO-EXTENSIVA E TRATAMENTOS DE DADOS

6.1 Bremsstrahlung from a Nonextensive Maxwellian Gas

Clusters of galaxies are the most massive bound systems in the Universe. They are luminous X-ray sources, with X-ray luminosity ranging from $10^{43} - 10^{46}$ ergs $^{-1}$, and typical sizes of 1 – 3 Mpc. For this reason, they are fair samples of the universe, and represent well properties like mass and baryon fractions of the universe^{171,223,199}. The great volumes of space between galaxies in clusters of galaxies are filled with a hot, diffuse plasma, with typical temperatures of $T \sim 10^7 - 10^8$ K. The X-ray emission of the intracluster medium (ICM) gas is primarily caused by Bremsstrahlung (free-free radiation).

Nowadays, there are increasing difficulties when we try to fit observational data with pure thermal bremsstrahlung models. With temperatures above 20 KeV, the X-ray spectrum show an excess that is not fitted by the thermal bremsstrahlung (Coma, Abell 2199 and others clusters), but have been fitted by power-law spectra, compelling to the investigation of alternatives to X-ray spectra models^{177,175,178}. The physical origin of these tails, however, is not well known until now^{176,174}.

Several nonthermal bremsstrahlung mechanisms in clusters of galaxies has been studied: Liang and collaborators¹⁸² proposed that the synchrotron-emitting relativistic electrons are accelerated in situ from the vast pool of thermal electrons producing a popula-

tion of suprathermal electrons responsible for the excess of hard X-ray emission through bremsstrahlung; Timokhin *et al.*¹⁸⁵ have suggest a new model assuming that the “non-thermal” excess is due to synchrotron radiation of ultra-relativistic (multi-TeV) electrons of “photonic” origin; Dogiel¹⁷³ show that in the case of in-situ acceleration of particles from the thermal pool, the hard X-rays in the range of Beppo-SAX observations (30-80 keV) are generated by bremsstrahlung radiation of thermal particles with the Maxwellian spectrum distorted by the acceleration; Enßlin *et al.*¹⁷⁶ believe that their origin could be due to an inverse-Compton (IC) emission by relativistic electrons.

Nonextensive effects in the fields of thermodynamics and statistical mechanics has been invoked as a possible generalization of entropy for the systems when the standard approach is not valid^{93,181}. We saw in Chapter 4 that, inspired on such problems, Tsallis⁷⁶ proposed a remarkable q -parameterized nonextensive entropic expression which reduces to the extensive Gibbs-Jaynes-Shannon entropy in the limiting case $q = 1$. We also saw in Chapter 4 that the generalized entropy indicate possibilities of association with systems presenting long range interactions (Coulombian and gravitational fields for which the additivity of the entropy is not applied), or presenting long duration memory or phase space with fractal structure. Nowadays a lot of work in cosmology treats the nonextensive approach as a real and even better possibility to many phenomena^{139,180}. Recent efforts on the fundamentals of kinetic theory of the q -nonextensive statistics proposed by Tsallis lead to an equilibrium velocity distribution of the form^{159,97}

$$f_o(v) = B_q \left[1 - (1 - q) \frac{mv^2}{2k_B T} \right]^{1-q}. \quad (6.1)$$

This is a thermal distribution, whose main effect at the level of the distribution function is to replace the standard Gaussian form by a power law. For $q < 1$, the distribution function (6.1) exhibits a thermal cutoff on the maximum value allowed for the velocity of the particles, which is given by $v_{max} = \sqrt{2k_B T/m(q-1)}$. The quantity B_q is a q -dependent normalization constant and can be expressed in terms of Gamma-function by

$$B_q = \begin{cases} (1 - q)^{1/2} \left(\frac{5-3q}{2}\right) \left(\frac{3-q}{2}\right) \\ \times \frac{\Gamma(1/2+1/(1-q))}{\Gamma(1/(1-q))} \left(\frac{m}{2\pi k_B T}\right)^{3/2} & \text{if } \frac{1}{3} < q \leq 1, \\ (q - 1)^{3/2} \frac{\Gamma(1/(q-1))}{\Gamma(1/(q-1)-3/2)} \left(\frac{m}{2\pi k_B T}\right)^{3/2} & \text{if } q \geq 1 \end{cases}, \quad (6.2)$$

where m is a mass, k_B is the Boltzmann constant and T is the temperature.

In principle, the q-nonextensive formalism may be very important for systems endowed with long range interactions as usually happens in astrophysics and plasma physics.

In this context, our aim is to extend the treatment of the bremsstrahlung emission for the nonextensive Maxwellian gas and derive important expressions in terms of simple algebraic functions which we hope will be very helpful to better fit the nowadays observational data.

The radiation due to the acceleration of a charge in the Coulomb field of another charge is called Bremsstrahlung emission. The classical formulas derived to explain such emission must to be extended by quantum corrections, known as Gaunt factors (g_{ff}), for a full understanding of the process. We treat the nonrelativistic Bremsstrahlung, so the total emission per unit time per unit volume per unit frequency range is

$$\frac{dW}{dV dt d\omega} = \frac{16\pi e^6}{3\sqrt{3}c^3 m^2 v} n_e n_i Z^2 g_{ff}(v, \omega), \quad (6.3)$$

where n_e and n_i are the electron and ion densities (respectively), m and e are the electron rest mass and module charge, Ze defines the ion charge, and v and c are the electron and light speed, respectively.

6.1.1 Maxwell-Boltzmann Thermal Bremsstrahlung Emission

To derive the thermal Bremsstrahlung formulae we average the single-speed equation (6.3) over a thermal distribution of speeds. The probability dP that a particle has velocity in the velocity range dv^3 is usually the Maxwellian

$$dP \propto \exp\left(\frac{-E}{kT}\right) dv^3 = \exp\left(\frac{-mv^2}{2kT}\right) dv^3. \quad (6.4)$$

Considering an isotropic distribution of velocities ($dv^3 = 4\pi v^2 dv$), the probability that a particle presents a speed in the speed range dv is

$$dP \propto v^2 \exp\left(\frac{-mv^2}{2kT}\right) dv, \quad (6.5)$$

and since the incident electron velocity must be large enough to at least a photon of energy $h\nu$ be created ($v_{\min} = \left[\frac{2h\nu}{m}\right]^{1/2}$), we have finally the thermal Bremsstrahlung using a Maxwell-Boltzmann distribution:

$$\frac{dW(T, \omega)}{dV dt d\omega} = \frac{\int_{v_{\min}}^{\infty} \left(\frac{dW_{(v, \omega)}}{dV dt d\omega} \right) v^2 \exp\left(\frac{-mv^2}{2kT}\right) dv}{\int_0^{\infty} v^2 \exp\left(\frac{-mv^2}{2kT}\right) dv}. \quad (6.6)$$

Using $\omega = 2\pi\nu$, the result of the upper expression gives

$$\frac{dW(T, \nu)}{dV dt d\nu} = \left[\frac{2^5 \pi e^6}{3mc^3} \left(\frac{2\pi}{3km} \right)^{\frac{1}{2}} T^{\frac{1}{2}} Z^2 n_e n_i \right] \cdot \exp\left(\frac{-h\nu}{kT}\right) \cdot \langle g_{ff} \rangle, \quad (6.7)$$

where the averaged Gaunt factor $\langle g_{ff} \rangle$ is

$$\langle g_{ff} \rangle = \int_{E=h\nu}^{\infty} g_{ff(E, \nu)} \exp\left(\frac{-[E - h\nu]}{kT}\right) \frac{dE}{kT}. \quad (6.8)$$

Using the relation $E' = E - h\nu$ we reach an easier integrable expression for $\langle g_{ff} \rangle$:

$$\langle g_{ff} \rangle = \int_{E'=0}^{\infty} g_{ff(E'+h\nu, \nu)} \exp\left(\frac{-E'}{kT}\right) \frac{dE'}{kT}. \quad (6.9)$$

For the sake of simplicity, we will consider since now the quantity

$$L = \left[\frac{2^5 \pi e^6}{3mc^3} \left(\frac{2\pi}{3km} \right)^{\frac{1}{2}} T^{\frac{1}{2}} Z^2 n_e n_i \right]. \quad (6.10)$$

6.1.2 Nonextensive Thermal Bremsstrahlung Emission

As we said before, we have several problems to fit nowadays observational data of Bremsstrahlung emission only using the thermal Bremsstrahlung formulae with the Maxwellian (6.7). We also saw that many non-thermal spectra have been proposed to fit well the data. In this work we want to show that we could possibly fit these data, in the pure thermal Bremsstrahlung emission, if we use the nonextensive Tsallis distribution instead of the Maxwellian one. But to compare these two distributions, we must first to show the new set of formulas obtained in the nonextensive case.

So, considering an isotropic distribution of velocities, the probability that a particle presents a speed in the range dv is

$$(dP)_{PL} \propto v^2 \left[1 - (1 - q) \frac{mv^2}{2kT} \right]^{\frac{1}{(1-q)}} dv.$$

Therefore the thermal Bremsstrahlung using the nonextensive Tsallis distribution can be derived as follows

$$\left(\frac{dW(T, \omega)}{dV dt d\omega}\right)_{PL} = \frac{\int_{v_{\min}}^{\alpha} \left(\frac{dW(v, \omega)}{dV dt d\omega}\right) v^2 \left[1 - (1-q) \frac{mv^2}{2kT}\right]^{\frac{1}{1-q}} dv}{\int_0^{\alpha} v^2 \left[1 - (1-q) \frac{mv^2}{2kT}\right]^{\frac{1}{1-q}} dv}, \quad (6.11)$$

where $v_{\min} = \sqrt{\frac{2h\nu}{m}}$, and the subscript ‘‘PL’’ means ‘‘Power Law’’ distribution.

The nonextensive distribution presents a particularity: the upper integral limit α of equation (6.11) tends to ∞ when the free parameter q is greater than 1 ($\alpha \rightarrow \infty$ when $q > 1$); but α also presents a cut-off for $[\frac{1}{3} < q < 1]$, where the quantity $(1-q) \frac{mv^2}{2kT}$ equals the unity, better saying, when $\alpha = v_{cut-off} = \sqrt{\frac{2kT}{m(1-q)}}$.

Solving the equation (6.11) and using $\omega = 2\pi\nu$, we have

$$\left(\frac{dW(T, \nu)}{dV dt d\nu}\right)_{PL} = L \cdot F_{(q)} \cdot \left[1 - (1-q) \frac{h\nu}{kT}\right]^{\frac{1}{1-q}+1} \cdot \langle g_{ff} \rangle_{PL}, \quad (6.12)$$

where L is the same of the equation (6.10); $F_{(q)}$ is a function of the free q -parameter so that

$$F_q = \begin{cases} \left(\frac{1}{4}\right) (1-q)^{\frac{1}{2}} (5-3q) (3-q) \frac{\Gamma(\frac{1}{1-q} + \frac{1}{2})}{\Gamma(\frac{1}{1-q})} & \text{if } 1/3 < q \leq 1, \\ (q-1)^{\frac{3}{2}} \frac{\Gamma(\frac{1}{q-1})}{\Gamma(\frac{1}{q-1} - \frac{3}{2})} & \text{if } q \geq 1 \quad , \end{cases} \quad (6.13)$$

and the averaged Gaunt factor $\langle g_{ff} \rangle_{PL}$ is

$$\langle g_{ff} \rangle_{PL} = \int_0^{\gamma} g_{ff} \cdot [1 - (1-q)x]^{\frac{1}{1-q}} dx, \quad (6.14)$$

where the upper integral limit γ tends to ∞ for $q > 1$ and have a cut-off when $\gamma = \frac{1}{1-q}$ for $[-1 < q < 1]$. For $q > 1$, there is also an analitical limit of mathematical validity of the formulas when $q = \frac{5}{3}$ (~ 1.7), so we must consider the analitical treatment in the segment $[1 < q < 1.7]$ in this case.

A peculiar characteristic of the nonextensive distribution is that, in the limit $q \rightarrow 1$, we retrieve the Maxwell distribution function. So we can consider such power-law distribution as an extension of the classical Maxwellian one, and the parameter q as a mesure of the non-extensivity of the system. We also have:

$$\lim_{q \rightarrow 1} \left(\frac{dW(T, \nu)}{dV dt d\nu}\right)_{PL} = \left(\frac{dW(T, \nu)}{dV dt d\nu}\right)_{Maxwellian} \quad (6.15)$$

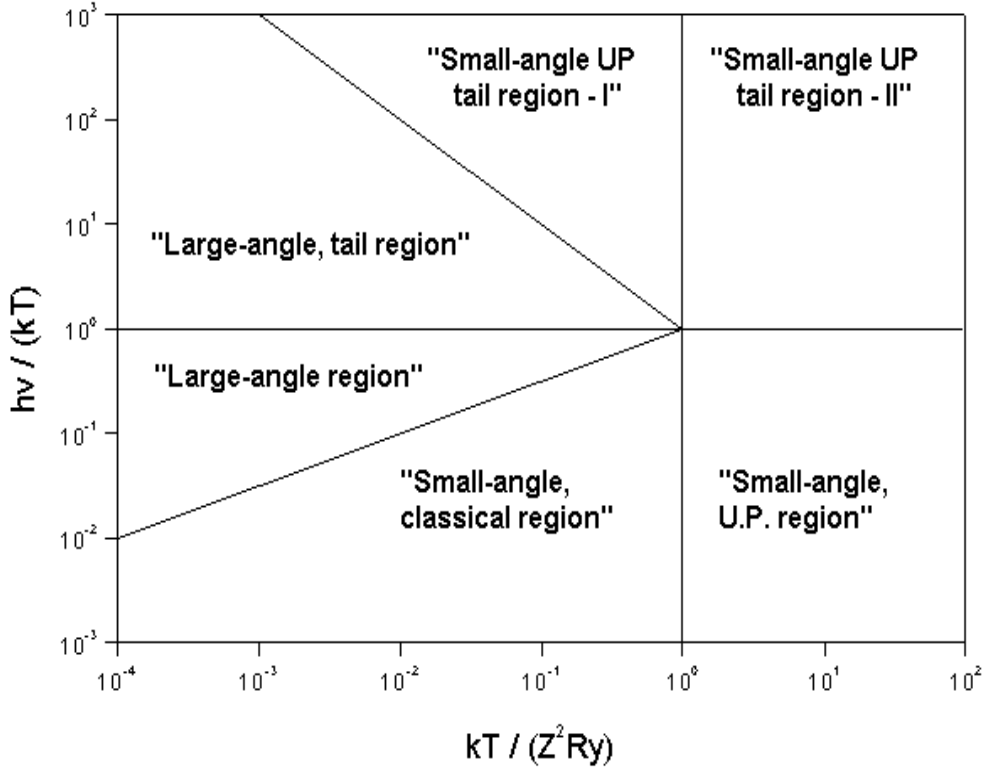


Figure 6.1: Plot from Novikov^{184,183}, showing different regions for the Gaunt factor.

6.1.3 Averaged Gaunt Factors

We present now an extensive derivation of all averaged Gaunt factors to five regions of Fig.(6.1), from Refs.^{184,183}. For each region of interest we have classical or quantum approximations which lead to a particular formulae of g_{ff} , which, calculated inside equations (6.8) and (6.14), gives the Maxwellian and Nonextensive averaged Gaunt factors $\langle g_{ff} \rangle$ for that specific region.

Below we show the region, the g_{ff} formulae and the derived $\langle g_{ff} \rangle$ and $\langle g_{ff} \rangle_{PL}$:

1. “Large-Angle Tail Region” and “Large-Angle Region” ($g_{ff} \simeq 1$):

- (a) $\langle g_{ff} \rangle = 1$.

- (b) $\langle g_{ff} \rangle_{PL} (q > 1 \text{ and } 1/3 < q < 1) = \frac{1}{2-q}$.

2. “Small-Angle UP Region” $\left(g_{ff} = \frac{\sqrt{3}}{\pi} \ln \left[4 \cdot \frac{\frac{1}{2}mv^2}{h\nu}\right]\right)$:
 - (a) $\langle g_{ff} \rangle = \frac{\sqrt{3}}{\pi} \ln \left[\frac{4kT}{h\nu\xi}\right]$.
 - (b) $\langle g_{ff} \rangle_{PL (q>1)} = \left(\frac{1}{2-q}\right) \frac{\sqrt{3}}{\pi} \left\{ \ln \left[\frac{4kT}{h\nu\xi}\right] + \ln \left(\frac{1}{q-1}\right) - \Psi \left(\frac{2-q}{q-1}\right) \right\}$.
 - (c) $\langle g_{ff} \rangle_{PL (1/3<q<1)} = \left(\frac{1}{2-q}\right) \frac{\sqrt{3}}{\pi} \left\{ \ln \left[\frac{4kT}{h\nu\xi}\right] + \ln \left(\frac{1}{1-q}\right) - \Psi \left(\frac{3-2q}{1-q}\right) \right\}$.

3. “Small-Angle Classical Region” $\left(g_{ff} = \frac{\sqrt{3}}{\pi} \ln \left[\frac{2}{\xi} \left(\frac{\frac{1}{2}mv^2}{h\nu}\right) \left(\frac{\frac{1}{2}mv^2}{Z^2R_y}\right)^{\frac{1}{2}}\right]\right)$:
 - (a) $\langle g_{ff} \rangle = \frac{\sqrt{3}}{\pi} \ln \left[\frac{4}{\xi^{\frac{5}{2}}} \left(\frac{kT}{h\nu}\right) \left(\frac{kT}{Z^2R_y}\right)^{\frac{1}{2}}\right]$.
 - (b) $\langle g_{ff} \rangle_{PL (q>1)} = \left(\frac{1}{2-q}\right) \frac{\sqrt{3}}{\pi} \left\{ \ln \left[\frac{4}{\xi^{\frac{5}{2}}} \left(\frac{kT}{h\nu}\right) \left(\frac{kT}{Z^2R_y}\right)^{\frac{1}{2}}\right] + \frac{3}{2} \ln \left(\frac{1}{q-1}\right) - \frac{3}{2} \Psi \left(\frac{2-q}{q-1}\right) \right\}$.
 - (c) $\langle g_{ff} \rangle_{PL (1/3<q<1)} = \left(\frac{1}{2-q}\right) \frac{\sqrt{3}}{\pi} \left\{ \ln \left[\frac{4}{\xi^{\frac{5}{2}}} \left(\frac{kT}{h\nu}\right) \left(\frac{kT}{Z^2R_y}\right)^{\frac{1}{2}}\right] + \frac{3}{2} \ln \left(\frac{1}{1-q}\right) - \frac{3}{2} \Psi \left(\frac{3-2q}{1-q}\right) \right\}$.

4. “Small-Angle U.P. Tail Region - I” $\left(g_{ff} = \frac{\sqrt{3}}{\pi} \ln \left(\frac{v_i+v_f}{v_i-v_f}\right)\right)$:
 - (a) $\langle g_{ff} \rangle = \left(\frac{3}{\pi} \frac{kT}{h\nu}\right)^{\frac{1}{2}}$.
 - (b) $\langle g_{ff} \rangle_{PL (q>1)} = \left(\frac{3}{\pi} \frac{kT}{h\nu}\right)^{\frac{1}{2}} (q-1)^{-3/2} \frac{\Gamma\left(\frac{1}{q-1}-\frac{3}{2}\right)}{\Gamma\left(\frac{1}{q-1}\right)}$.
 - (c) $\langle g_{ff} \rangle_{PL (1/3<q<1)} = \left(\frac{3}{\pi} \frac{kT}{h\nu}\right)^{\frac{1}{2}} \frac{4}{(1-q)^{1/2}(5-3q)(3-q)} \frac{\Gamma\left(\frac{1}{1-q}\right)}{\Gamma\left(\frac{1}{1-q}+\frac{1}{2}\right)}$.

5. “Small-Angle U.P. Tail Region - II” $\left(g_{ff} \sim \frac{2\sqrt{3}}{\pi} \left[1 - \exp\left(-2\pi\sqrt{\frac{Z^2R_y}{h\nu}}\right)\right]\right)$:
 - (a) $\langle g_{ff} \rangle = 2 \left(12 \frac{Z^2R_y}{h\nu}\right)^{\frac{1}{2}}$.
 - (b) $\langle g_{ff} \rangle_{PL (q>1) \text{ and } (1/3<q<1)} = 2 \left(12 \frac{Z^2R_y}{h\nu}\right)^{\frac{1}{2}} \frac{1}{(2-q)}$,

where $\xi = \exp(C)$, C being the Euler Constant (Ref.¹⁷⁹):

$$C = - \int_0^{\infty} \ln t \cdot \exp(-t) dt = 0.577\dots, \quad (6.16)$$

$\Psi(x)$ is the Euler Psi function of x , and the Rydberg energy $R_y = 13.6 \text{ eV}$ is the energy unit.

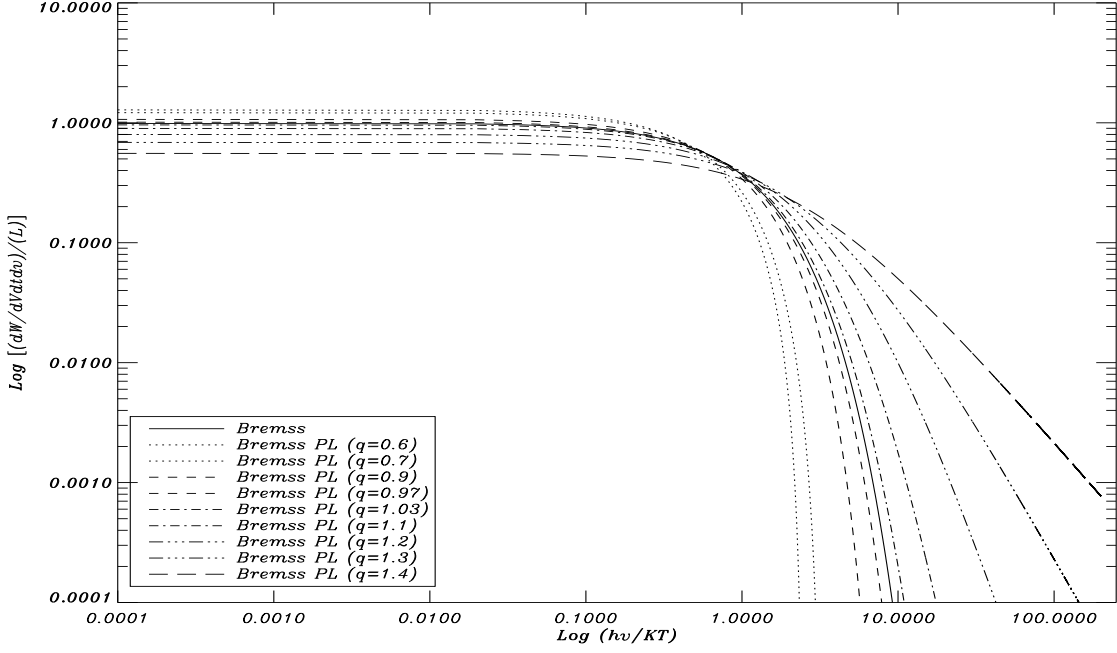


Figure 6.2: Thermal Bremsstrahlung emission of the “Large-Angle” and the “Large-Angle Tail” region. We obtain the solid line using the Maxwellian distribution, and the other lines using our Power Law one with different q parameters. We can easily observe the flexibility of the Power Law free q -parameter after the $\log\left(\frac{h\nu}{KT}\right) = 1$ limit.

6.1.4 Analysis

Considering the results from equations (6.7) and (6.12), and taking the L constant value as in equation (6.10), we obtain equations relating the thermal Bremsstrahlung emission spectrum versus the frequency ν as follows:

$$\frac{\left(\frac{dW_{(T,\nu)}}{dVdtd\nu}\right)}{L} = \langle g_{ff} \rangle \cdot \exp\left(\frac{-h\nu}{kT}\right) \quad (6.17)$$

$$\frac{\left(\frac{dW_{(T,\nu)}}{dVdtd\nu}\right)_{PL}}{L} = F_{(q)} \cdot \langle g_{ff} \rangle_{PL} \cdot \left[1 - (1 - q) \frac{h\nu}{kT}\right]^{\frac{1}{(1-q)} + 1} \quad (6.18)$$

where $\langle g_{ff} \rangle$ and $\langle g_{ff} \rangle_{PL}$ were previously obtained in section 6.1.3 for each region of Fig. 6.1, and $F_{(q)}$ is a q -dependent function given by equation (6.13).

Using equations (6.17) and (6.18) we plot the figures 6.2, 6.3 and 6.4, in order to compare the behavior of the Maxwellian and the Nonextensive distributions under the Bremsstrahlung thermal emission model.

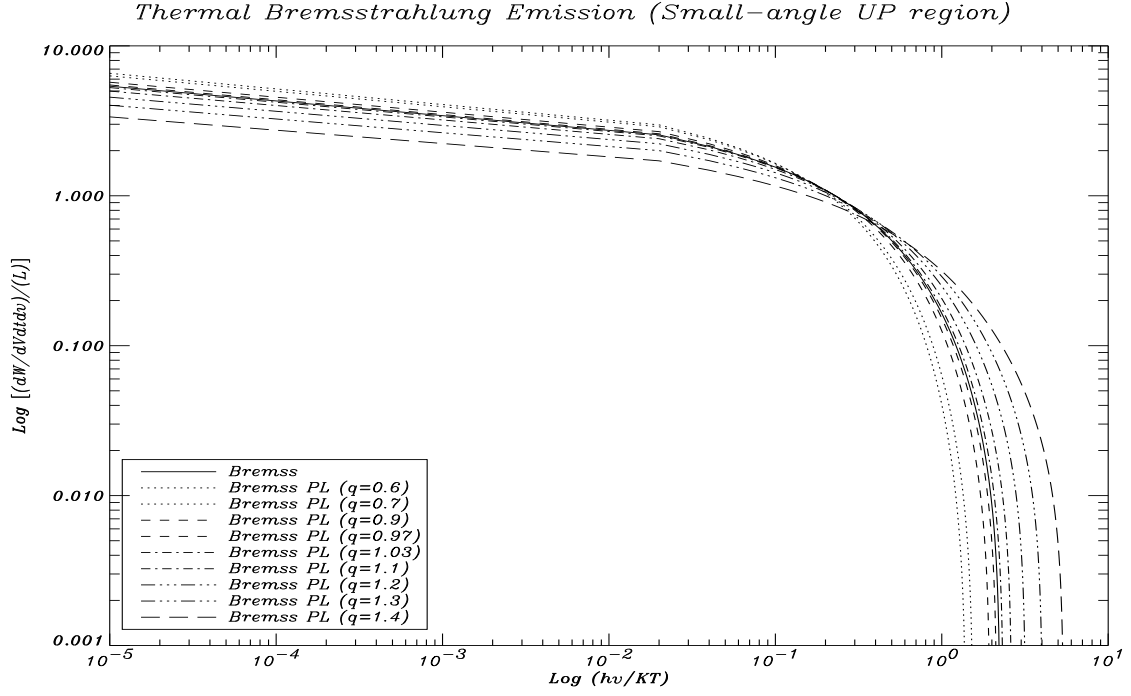


Figura 6.3: Same explanation as Fig.(6.2), but for the “Small-Angle UP” region.

In the figure 6.2 we see the thermal Bremsstrahlung emission of the “Large-Angle” and the “Large-Angle Tail” region. The solid line presents the Maxwellian behavior, which is almost constant until $\log\left(\frac{h\nu}{KT}\right) = 1$, and after that it falls faster to greater $\log\left(\frac{h\nu}{KT}\right)$ values, but at these same values the nowadays observational data show higher values of $\log\left[\left(\frac{dW_{(T,\nu)}}{dV dtd\nu}\right)/L\right]$, and these data continue the tail to even higher values of $\log\left(\frac{h\nu}{KT}\right)$. It is very clear that the pure Maxwellian thermal Bremsstrahlung emission cannot fit well these data. But note the Nonextensive distribution behavior at the same figure: the $\log\left[\left(\frac{dW_{(T,\nu)}}{dV dtd\nu}\right)_{PL}/L\right]$ values are also constant until $\log\left(\frac{h\nu}{KT}\right) = 1$ (and are approximately the same of the Maxwellian case); so we can conclude that, where the Maxwellian case explains well the observational data, so our distribution does. The nonextensive emission presents, however, a free q parameter, which plays an important role after the $\log\left(\frac{h\nu}{KT}\right) = 1$ limit; after that limit, for $q < 1$ values the curves falls even faster than the Maxwellian one, and so these parameters presents even worst fits to the data; but for $q > 1$ the curves presents higher emission values and “smoother falls” when compared to the Maxwellian curve. So in our nonextensive thermal emission framework, for $q > 1$ values we expect better fits to nowadays observational data, without assuming any non-thermal emissions or non-physical power-law adjustments.

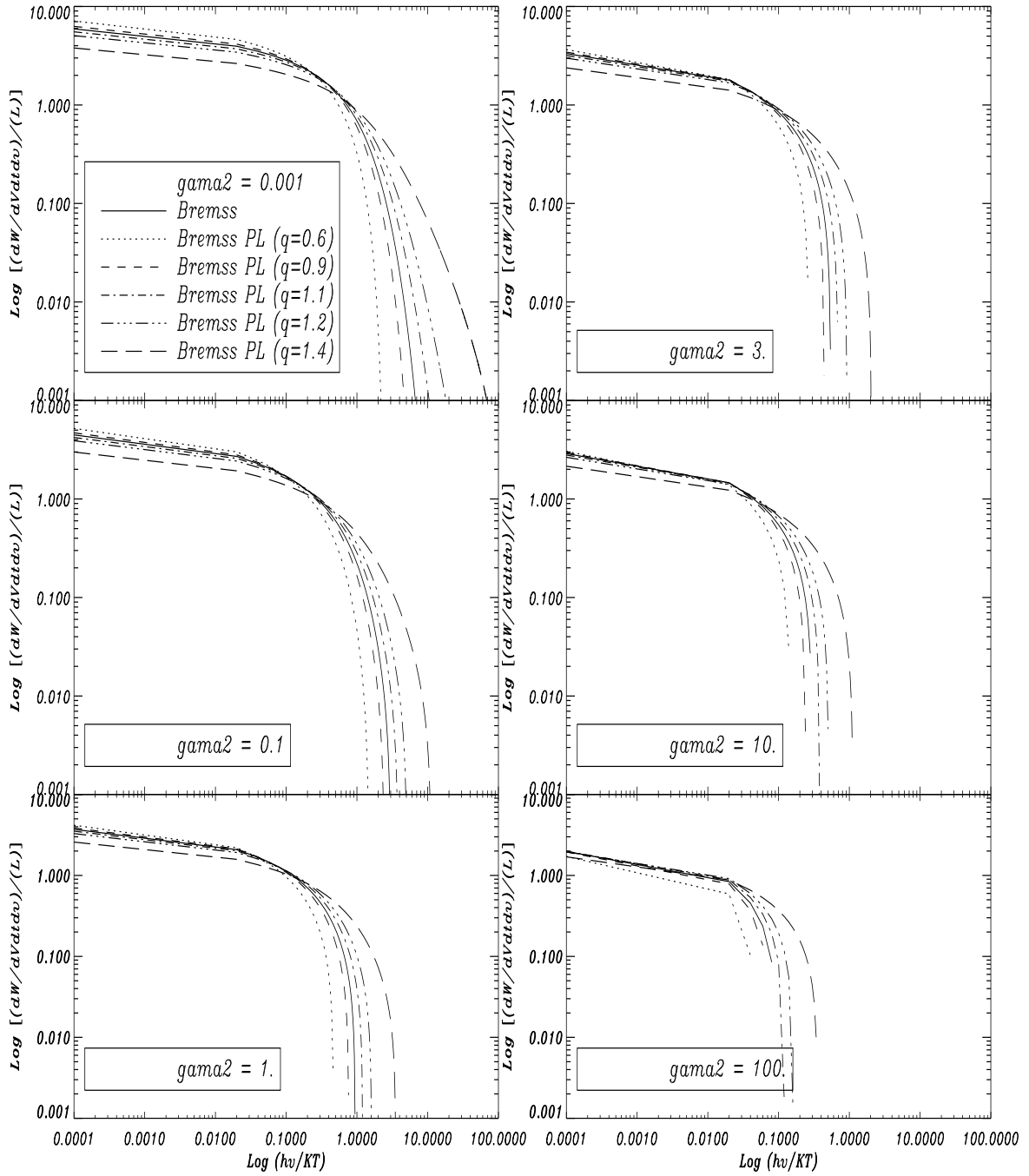


Figure 6.4: The behavior of the Thermal Bremsstrahlung Emission in the “Small-Angle Classical” region, using the Maxwellian and our PL distribution, for different $\text{gamma}2 = \left(\frac{kT}{Z^2 R_y}\right)$ values.

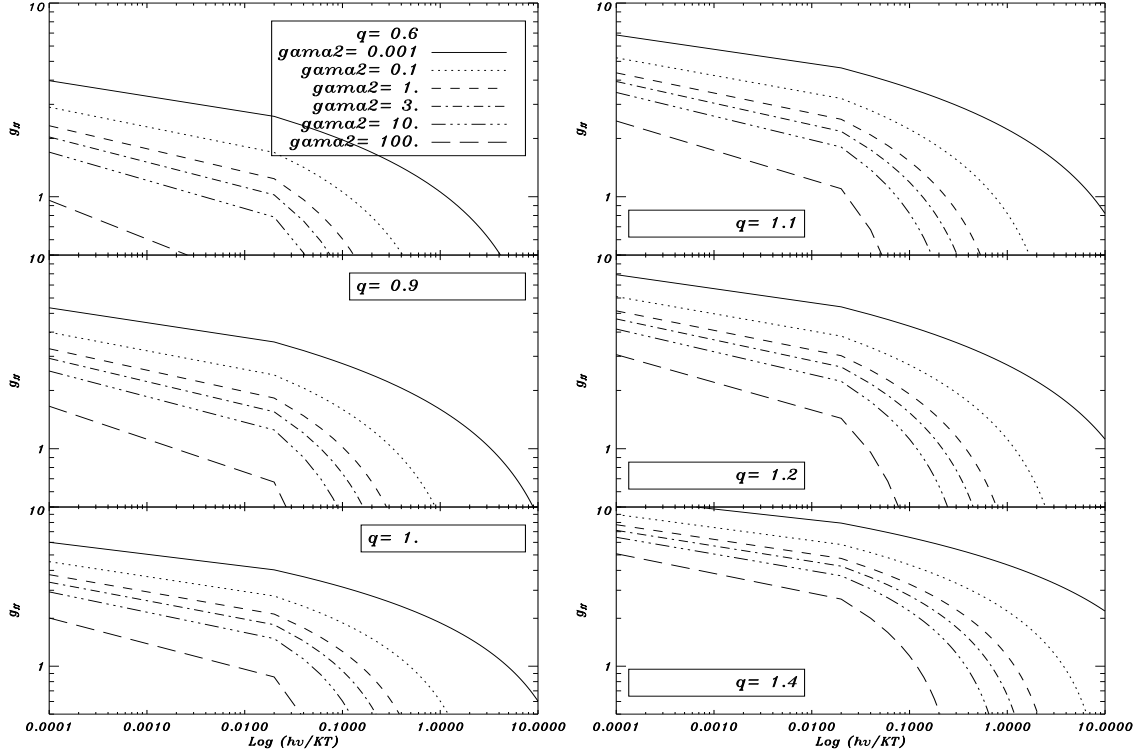


Figure 6.5: The behavior of the averaged Gaunt Factor in the “Small-Angle Classical” region, using only our PL distribution, for different q parameter values. Each curve is plotted using a different $\text{gamma}2 = \left(\frac{kT}{Z^2 R_y}\right)$ value. We can easily see that our nonextensive method presents the same averaged Gaunt Factor behavior as using the classical method; better saying, we can also use the same approximations in the Gaunt Factor, which is of the order of a unity, even for a large range of q parameter values.

In Fig. 6.3 we see the same explanation as in the Fig. 6.2 for the “Small-Angle UP” region; but here we note that the tail is not so pronounced as in the “Large-Angle” and the “Large-Angle Tail” region of Fig. 6.2. In Fig. 6.4 we present the behavior of the thermal Bremsstrahlung emission in the “Small-Angle Classical” region, using the Maxwellian and our PL distribution, for different $\text{gamma}2 = \left(\frac{kT}{Z^2 R_y}\right)$ values (the curves are cut-off in the limit of numerical treatment).

Finally, in Fig. 6.5 we show the behavior of the averaged Gaunt Factor in the “Small-Angle Classical” region, using only our PL distribution, for different q parameter values. Each curve is plotted using a different $\text{gamma}2 = \left(\frac{kT}{Z^2 R_y}\right)$ value. Note that in the left-bottom panel we see the same behavior as using the Maxwellian distribution, because our PL one turns to a Maxwellian when q tends to 1. We can easily see that our nonextensive

method presents the same averaged Gaunt Factor behavior as using the classical method; better saying, we can also use the same approximations in the Gaunt Factor, which is of the order of a unity, even for a large range of q parameter values.

6.2 Nonextensivity in the Plasma Probe

We investigate the consequences of a nonextensive q -distribution function in a plasma probe in the presence of an external field of force possessing a potential $V(\mathbf{r})$. We show that this statistics explains the plasma probe data very well for a given q parameter, covering a region of data never explained theoretically by the classic Boltzmann-Gibbs (BG) statistics. This result will improve the plasma diagnostic and give us a better knowledge of several plasma treatments of materials.

6.2.1 Maxwellian velocity distribution

As widely known, the Maxwellian velocity distribution is

$$f(v)_{BG} = n_o \left(\frac{m}{2\pi k_B T} \right)^{3/2} \exp \left(-\frac{mv^2}{2k_B T} \right), \quad (6.19)$$

where m is the mass of the particles, T is the temperature and n_o is the particle number density in the absence of the external force field.

As we known, a classical gas under steady state conditions and immersed in a conservative force field, $\mathbf{F} = -\nabla U(\mathbf{r})$, is described by a distribution function that differs from the Maxwellian velocity distribution by an extra exponential factor involving the potential energy. In this case, the total equilibrium distribution function reads

$$f(\mathbf{r}, v) = n_o \left(\frac{m}{2\pi k_B T} \right)^{3/2} \exp \left(-\frac{\frac{1}{2}mv^2 + U(\mathbf{r})}{k_B T} \right), \quad (6.20)$$

where m is the mass of the particles, k_B is the Boltzmann constant, T is the temperature and n_o is the particle number density in the absence of the external force field. In addition, since this distribution function is normalized, it is easy to see that the number density is given by

$$n(\mathbf{r}) = n_o \exp \left[-\frac{U(\mathbf{r})}{k_B T} \right], \quad (6.21)$$

where the factor, $\exp[-U(\mathbf{r})/k_B T]$, which is responsible for the inhomogeneity of $f(\mathbf{r}, v)$, is usually called the Boltzmann factor. Expression (6.20) follows naturally from an integration of the collisionless Boltzmann's equation

$$\frac{\partial f}{\partial t} + \mathbf{v} \cdot \frac{\partial f}{\partial \mathbf{r}} + \frac{\mathbf{F}}{m} \cdot \frac{\partial f}{\partial \mathbf{v}} = 0, \quad (6.22)$$

when stationary conditions are adopted along with the assumption that the total distribution can be factored

$$f(\mathbf{r}, v) = f_0(v)\chi(\mathbf{r}), \quad (6.23)$$

where $f_0(v)$ represents the Maxwell equilibrium distribution function, and $\chi(\mathbf{r})$ is a scalar function of \mathbf{r} . As one may show, after a simple normalization, the resulting expression for $\chi(\mathbf{r})$ is exactly the Boltzmann factor for the potential energy of the external field, namely:

$$\chi(\mathbf{r}) = \exp \left[-\frac{U(\mathbf{r})}{k_B T} \right], \quad (6.24)$$

and combining this result with equation (6.23) the Boltzmann stationary distribution (6.20) is readily obtained.

6.2.2 Power Law velocity distribution

On the other hand, recent efforts on the kinetic foundations of the q -nonextensive statistics proposed by Tsallis⁷⁶ lead to an equilibrium velocity distribution of the form¹⁵⁹

$$f_0(v) = B_q \left[1 - (1 - q) \frac{mv^2}{2k_B T} \right]^{\frac{1}{1-q}}. \quad (6.25)$$

The equation (6.25) reduces to the Maxwellian result in the limit $q = 1$. This is a thermal distribution, whose main effect at the level of the distribution function is to replace the standard Gaussian form by a power law. For $q < 1$, the distribution function exhibits a thermal cutoff on the maximum value allowed for the velocity of the particles, which is given by $v_{max} = \sqrt{2k_B T/m(q-1)}$. The quantity B_q is a q -dependent normalization constant and can be expressed in terms of Gamma-function by

1. $B_q = (1 - q)^{1/2} \left(\frac{5-3q}{2} \right) \left(\frac{3-q}{2} \right) \cdot \frac{\Gamma(1/2+1/(1-q))}{\Gamma(1/(1-q))} \left(\frac{m}{2\pi k_B T} \right)^{3/2}$, if $1/3 < q < 1$.
2. $B_q = (q - 1)^{3/2} \frac{\Gamma(1/(q-1))}{\Gamma(1/(q-1)-3/2)} \left(\frac{m}{2\pi k_B T} \right)^{3/2}$, if $q > 1$.

The q -parameter quantifies the nonadditivity (nonextensivity) property of the associated gas entropy, responsible to replace the standard Gaussian form by a power law.

The BG statistics is valid only for sufficiently short-range interactions. It fails when gravitational or unscreened Coulombian fields are present, and that is precisely the case of a plasma. We must to note that several experimental works on surface and coatings technology (plasma sputtering deposition, hollow cathode probe techniques, ion-beam sputtering in collision cascade statistics etc.) point out a severe difference between the plasma data obtained and the theoretical expectation (using the BG statistics)^{186–188}; Based upon these evidences, and also based on many recent theoretical work about this subject^{139,146} we must infer that a plasma probe will describe better the behavior of the system with a nonextensive statistics.

Let us now consider a spatially inhomogeneous dilute gas supposed in equilibrium at temperature T . It is immersed in a conservative external field in such a way that $f(\mathbf{r}, v)d^3v d^3r$ is the number of particles with velocity lying within a volume element d^3v about \mathbf{v} and positions lying within a volume element d^3r around \mathbf{r} . The stationary Boltzmann equation can be rewritten as

$$\mathbf{v} \cdot \nabla_{\mathbf{r}} f - \frac{1}{m} \nabla_{\mathbf{r}} U \cdot \nabla_{\mathbf{v}} f = 0. \quad (6.26)$$

Using the functions q -exp and q -log, $e_q(f)$, $\ln_q(f)$, defined by

$$e_q(f) = [1 + (1 - q)f]^{1/(1-q)}, \quad (6.27)$$

$$\ln_q f = \frac{f^{1-q} - 1}{1 - q} \quad (6.28)$$

(note that in the limit $q \rightarrow 1$ we recover the exponential and logarithm functions), we obtain the complete q -distribution function in the presence of an external field¹⁸⁹

$$f(\mathbf{r}, v) = B_q \left[1 - (1 - q) \left(\frac{m\mathbf{v}^2}{2k_B T} + \frac{U(\mathbf{r})}{k_B T} \right) \right]^{1/(1-q)} \equiv B_q e_q(-E/k_B T), \quad (6.29)$$

where E is the total energy of the particles. The particle number density, $n(\mathbf{r}) = \int f(\mathbf{r}, \mathbf{v}) d^3v$, also becomes a function of the position given by

$$n(\mathbf{r}) = n_0 \left[1 - (1 - q) \frac{U(\mathbf{r})}{k_B T} \right]^{(5-3q)/2(1-q)} \equiv n_0 [e_q(-U/k_B T)]^{\frac{5-3q}{2}}, \quad (6.30)$$

and as should be expected, in the extensive limit ($q \rightarrow 1$), the standard exponential Maxwellian expressions for $f(\mathbf{r}, v)$ and $n(\mathbf{r})$ are readily recovered.

6.2.3 The Plasma Probe - Maxwellian Case

An approximate expression for the magnitude of the electron current density, away from the region of saturation, can be obtained from Eq.(6.21) as

$$J_e = J_{e0} \exp \left[\frac{e\phi}{k_B T_e} \right], \quad (6.31)$$

where J_{e0} is the electron current density when the electric potential is zero and ϕ is the electric potential. When ϕ is negative the ions reaching the plasma sheath continue to fall into the negative potential of the probe, and we have a constant ion current density (J_i) in the negative potential region. So the probe current density when $\phi < 0$ is

$$J_p = J_{e0} \exp \left[\frac{e\phi}{k_B T_e} \right] - J_i. \quad (6.32)$$

If we take the logarithm on both sides of Eq.(6.32) we get

$$\ln (J_p + J_i) = \ln (J_{e0}) + \left(\frac{1}{T_{BG} [ev]} \right) \phi. \quad (6.33)$$

If we plot $\ln (J_p + J_i)$ as a function of ϕ , this curve has a straight-line section corresponding to the probe potential less than the plasma potential (this region is believed to be well described by this BG statistics used until here), followed by a slope, and then a region where the plasma potential dominates and cannot be described by the BG theory. The problem is that experimentally the first section contains noises that interfere in our data, troubling the diagnostic of the plasma system. With the nonextensive statistics we will show that we can describe the plasma behavior of the second section of this curve, allowing a better knowledge of the system as a whole. As a last remark, note that we can obtain the BG temperature T_{eBG} from the slope of this same curve, using the derivative of Eq.(6.33):

$$T_{BG} = \left(\frac{d \ln (J_p + J_i)}{d\phi} \right)^{-1}. \quad (6.34)$$

6.2.4 The Plasma Probe - Power Law Case

Using the same procedure, we can derive the nonextensive (hereafter PL, from ‘‘Power Law’’) electron current density from Eq.(6.30). So the PL probe current density when

$\phi < 0$ is

$$J_p = J_{e0} \left[1 + (1 - q) \frac{e\phi}{k_B T_e} \right]^{(5-3q)/2(1-q)} - J_i, \quad (6.35)$$

and again applying the logarithm on both sides we have

$$\ln(J_p + J_i) = \ln(J_{e0}) + \left(\frac{5 - 3q}{2(1 - q)} \right) \ln \left(1 + (1 - q) \frac{1}{T_{PL} [ev]} \right) \phi. \quad (6.36)$$

We can easily see an evident relation between T_{PL} and T_{BG} deriving Eq.(6.36), if we consider that $e\phi \ll k_B T_e$. So

$$T_{PL} = \left(\frac{5 - 3q}{2} \right) \cdot T_{BG}. \quad (6.37)$$

With Eq.(6.37) and knowing that the PL q-parameter is limited as $[1/3 \leq q < 1]$ if $q < 1$ and $[1 < q < 2]$ if $q > 1$, then

$$0 < \frac{\Delta T}{T_{BG}} < 1.5. \quad (6.38)$$

which provides, certainly, theoretical conclusions yet to be massively tested experimentally.

6.2.5 The Density of Electrons

We focus now on the derivation of the density of electrons for the nonextensive approach, and we compare it with the classical one.

The particle current density (or particle flux) is defined as the number of particles passing through a given surface, per unit area and per unit time. Since we assume that the average velocity is zero, the flux will be also zero. In this case, it is of interest to consider only the flux of particles that cross the surface element from the same side, due to their random motions. Using spherical coordinates we can derive the particle flux as¹⁹⁰

$$F = \pi \int_0^\infty f(v) \cdot v^3 dv \quad (6.39)$$

If we use the Maxwellian velocity distribution 6.19 in Eq.(6.39) we obtain

$$F_{BG} = n_o \left(\frac{k_B T}{2\pi m} \right)^{1/2} \quad (6.40)$$

Since the Maxwellian distribution is isotropic, Eq.(6.40) applies to any direction inside the gas. Note that the random particle flux is inversely proportional to the square root of the particle mass, so the plasma electron density is therefore much larger than that for ions, and this property plays a very important role in the interaction of a plasma with a material body immersed in it¹⁹⁰.

If we use, instead, the nonextensive distribution in the interval $1/3 < q < 1$ of Eq.(6.25) with the correspondent normalization, we read

$$F_q = F_{BG} \cdot \left(\frac{5-3q}{2}\right) \left(\frac{3-q}{2}\right) \left(\frac{1}{3-2q}\right) \left(\frac{1}{2-q}\right) (1-q)^{1/2} \frac{\Gamma\left(\frac{1}{2} + \frac{1}{1-q}\right)}{\Gamma\left(\frac{1}{1-q}\right)} \quad (6.41)$$

We can therefore easily see that F_q tends to F_{BG} in the limit $q \rightarrow 1$. When we calculate the particle flux using the nonextensive distribution in the interval $q > 1$ we have

$$F_q = F_{BG} \cdot \left(\frac{1}{q-1}\right)^{1/2} \frac{\Gamma\left(\frac{1}{q-1} - 2\right)}{\Gamma\left(\frac{1}{q-1} - \frac{3}{2}\right)} \quad (6.42)$$

which also tends to F_{BG} if $\left(\frac{1}{q-1}\right) \gg 3/2$ in the limit $q \rightarrow 1$.

From the probe current density (Eqs. (6.32) and (6.35)) we have J_{e0} , the electron current density when the electric potential is zero. So that

$$J_{e0} = e \cdot F \quad (6.43)$$

where F is F_{BG} for the Maxwellian distribution, and F_q for the nonextensive one. Each particle flux is in function of the n_o quantity, which is the electron number density in the unperturbed plasma region. We can then derive the electron number density for the Maxwell distribution as

$$n_{oBG} = \frac{J_{e0}}{e} \left(\frac{2\pi m_e}{k_B T_e}\right)^{1/2} \quad (6.44)$$

and using the same procedure we derive the electron number density for the nonextensive distribution in the interval $1/3 < q < 1$:

$$n_{oq} = n_{oBG} \cdot \left(\frac{2}{5-3q}\right) \left(\frac{2}{3-q}\right) (3-2q) (2-q) \left(\frac{1}{1-q}\right)^{1/2} \frac{\Gamma\left(\frac{1}{1-q}\right)}{\Gamma\left(\frac{1}{2} + \frac{1}{1-q}\right)} \quad (6.45)$$

and using the nonextensive distribution in the interval $q > 1$ we have

$$n_{oq} = n_{oBG} \cdot (q - 1)^{1/2} \frac{\Gamma\left(\frac{1}{q-1} - \frac{3}{2}\right)}{\Gamma\left(\frac{1}{q-1} - 2\right)} \quad (6.46)$$

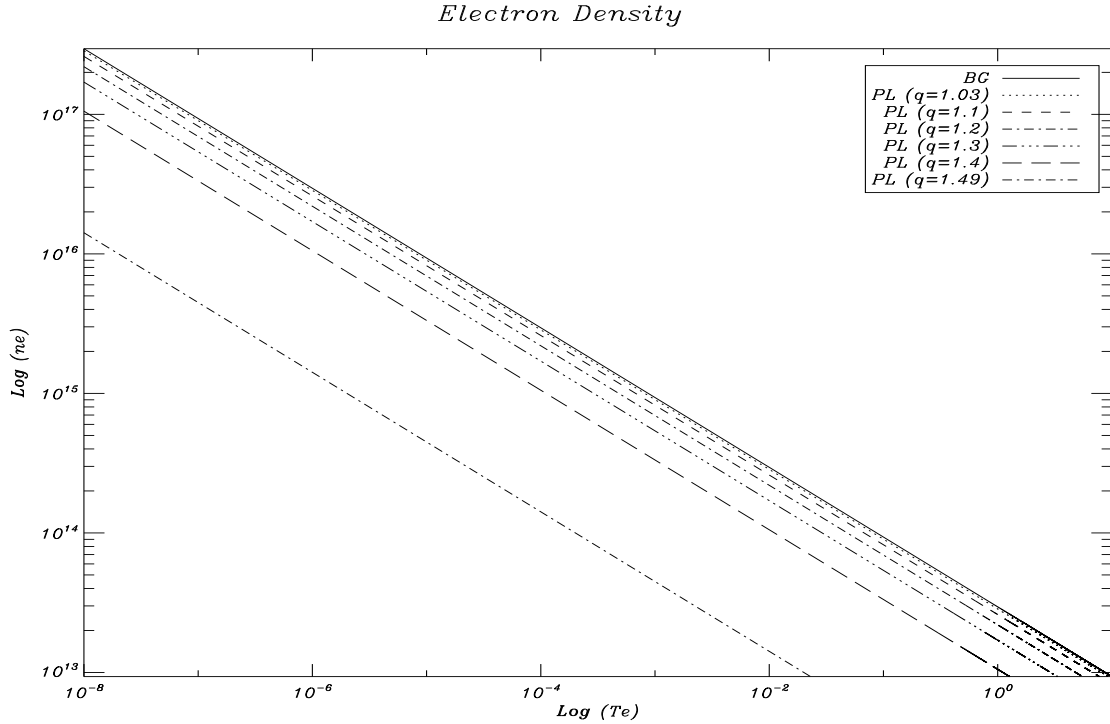


Figura 6.6: The BG (Boltzmann-Gibbs) and the PL (Power Law, nonextensive) results for the electron density, where we fix the J_{e0} value ($J_{e0} = 0.792$ Ampères), in function of the electron temperature. In the $q > 1$ interval.

6.2.6 The Results

The electron temperature are obtained by the probe data using Eqs. (6.34) and (6.37). With this temperature we can quantify the electron density of the plasma using Eqs. (6.44), (6.45) and (6.46). In the Fig. 6.6 and Fig. 6.7 we can see the BG (Boltzmann-Gibbs) and the PL (Power Law, nonextensive) results for the electron density, where we fix the J_{e0} value ($J_{e0} = 0.792$ Ampères), in function of the electron temperature (the correction of Eq.(6.37) for the PL temperatures are performed in all PL curves). In Fig. 6.6 we see the curves for $q > 1$ (were an upper limit of $q \cong 1.5$ is obtained from the mathematical derivation of Eq.(6.42)), although in Fig. 6.7 we see PL curves in the $1/3 < q < 1$ interval.

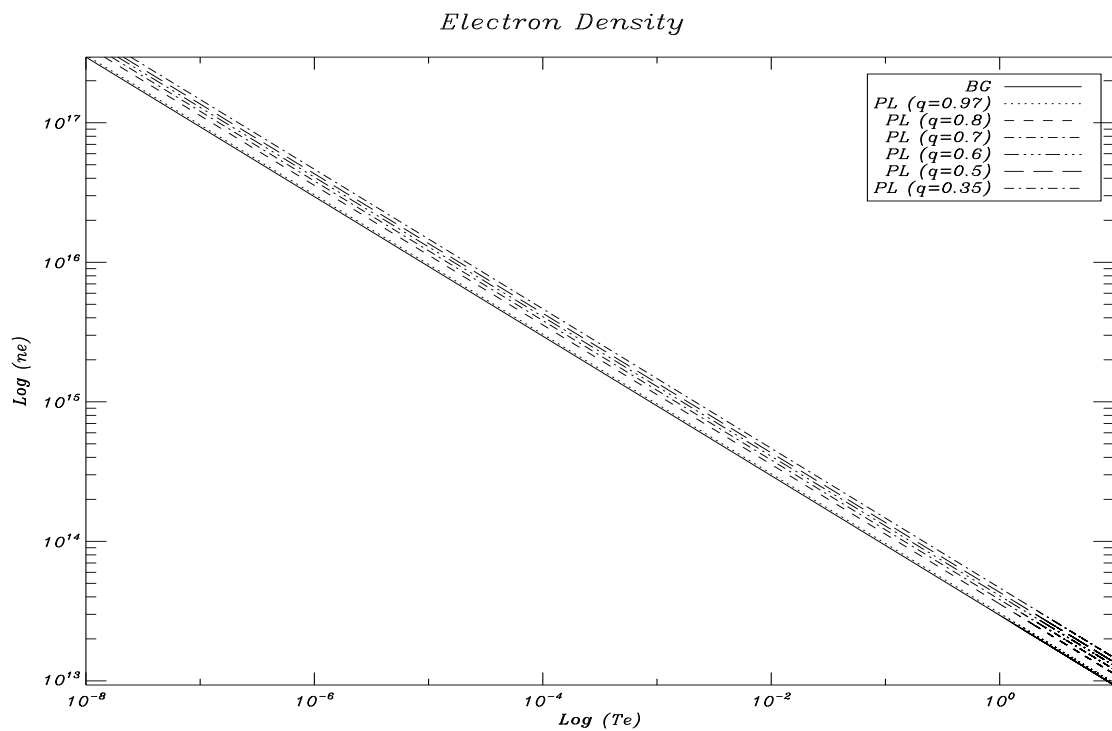


Figura 6.7: The BG (Boltzmann-Gibbs) and the PL (Power Law, nonextensive) results for the electron density, where we fix the J_{e0} value ($J_{e0} = 0.792$ Ampères), in function of the electron temperature. In the $1/3 < q < 1$ interval.

In the Fig. 6.8 we show comparisons between the plasma probe data and the theoretical behavior of the BG and the PL curves, varying the q parameter of this last one. The thick solid line is the BG prediction of Eq.(6.33); we see that in both panels we must to shift up the BG curve by the same factor to effectively compare the curve to the experimental data. The shifted BG curve is shown as a thick dashed line. All the thin lines are PL curves with different q parameter, which goes from $q = 1.01$ to $q = 1.6$ in the bottom-up direction (after $q = 1.65$ we cease to obtain results). We note in both panels that the shifted BG curve fits well the straight line before the slope of the data curve (were the probe potential is less than the plasma potential, so attracting more ions; the velocity and collisions of the particles in this region makes the kinetics surpass the plasma behavior) , but it is completely unable of fit any data points in the region after the slope, were the plasma behavior is stronger. The PL curves show in both panels that with a $q \sim 1.6$ we can describe all data points in the after-slope region (and, as a bonus, without need to shift the curve as we must to do with the BG one).

In the Fig. 6.9 we show essentially the same, but now we note that in the top panel the PL curve at $q = 1.6$ begins to be unable to do a good description of the data behavior after the slope, although in the bottom panel we see that the PL curve cannot describe the data at all, and we note that the BG curve fits very well the data (discounting the fact that we must to use the shift up procedure here again, and worse, the shift parameter is different of the one used in Fig. 6.8). But the behavior of both theoretical curves is physically expected. The distance of the probe from the cathode in the top panel puts the probe in the limit of the plasma sheath that surrounds the basis (were the material is treated); the distance of the probe in the bottom panel is even more closer to the basis, completely immersed in the cathode plasma sheath (that surrounds the basis and also the sample treated). In both panels the plasma behavior is overcome by the kinetic of the present particles (in the bottom panel we can easily see that the plasma behavior is completely overwhelmed by the random movement presented by the local particles, and we already know that the BG theory is very effective in such kind of strong-chaos regime).

So in Fig. 6.8 and Fig. 6.9 , we show the expected theoretical behavior of both curves. In Fig.6.9 ,inside the sheath of the basis, the random displacement of the particles is characteristic of strong chaos (short-range colisional interactions, better explained by the

Figura 6.8: Probe outside the plasma sheath of the cathode. Region of long-range Coulombian interactions, weak chaos, plasma behavior. The PL curve with $q=1.6$ explains very well the region after the slope of the data probe (were the probe potential is overwhelmed by the plasma potential). This PL curve describes the region outside the sheath *of the probe*, where we can detect the *real* macroscopic variables of the plasma (temperature, pressure, density, etc.), and we do not need to shift the curve, as we must to do in the BG case.

Figura 6.9: Probe inside the plasma sheath of the cathode. Region of short-range collisional interactions, strong chaos, random kinetic behavior. The BG curve explains very well the data, specially in the bottom panel, where the probe is completely immersed in the cathode sheath region (But the shift up parameter is needed in both panels, with different values in each one).

Figura 6.10: The first column shows the region outside the cathode sheath. The second column shows the region inside the sheath.

BG theory), so the BG curve describes better the data here; while in Fig. 6.8 we see that outside the sheath of the basis, where the plasma behavior is stronger (long-range Coulombian interactions of particles), the PL curve at $q = 1.6$ is better in explain the data.

The bonus of using the PL curve over the BG one is that we can describe the region outside the sheath *of the probe*, where we can detect the *real* macroscopic variables of the plasma (temperature, pressure, density, etc.), and we do not need to shift the curve to obtain good results in this case. So the nonextensive theory can indeed improve the diagnostic of the plasma probe technic.

6.3 New Cosmological Constraints using Dark Energy, X-Ray Gas Mass Fractions and SNe Ia

Recent measurements are suggesting that we live in a flat Universe and that its present accelerating stage is driven by a dark energy component whose equation of state may evolve in time. Assuming two different parameterizations for the function $\omega(z)$, we constrain their free parameters from a joint analysis involving measurements from X-Ray luminosity of galaxy clusters and SNe type Ia data.

A cosmological constant (Λ), the oldest and by far the most natural candidate for dark energy, faces some theoretical difficulties. The most puzzling of them is the so-called cosmological constant problem: the present cosmological upper bound, $\Lambda_o/8\pi G \sim 10^{-47} GeV^4$, differs from natural theoretical expectations from quantum field theory, $\sim 10^{71} GeV^4$, by more than 100 orders of magnitude. Actually, such a problem has also inspired many scenarios driven by a $\Lambda(t)$ or a time varying decaying vacuum with constant equation of state¹⁹¹. Among the remaining candidates to dark energy, the most promising ones lead to a time dependent equation of state (EOS), usually associated to a dynamical scalar field component. Such quintessence models may also parameterically be represented by an equation of state, $\omega(z)$, as proposed by Cooray and Huterer¹⁹², as well as the one discussed by Linder¹⁹⁵, and, independently, by Padmanabhan and Choudhury¹⁹⁶. In principle, the time variation of the EOS parameter, $\omega(z) \equiv p/\rho$, may allow a clear distinction between a cosmological constant model and the one driven by a rolling scalar

field.

Maor *et al.*¹⁹³ and Weller and Albrecht¹⁹⁴, have also observed that in order to constrain the evolution of the EOS with SNe observations, it is necessary to use a tight prior on the mean matter density of the Universe. A natural way to circumvent such a problem is to consider the constraints on the density parameter from measurements of the X-Ray luminosity of galaxy clusters together in a joint analysis involving SNe Ia observations.

We investigate the cosmological implications from X-ray of galaxy clusters and SNe data by considering two different classes of EOS evolving with redshift. In the first scenario (hereafter Model 1), the EOS parameter is defined by¹⁹²

$$\text{Model 1 : } \omega(z) = \omega_o + \omega_1 z, \quad (6.47)$$

whereas in the second, the EOS parameter reads^{195,196}

$$\text{Model 2 : } \omega(z) = \omega_o + \frac{\omega_1 z}{1 + z} \quad (6.48)$$

where ω_o and ω_1 are constants.

It should be noticed that the linear expression of model 1 yields a reasonable approximation for most quintessence models out to redshift of a few, and, of course, it should be exact for models where $\omega(z)$ is a constant or varies slowly. The unsuitable aspect of the first expression is that it grows with no limit at high redshifts $z > 1$ (for example, distance to the last scattering surface at $z_{lss} \simeq 1100$). In order to fix such a problem, some authors^{195,196} have proposed the second form which has the advantage of giving finite $\omega(z)$ for all z . In both cases, ω_o is the current value of the EOS parameter and ω_1 defines its variation rate for R close to the present epoch ($z = 0$).

6.3.1 Basic Equations

It is assumed that the Universe is flat and its dynamics is driven by a cold dark matter (CDM) fluid plus a quintessence component. Both components are separately conserved and the EOS parameter of the quintessence component is represented by one of the parameterizations from Eqs. (6.47) and (6.48). By integrating the energy conservation laws for each component and combining the result with the FRW equation, it is straightforward to show that the Hubble parameter for both models can be written as:

$$H_{Model1}^2 = H_0^2 \left[\Omega_M (1+z)^3 + (1 - \Omega_M) (1+z)^{3(1+\omega_0-\omega_1)} e^{3\omega_1 z} \right], \quad (6.49)$$

and

$$H_{Model2}^2 = H_0^2 \left[\Omega_M (1+z)^3 + (1 - \Omega_M) (1+z)^{3(1+\omega_0+\omega_1)} e^{-3\omega_1(z/1+z)} \right], \quad (6.50)$$

where the subscript “0” denotes a present day quantity and Ω_M is the CDM density parameter.

The first attempts involving gas mass fraction as a cosmological test were originally performed by Pen¹⁹⁷ and Sasaki¹⁹⁸, and further fully developed by Allen *et al.*²⁰⁰ who analyzed the X-ray observations for six relaxed lensing clusters observed with Chandra in the redshift interval $0.1 < z < 0.5$. A similar analysis has also been done for conventional quintessence models having constant EOS parameter by Lima *at al.*¹⁹⁹. These authors also discussed the case for a cosmological scenario driven by phantom energy ($\omega < -1$). Further, this test was also applied in the context of a Chaplygin gas EOS²²³. More recently, a detailed analysis using an improved sample observed with Chandra (26 clusters) was performed by Allen and collaborators¹⁷¹ also considering a constant EOS parameter. In such studies, it is usually assumed that the baryonic gas mass fraction in galaxy clusters provides a fair sample of the distribution of baryons in the universe. In what follows, the gas mass fraction is defined as^{199,171}

$$f_{\text{gas}}(z_i) = \frac{b\Omega_b}{(1 + 0.19h^{3/2})\Omega_M} \left[2h \frac{D_A^{\text{SCDM}}(z_i)}{D_A^{\text{DE}}(z_i)} \right]^{1.5}, \quad (6.51)$$

where b is a bias factor motivated by gas dynamical simulations that takes into account the fact that the baryon fraction in clusters seems to be lower than for the universe as a whole, Ω_b stands for the baryonic mass density parameter, with the term $(2h)^{3/2}$ representing the change in the Hubble parameter between the default cosmology and quintessence scenarios while the ratio $D_A^{\text{SCDM}}(z_i)/D_A^{\text{DE}}(z_i)$ accounts for deviations in the geometry of the universe from the Einstein-de Sitter CDM model.

In order to derive the constraints from X-ray gas mass fraction we shall use the concept of angular diameter distance, $D_A(z)$. Such a quantity is readily derived in the present context (see, for instance, Refs.¹⁹⁹ and²²³):

$$D_A^{\text{DE}} = \frac{H_o^{-1}}{(1+z)} \int_{x'}^1 \frac{dx}{x^2 H(x)}. \quad (6.52)$$

where $x = \frac{R(t)}{R_o} = (1+z)^{-1}$ is a convenient integration variable. In what follows, we will consider in our statistical modeling only flat cosmological models with Gaussian priors of $h = 0.72 \pm 0.08$ ²⁰¹ with $b = 0.824 \pm 0.089$ ¹⁷¹ and $\Omega_b h^2 = 0.0214 \pm 0.002$ ²⁰².

6.3.2 Observational Constraints

Let us now discuss the constraints from X-ray luminosity of galaxy clusters and SNe type Ia data. First, it is worth notice that the 26 clusters cataloged by Allen *et al.*¹⁷¹ are all regular, relatively relaxed systems for which independent confirmation of the matter density parameter results is available from gravitational lensing studies.

In order to determine the cosmological parameters ω_o and ω_1 we use a χ^2 minimization for the range of ω_o and ω_1 spanning the interval $[-2.3, -0.4]$ and $[-4, 6.5]$, respectively, in steps of 0.025. The 68.3%, 90.0% and 95.4% confidence levels are defined by the conventional two-parameters χ^2 levels 2.30, 4.61 and 6.17, respectively. It is very important to note that we do not consider any prior in Ω_M , as usually required by the SNe Ia test.

In addition to our gas mass fraction analysis we consider the SNe Ia measurements as given by Riess *et al.*²⁰³. The best fit of the model of Eq.(6.49) is $\chi^2 = 202.06$, $\omega_o = -1.25$, $\omega_1 = 1.3$ and $\Omega_M = 0.26$. For the Model 2, the best fit is $\chi^2 = 202.02$, $\omega_o = -1.4$, $\omega_1 = 2.57$ and $\Omega_M = 0.26$.

We now present our joint analysis (X-Ray luminosity from galaxy clusters and SNe Ia data). In the first EOS parameter we find at 2σ of likelihood that $-1.78 \leq \omega_o \leq -0.82$ and $-1.2 \leq \omega_1 \leq 2.7$. For the other model we get $-2.0 \leq \omega_o \leq -0.8$ and $-2.0 \leq \omega_1 \leq 5.5$ with 2σ . In Fig. 1, we show contours of constant likelihood in the ω_o - ω_1 plane. Note that the allowed range for both ω_o and ω_1 is reasonably large thereby showing the impossibility of placing restrictive limits on these quintessence scenarios. However, these limits are better than those obtained by a simple SNe Ia analysis since in this case, the uncertainties on both parameters are strongly correlated when one marginalizes over Ω_M .

At this point, it is interesting to compare our results with other recent determinations of ω_o and ω_1 derived from independent methods. For example, the age constraints recently derived by Jain and Dev²⁰⁴ are $\omega_o \leq -0.31$ and $\omega_1 \leq 0.96$ for the first model, and $\omega_o \leq -0.31$ and $\omega_1 \leq 3.29$ for the second one. Riess *et al.*²⁰³ found $\omega_o = -1.31_{-0.28}^{+0.22}$ (1σ) and $\omega_1 = 1.48_{-0.90}^{+0.81}$ (1σ) with the uncertainties in both parameters strongly correlated. In the article of Padmanabhan and Choudhury¹⁹⁶ we must to use a constant Ω_M in order to analyze the $\omega_o - \omega_1$ plane. It should be stressed that the EOS corresponding to the cosmological constant is within the 1σ contour for $0.21 < \Omega_M < 0.41$, and models with $\omega_o > -1/3$ are ruled out at a high significance level for $\Omega_M < 0.4$ (we must to have very

high negative values of ω_1 in this case, and despite the high uncertainties in ω_1 present in this data set, we know that it cannot vary but a few from ω_o); this supernova observation analysis clearly indicates that the data are not sensitive to ω_1 as compared to ω_o .

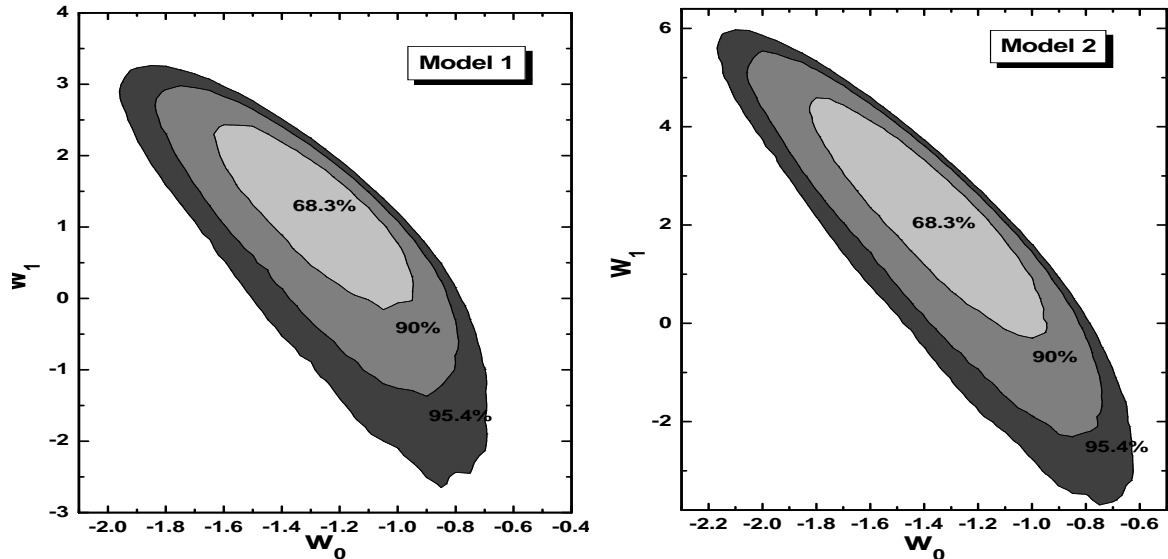


Figure 6.11: Marginalized constraints on plane ω_0 and ω_1 from joint analysis of the Chandra $f_{\text{gas}}(z)$ and SNe Ia data shown above for models 1 (left panel) and 2 (right panel). The solid lines mark the 1, 2 and 3 σ confidence limits. See text for more details.

6.3.3 Perspectives

We have discussed here two simple possible parameterizations of the EOS obeyed by quintessence models as recently presented in the literature. Our results suggest that it is worthwhile to use the estimates of the gas mass fraction from galaxy clusters in joint analysis with the SNe Ia data since the derived constraints for Ω_M (and other quantities) do not require any prior to this parameter. More important, we have also obtained constraints for w_o and w_1 which have not been obtained before without a prior in Ω_M .

The parameterizations seems to be more efficient to explain these data set, once they get a lower χ^2 ; however they also have an additional parameter, and that is worthy of a study with more specific statistical criteria (Akaike or Bayesian information criteria, for example). A more detailed analysis of this kind will be investigated in the near future.

6.4 Constraining H_0 from Sunyaev-Zel'dovich effect, Galaxy Clusters X-ray data, and Baryon Oscillations

In the current Λ CDM flat cosmology, a possible technique to broke the degenerescency on the mass density parameter (Ω_m) is to apply a joint analysis involving the baryon acoustic oscillations (BAO). By adopting this technique to the (H_0, Ω_m) parameter space, we obtain new constraints on the Hubble constant H_0 from BAO signature as given by the Sloan Digital Sky Survey (SDSS) catalog. Our analysis based on the SZE/X-ray data for a sample of 25 clusters yields $H_0 = 74_{-3.5}^{+4}$ km s⁻¹ Mpc⁻¹ (1σ , neglecting systematic uncertainties). This result is in good agreement with independent studies from the *Hubble Space Telescope* key project and the recent estimates of WMAP, thereby suggesting that the combination of these three independent phenomena provides an interesting method to constrain the Hubble constant.

Galaxy clusters are one of the most impressive evolving structures from an earlier stage of the Universe. Usually, they congregate thousands of galaxies and are endowed with a hot gas (in the intra cluster medium), emitting X-rays primarily through thermal bremsstrahlung. Several studies in the last decade have suggested that the combination of data from different physical processes in galaxy clusters provides a natural method for estimating cosmological parameters.

An important phenomena occurring in clusters is the Sunyaev-Zel'dovich Effect (SZE), a small distortion of the Cosmic Microwave Background (CMB) spectrum provoked by the inverse Compton scattering of the CMB photons passing through a population of hot electrons (Sunyaev & Zel'dovich 1972²²⁸). Since the SZE is insensitive to the redshift of galaxy clusters, it provides a very convenient tool for studies at intermediate redshifts where the abundance of clusters depends strongly on the underlying cosmology (the unique redshift dependence appear in the total SZE flux due to the apparent size of the cluster). Another fundamental process is the X-ray emission from the hot electrons in the intracluster medium. When the X-ray surface brightness is combined with the SZE temperature decrement in the CMB spectrum, the angular diameter distance of galaxy clusters is readily obtained.

The possibility to estimate the galaxy cluster distances through SZ/X-ray technique was suggested long ago by many authors^{205,206}, but only recently it has been applied for a fairly large number of clusters (for reviews, see Ref.²⁰⁶). Such a method is based on the different dependence of the cluster electron density (n_e) and the temperature T_e of the SZE ($\propto n_e T_e$) and X-ray bremsstrahlung ($\propto n_e^2 T_e^{1/2}$). Combining both measurements it is possible to estimate the angular diameter distance and infer the value of the Hubble constant whether the cosmology is fixed. The main advantage of this method for estimating H_0 is that it does not rely on extragalactic distance ladder being fully independent of any local calibrator. A basic disadvantage rests on the difficulty of modeling the cluster gas which causes great systematic uncertainties in its determination. In particular, this means that systematic effects on H_0 are quite different from the ones presented by other methods, like the traditional distance ladder or gravitational lensing^{207,209}.

In order to estimate the distance to the cluster from its X-ray spectroscopy, one needs to add some complementary assumptions about its geometry. The importance of the intrinsic geometry of the cluster has been emphasized by many authors^{211,210}. The standard spherical geometry has been severely questioned, since Chandra and XMM-Newton observations have shown that clusters usually exhibit an elliptical surface brightness. In a point of fact, the cluster shape estimation problem is a difficult matter since many clusters do not appear in radio, X-ray, or optical. Another source of difficulty is related to the error bars. Assuming that the clusters have an axisymmetric form, different authors introduced a roughly random uncertainty in H_0 between 15%–30%^{207,212}. The assumed cluster shape also affects considerably the SZE/X-ray distances, and, therefore, the Hubble constant estimates.

Fox and Pen²¹¹ estimate the Hubble constant by assuming triaxial clusters and measuring the distance to artificial observations corrected for asphericity. De Filippis and collaborators²⁰⁹ showed that the spherical hypothesis is strongly rejected for most members of the sample studied. By taking into account such an effect for two samples, a better agreement with the cosmic concordance model ($\Omega_m = 0.3$, $\Omega_\Lambda = 0.7$) was obtained. Triaxial clusters may also be useful for reconciling the observed discrepancies in the total mass of clusters as computed with lensing and X-ray measurements (in this connection see Ref.²¹³).

The determination of H_0 has a practical and theoretical importance to many astrophysical properties of galaxies and quasars, and several cosmological calculations, like the age of the Universe, its size and energy density, primordial nucleosynthesis, and others^{214,215}. Spergel *et al.*¹⁶⁴ have shown that CMB studies can not supply strong constraints on the value of H_0 on their own. This problem occurs due to the degenerescency on the parameter space, and may be circumvented only by using independent measurements of H_0 ²¹⁶.

On the other hand, according to cold dark matter (CDM) picture of structure formation, large-scale fluctuations have grown since $z \sim 1000$ by gravitational instability. The cosmological perturbations excite sound waves in the relativistic plasma, producing the acoustic peaks in the early universe. Eisenstein *et al.*²¹⁷ presented the large scale correlation function from the Sloan Digital Sky Survey (SDSS) showing clear evidence for the baryon acoustic peak at $100h^{-1}$ Mpc scale, which is in excellent agreement with the WMAP prediction from the CMB data. The Baryon Acoustic Oscillations (BAO) method is *independent of the Hubble constant* H_0 which means that we can use BAO signature to break the degenerescency of the mass parameter Ω_m . Hence, combining SZE/X-ray method to obtain \mathcal{D}_A with BAO it is possible to improve the limits over H_0 (for recent applications of BAO see Ref.²¹⁸).

Assuming that the clusters are ellipsoids with one axis parallel to the line of sight, we derive new constraints on the Hubble constant H_0 . By considering the sample of 25 triaxial clusters given by De Filippis *et al.*²⁰⁹, we perform a joint analysis combining the data from SZE and X-ray surface brightness with the recent SDSS measurements of the baryon acoustic peak²¹⁷.

6.4.1 Basic Equations and Sample

Let us now consider that the Universe is described by a flat Friedmann-Robertson-Walker (FRW) geometry driven by cold dark matter plus a cosmological constant. In this case, we have only two free parameters (H_0, Ω_m) and the angular diameter distance, \mathcal{D}_A reads^{199,219,209}

$$\mathcal{D}_A(z; h, \Omega_m) = \frac{3000h^{-1}}{(1+z)} \int_0^z \frac{dz'}{\mathcal{H}(z'; \Omega_m)} \quad \text{Mpc}, \quad (6.53)$$

where $h = H_0/100 \text{ km s}^{-1} \text{ Mpc}^{-1}$ and the dimensionless function $\mathcal{H}(z'; \Omega_m)$ is given by

$$\mathcal{H} = \left[\Omega_m (1 + z')^3 + (1 - \Omega_m) \right]^{1/2}. \quad (6.54)$$

Following De Filippis *et al.*²⁰⁹, a general triaxial morphology it will adopted here. In this case, the intra cluster medium is described by an isothermal triaxial β -model distribution and the SZE decrement reads

$$\begin{aligned} \Delta T_{SZ} &\equiv T_0 f(\nu, T_e) \frac{\sigma_T k_B T_e}{m_e c^2} n_{e0} \sqrt{\pi} \\ &\times \frac{\mathcal{D}_A \theta_{c,\text{proj}}}{b^{3/4}} \sqrt{\frac{e_1 e_2}{e_{\text{proj}}}} g(\beta), \end{aligned} \quad (6.55)$$

where $T_0 = 2.728K$ is the CMB temperature, T_e is the gas temperature, σ_T is the Thompson cross section, the factor $f(\nu, T_e)$ accounts for frequency shift and relativistic corrections, n_{e0} is the central number density of the cluster gas, b is a function of the cluster shape and orientation, e_{proj} is the axial ratio of the major to the minor axes of the observed projected isophotes, $\theta_{c,\text{proj}}$ is the projection on the plane of the sky of the intrinsic angular core radius, and $g(\beta) = \Gamma(3\beta - 1/2)/\Gamma(3\beta)$ (Γ denotes the Gamma function).

Similarly, the X-ray central surface brightness S_{X0} can be written as

$$S_{X0} \equiv \frac{\Lambda_{eH} \mu_e / \mu_H}{4\sqrt{\pi}(1+z)^4} \frac{n_{e0}^2 \mathcal{D}_A \theta_{c,\text{proj}}}{b^{3/4}} \sqrt{\frac{e_1 e_2}{e_{\text{proj}}}} g(\beta), \quad (6.56)$$

where z is the redshift of the cluster, Λ_{eH} is the X-ray cooling function of the ICM in the cluster rest frame and μ is the molecular weight ($\mu_i \equiv \rho/n_i m_p$).

De Filippis and collaborators (2005)²⁰⁹ studied and corrected the \mathcal{D}_A measurements for 25 clusters, getting a better agreement with the Λ CDM models. We used two samples studied by them to investigate the bounds arising from SZE/X-ray observations. One of the samples, compiled by Reese *et al.* (2002)²⁰⁷, is a selection of 18 galaxy clusters distributed over the redshift interval $0.14 < z < 0.8$. The other one, the sample of Mason *et al.* (2001)²²⁰, has 7 clusters from the X-ray limited flux sample of Ebeling *et al.* (1996)²²¹. De Filippis *et al.* (2005)²⁰⁹ show that the samples turn out slightly biased, with strongly elongated clusters preferentially aligned along the line of sight. Their results suggest that 15 clusters are in fact more elongated along the line of sight, while the remaining 10 clusters are compressed.

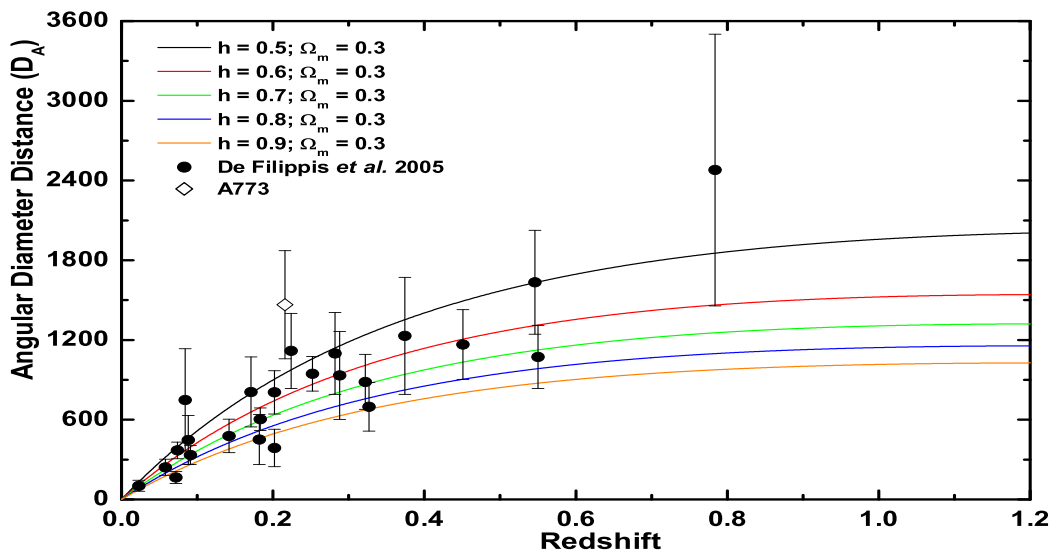


Figura 6.12: Angular diameter distance as a function of redshift for $\Omega_m = 0.3$ and some selected values of the h parameter. The data points correspond to the the SZE/X-ray distances for 25 clusters from De Filippis *et al.*²⁰⁹. The open diamond indicates the Abell 773 outlier cluster, which has been excluded from our statistical analysis.

In Fig. 6.12, the galaxy cluster sample is plotted on a residual Hubble diagram using a flat cosmic concordance model ($\Omega_m = 0.3, \Omega_\Lambda = 0.7$). We see that the *A773* cluster is the largest outlier, and our statistical analysis confirms that its inclusion leads to the highest χ^2 . For that reason we have excluded this data point from the statistical analysis.

6.5 Analysis and Results

Now, let us perform a χ^2 fit over the $h - \Omega_m$ plane. In our analysis we use a maximum likelihood that can be determined by a χ^2 statistics,

$$\chi^2(z|\mathbf{p}) = \sum_{\mathbf{i}} \frac{(\mathcal{D}_{\mathbf{A}}(\mathbf{z}_i; \mathbf{p}) - \mathcal{D}_{\mathbf{A}o,i})^2}{\sigma_{\mathcal{D}_{\mathbf{A}o,i}}^2}, \quad (6.57)$$

where $\mathcal{D}_{\mathbf{A}o,i}$ is the observational angular diameter distance, $\sigma_{\mathcal{D}_{\mathbf{A}o,i}}$ is the uncertainty in the individual distance and the pair, $\mathbf{p} \equiv (\mathbf{h}, \Omega_m)$, is the complete set of parameters.

In what follows, we first consider the SZE/X-ray distances separately, and, further, we present a joint analysis including the BAO signature from the SDSS catalog. Note that a specific flat cosmology has not been fixed by hand in the analyzes below.

6.5.1 Limits from SZE/X-ray

We now consider the 24 clusters (without the A773, see Fig. 6.12), which constitutes the SZE/X-ray data from De Filippis *et al.* (2005)²⁰⁹. Our analysis indicated that any cosmological model could be accepted by that sample until 3σ (with 2 free parameters). It also shows that using only the ellipsoidal cluster sample we cannot constrain the energetic components of the cosmological model. This happens basically because the error bars are large, mainly at intermediate and high redshifts.

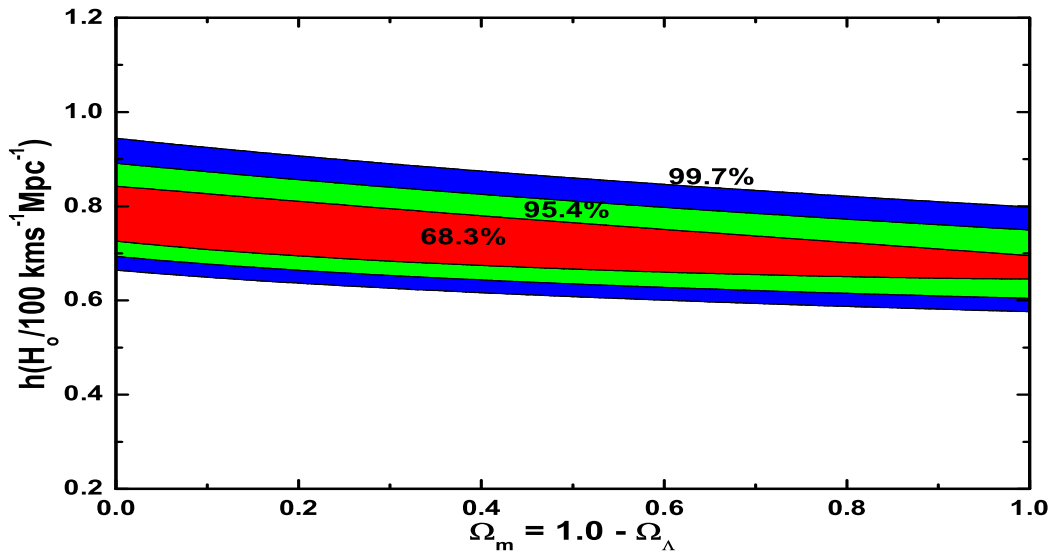


Figure 6.13: Confidence regions (68.3%, 95.4% and 99.7%) in the (Ω_m, h) plane provided by the SZE/X-ray data from De Filippis *et al.* (2005)²⁰⁹. The best fit values are $h = 0.75$ and $\Omega_m = 0.15$.

In Fig. 6.13 we show the contours of constant likelihood (68.3%, 95.4% and 99.7%) in the space parameter $h - \Omega_m$ for the SZ/X-ray data discussed earlier. Note that only a small range for the h parameter is allowed, ($0.64 \leq h \leq 0.85$), at 1σ of confidence level. In particular, we found $h = 0.75^{+0.07}_{-0.07}$ and $\Omega_m = 0.15^{+0.57}_{-0.15}$ with $\chi^2_{min} = 24.4$ at 68.3% c.l. for 1 free parameter. Naturally, such bounds on h are reasonably dependent on the cosmological model adopted. For example, if we fix $\Omega_m = 0.3$ we have $h = 0.74$, for $\Omega_m = 1.0$ we have $h = 0.67$, and both cases are permitted with high degree of confidence. Clearly, we see that an additional cosmological test (fixing Ω_m) is necessary in order to break the degeneracy on the (Ω_m, h) plane.

Systematic effects still need to be considered. The common errors are: SZ $\pm 8\%$, X-ray $\pm 10\%$, radio halos -3% , 5% for Galactic N_H , 10% for isothermality, 2% kinetic SZ, clumping causes -20% , radio source confusion $\pm 12\%$, primary beam $\pm 3\%$ and 1% on the CMB. When we combine the errors in quadrature, we find that the typical error are of $20\% - 30\%$, in agreement with others works^{220,207,208}.

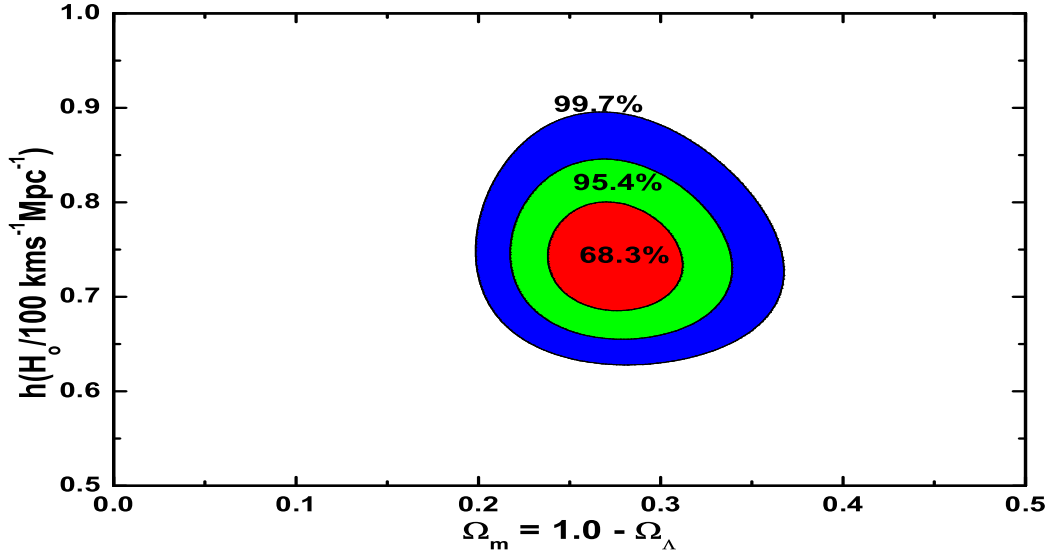


Figure 6.14: Contours in the $\Omega_m - h$ plane using the SZE/X-ray and BAO joint analysis. The contours correspond to 68.3%, 95.4% and 99.7% confidence levels. The best-fit model converges to $h = 0.74$ and $\Omega_m = 0.27$.

6.5.2 Joint Analysis for SZE/X-ray and BAO

As remarked earlier, more stringent constraints on the space parameter (h, Ω_m) can be obtained by combining the SZE/X-ray with the BAO signature²¹⁷. The peak detected (from a sample of 46748 luminous red galaxies selected from the SDSS Main Sample) is predicted to arise precisely at the measured scale of $100 h^{-1}$ Mpc. Basically, it happens due to the baryon acoustic oscillations in the primordial baryon-photon plasma prior to recombination. Let us now consider it as an additional cosmological test over the ellipsoidal cluster sample. Such a measurement is characterized by²¹⁷

$$\mathcal{A} \equiv \frac{\Omega_m^{1/2}}{\mathcal{H}(z_*)^{1/3}} \left[\frac{1}{z_*} \Gamma(z_*) \right]^{2/3} = 0.469 \pm 0.017, \quad (6.58)$$

where $z_* = 0.35$ is the redshift at which the acoustic scale has been measured, and $\Gamma(z_*)$ is the dimensionless comoving distance to z_* .

Note that the above quantity is independent of the Hubble constant, and, as such, the BAO signature alone constrains only the Ω_m parameter. This property is very characteristic of the BAO signature, thereby differentiating it from many others classical cosmological tests, like the gas mass fraction^{199,171,127}, luminosity distance²²², or the age of the universe^{223,224}.

In Fig. 6.14, we show the confidence regions for the SZE/X-ray cluster distance and BAO joint analysis. By comparing with Fig. 6.13, one may see how the BAO signature breaks the degeneracy in the (Ω_m, h) plane. As it appears, the BAO test presents a striking orthogonality centered at $\Omega_m = 0.27_{-0.02}^{+0.03}$ with respect to the angular diameter distance data as determined from SZE/X-ray processes. We find $h = 0.738_{-0.033}^{+0.042}$ and $\chi_{min}^2 = 24.5$ at 68.3% (c.l.) for 1 free parameter. An important lesson here is that the combination of SZE/X-ray with BAO provides an interesting approach to constrain the Hubble constant.

In Fig. 6.15, we have plotted the likelihood function for the h parameter in a flat Λ CDM universe for the SZE/X-ray + BAO data set. The dotted lines are cuts in the regions of 68.3% probability and 95.4%.

Our results are in line with some recent analyzes based on different cosmological observations, like the one provided by the WMAP team $h = 0.73 \pm 0.03$ ¹⁶⁴, and the HST Project $h = 0.72 \pm 0.08$ ²⁰¹. Note, however, that it does not agree with the recent determination, $h = 0.62 \pm 0.013$ (random) ± 0.05 (systematics), recently advocated by Sandage and collaborators (2006)²²⁵. A result obtained with basis on Type Ia Supernovae, calibrated with Cepheid variables in nearby galaxies that hosted them.

At this point, it is interesting to compare our results with others recent works in which the limits on h were obtained by fixing the cosmology ($\Omega_m = 0.3$, $\Omega_\Lambda = 0.7$, cosmic concordance), and assuming spherical geometry. A measurement using SZ effect was accomplished by Mason *et al.* (2001)²²⁰, using 5 clusters, and gives $h = 0.66_{-0.11}^{+0.14}$; Reese and coauthors (2002)²⁰⁷, using 18 clusters, found $h = 0.60 \pm 0.04$, and in a posterior analysis²⁰⁸, with 41 clusters, obtains $h \approx 0.61 \pm 0.03$; Jones *et al.* (2005)²¹² derived $h = 0.66_{-0.10}^{+0.11}$, using a sample of 5 clusters free of any orientation bias. In a recent paper,

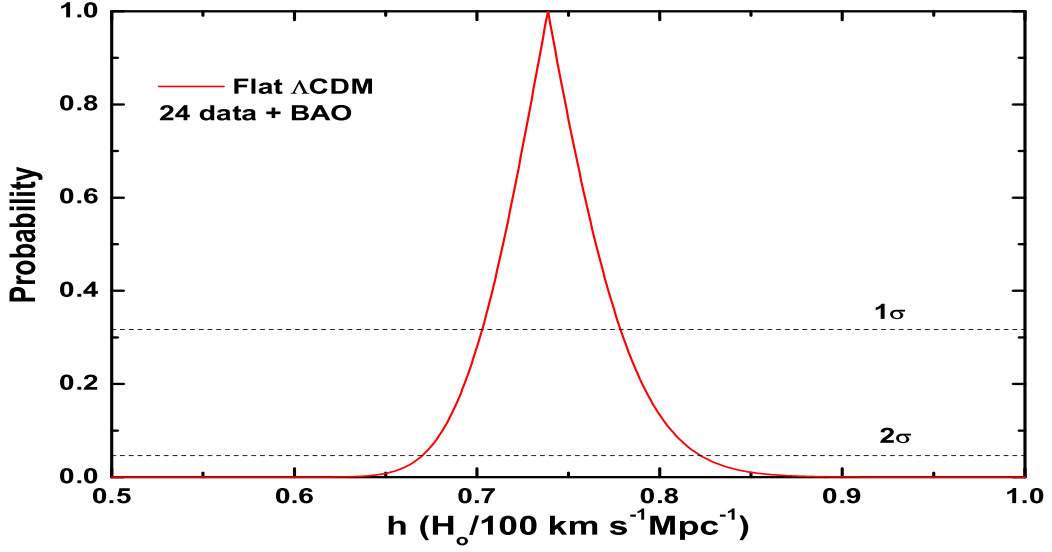


Figura 6.15: Likelihood function for the h parameter in a flat Λ CDM universe, from SZE/X-ray emission. The shadow lines are cuts in the regions of 68.3% probability and 95.4%. We see that the region permitted is well constrained and in concordance with others studies^{201,164}.

Tabela 6.1: **SZ/X-ray method**: Limits to h from galaxy clusters (Λ CDM).

Reference (data)	Ω_m	h (1σ)	χ^2
Mason <i>et al.</i> 2001 (7) ²²⁰	0.3	$0.66^{+0.14}_{-0.11}$	$\simeq 2$
Reese <i>et al.</i> 2002(18) ²⁰⁷	0.3	$0.60^{+0.04}_{-0.04}$	16.5
Reese 2004 (41) ²⁰⁸	0.3	$0.61^{+0.03}_{-0.03}$	–
Jones <i>et al.</i> 2005 (5) ²¹²	0.3	$0.66^{+0.11}_{-0.10}$	–
Bonamente <i>et al.</i> 2006 (38) ²¹³	0.3	$0.77^{+0.04}_{-0.03}$	31.6
Present work (24)	$0.15^{+0.57}_{-0.15}$	$0.75^{+0.07}_{-0.07}$	24.4
Present work (24)+BAO	$0.27^{+0.04}_{-0.03}$	$0.74^{+0.04}_{-0.03}$	24.5

Bonamente *et al.* (2006)²¹³, using 38 clusters, obtained $h = 0.769_{-0.034}^{+0.039}$. All these results, using SZ/X-ray technique, presented a systematic uncertainty of 10%-30%. In Table 6.1, we summarize the estimates of H_0 from clusters in the framework of Λ CDM models (the data in round brackets is the number of clusters).

It is worth notice that the best-fit scenario derived here, $\Omega_m = 0.27_{-0.02}^{+0.03}$ and $h = 0.738_{-0.033}^{+0.042}$, corresponds to an accelerating Universe with $q_0 = -0.6$, a total evolutionary age of $t_o \simeq 10h^{-1}$ Gyr, and a transition redshift (from deceleration to acceleration) $z_t \simeq 0.6$. At 95.4% c.l. (2σ) the BAO+SZE/X-ray analysis also provides $h = 0.74_{-0.07}^{+0.08}$. Hopefully, future developments related to the physics of clusters may shed some light on the nature of the dark energy (for reviews see Refs.^{226,227}).

6.5.3 Conclusions

Since the original work of Hubble, the precise determination of the distance scale (H_0) has been a recurrent problem in the development of physical cosmology. In this letter we have discussed a new determination of the Hubble constant based on the SZE/X-ray distance technique for a sample of 24 clusters as compiled by De Filippis *et al.* (2005)²⁰⁹. The degenerescency on the Ω_m parameter was broken using the baryon acoustic oscillation signature from the SDSS catalog. The Hubble constant was constrained to be $h = 0.74_{-0.035}^{+0.04}$ and $_{-0.07}^{+0.08}$ for 1σ and 2σ , respectively. These limits were derived assuming elliptical β -model and a flat Λ CDM scenario.

As we have seen, the baryon acoustic signature is an interesting tool for constraining directly the mass density parameter, Ω_m , and, indirectly, it also improves the Hubble constant limits acquired from other cosmological techniques (like the SZE/X-ray cluster distance). Our Hubble constant estimation using the joint analysis SZE/X-ray + BAO is largely consistent with some recent cosmological observations, like the third year of the WMAP and the HST Key Project. Implicitly, such an agreement suggests that the elliptical morphology describing the cluster sample and the associated isothermal β -model is quite realistic. It also reinforces the interest to the observational search of galaxy clusters in the near future, when more and larger samples, smaller statistic and systematic uncertainties will improve the limits on the present value of the Hubble parameter.

CONCLUSÕES E PERSPECTIVAS

Mostramos no capítulo 5 os resultados de um recente trabalho¹³⁹, em que propusemos um novo formalismo analítico baseado na estatística não-extensiva de Tsallis, onde uma distribuição de lei de potência (Power Law - PL) é empregada para o campo primordial que representa o contraste de densidade. Tal distribuição possui um parâmetro livre q que regula o grau de *não-gaussianidade* do campo primordial. A distribuição PL recupera a forma Gaussiana padrão quando $q \rightarrow 1$. Em outro recente artigo¹⁴⁶ analisamos as propriedades estatísticas, especialmente a normalização, de diversas distribuições (incluindo a distribuição PL) aplicadas ao campo primordial do contraste de densidade, e descobrimos que a conhecida distribuição de Burr, além de possuir 2 parâmetros livres e permitir com isso a mesma maleabilidade que nossa distribuição PL, tem ainda a vantagem de corrigir o problema de normalização do formalismo original de PS.

Após termos definido o novo formalismo PL baseado na estatística não-extensiva de Tsallis, precisávamos verificar se o parâmetro livre q permitia efetivamente explicar os atuais dados observacionais. No caso do catálogo de raio-X de galáxias HIFLUGCS¹⁵⁶, baseado no ROSAT All-Sky Survey, a função de massa de PS que se adequa aos dados fornece parâmetros de σ_8 (a amplitude das flutuações de densidade em esferas de raio $8h^{-1}Mpc$) e Ω_m (a densidade de matéria do universo) claramente fora (em 3σ ou mais) dos atuais limites definidos pelo 3º ano do WMAP¹⁶⁴. Em outras palavras, o método de PS padrão não explica os atuais dados de raio-X de galáxias. Calculando o χ^2 pelo método de máxima verossimilhança nós asseguramos que, usando a distribuição PL com os dados do catálogo HIFLUGCS, obtemos parâmetros σ_8 e Ω_m plenamente compatíveis com os dados do WMAP⁴. Vemos claramente que o método PL se ajusta às observações

com parâmetros compatíveis com o WMAP, enquanto o mesmo não se processa no método PS padrão⁴. Naturalmente, tais resultados devem depender do tipo de energia escura que está acelerando o universo. Os resultados descritos até aqui foram obtidos para o caso de uma constante cosmológica.

Estudamos também a influência da *energia escura* no processo de formação de estruturas. O trabalho de incorporar modelos de energia escura na formação de estruturas do universo está começando a ser implementado na literatura. Por exemplo, o modelo de colapso esférico com energia escura homogênea foi discutido por Wang (2005)³; também no estudo da virialização, modelos onde energia escura imita o efeito de uma constante cosmológica foram implementados¹⁴⁵; Independentemente, recentes catálogos de raio-X de altos redshifts ($z \geq 0.3$), como o EMSS, permitem limites restritos para a equação de estado da energia escura². Nossos estudos nesta vertente já se encontram em andamento. Seguimos o trabalho de Percival (2005)¹⁵², que analisou a formação de estruturas em um fundo homogêneo de energia escura, fornecendo uma fórmula de ajuste para o fator de crescimento linear, em cosmologias com ω constante. A incorporação desse ajuste com energia escura já foi concluído no formalismo PS padrão, e está sendo implementado em nosso formalismo PL. O passo seguinte será aplicá-lo para os demais modelos de energia escura presentes na literatura. Devemos também considerar diversas parametrizações $\omega(z)$, procurando empregá-las no modelo analítico de formação de estruturas, em conjunto com o método PL descrito anteriormente. Com tais análises pretendemos verificar a real influência da energia escura no processo de formação de estruturas.

No capítulo 6 a cosmologia não extensiva é ainda abordada na radiação de Bremsstrahlung, a radiação primária dos aglomerados de raio-X, e também na sonda de plasma, com evidentes aplicações em astrofísica experimental. Por fim, tratamentos de dados dos atuais catálogos de galáxias nos permitiram análises conjuntas^{127,17} que limitaram melhor os principais parâmetros dos modelos, objetivando eleger o candidato mais adequado para o novo paradigma cosmológico.

Poderemos futuramente realizar simulações de N-Corpos para determinarmos a função de massa ideal de halos de matéria escura na fase não-linear. É bem compreendido hoje que o modelo de Press-Schechter se ajusta muito mal aos dados computacionais atuais, e isso em todas as épocas de formação. O modelo modificado da função de massa, de

Sheth-Tormen^{158,1} fornece um melhor ajuste, mas ainda apresenta um número muito alto da abundância de objetos raros, em todas as épocas, por um valor acima de 50%. Desse modo, um grande estudo foi empreendido usando diversas simulações de N-Corpos em diversos redshifts, para determinar uma equação ideal para a função de massa, com ajuste superior à função de massa de PS e de Sheth-Tormen¹⁶. Nosso intento será comparar todas as funções de massa apresentadas, incluindo a das simulações de N-Corpos, com nossa função de massa PL, e assim verificar as previsões e o poder de ajuste dessa última face às demais.

Estudaremos a formação de grandes estruturas usando nosso formalismo de Lei de Potências (PL) para o campo inicial das perturbações, implementando o modelo de energia escura do trabalho de Percival¹⁵², como descrito anteriormente. Submeteremos igualmente trabalhos visando analisar um campo inicial de perturbações regido pela distribuição de Burr, que como vimos é capaz de resolver o problema de normalização de Press-Schechter; veremos nas análises subsequentes se tal distribuição oferece a maleabilidade necessária para explicar os atuais dados em raio-X dos aglomerados de galáxias, assim como já verificamos ser o caso com nosso método PL. Visamos igualmente submeter artigos usando a distribuição de Burr junto com o modelo de energia escura de Percival¹⁵², para termos um quadro geral da influência da energia escura no processo de formação de estruturas, usando um campo primordial de perturbações não-gaussiano.

Poderemos analisar aglomerados de galáxias, em médios e altos redshifts, utilizando os testes de raio-X, SNe Ia, diâmetro angular, *Gamma-Ray Bursts*, idade, efeito Sunyaev-Zel'dovich (ESZ) e Baryon Acoustic Oscillations (BAO); estudaremos então os mais recentes catálogos observacionais, usando diversos modelos cosmológicos nas análises, incluindo matéria e energia escura (diversos modelos de energia escura, parametrizações, além do caso da phantom-energy). Faremos assim um estudo sistemático pondo a prova os modelos mais cogitados na literatura. Com isso teremos uma base real de validação dos modelos que melhor explicam os atuais dados observacionais, além de precisarem ser coerentes com os mais recentes dados do WMAP. Tais trabalhos certamente excluirão diversos modelos cosmológicos, e aumentarão nosso conhecimento sobre a formação das estruturas no universo.

Critérios estatísticos mais poderosos poderão ser usados na análise dos aglomerados

de galáxias. Diversas análises estatísticas serão empregadas no mesmo problema, para verificarmos se a adequação do modelo aos dados é um problema do modelo cosmológico empregado ou do tratamento estatístico escolhido. Ainda submeteremos trabalhos sobre formação de estruturas, incluindo comparações diretas com os mais recentes dados computacionais (simulações massivas de N-Corpos), do espectro de potências e da função de massa; pretendemos com isso verificar se nosso modelo PL, ou mesmo o de Burr, seriam mais efetivos que os de Sheth-Tormen^{158,1} para corrigir os ajustes em relação ao modelo original de PS.

No ano de 2007 o satélite Planck fornecerá ao mundo os dados cosmológicos mais recentes e precisos jamais vistos até então. Pretendemos em um futuro bem próximo focar nossa atenção em análises profundas desses dados, utilizando todo o arcabouço teórico desenvolvido acima, e comparando aos dados anteriores, e também às observações independentes de outras fontes. Muitos trabalhos serão desenvolvidos nessa linha, no espírito dos desenvolvimentos anteriores. Certamente deveremos descartar vários modelos, assim como iremos apontar os mais aptos a explicar o paradigma cosmológico atual. O objetivo básico é obter uma melhor compreensão da formação de estruturas e, conseqüentemente, do comportamento da matéria escura e da energia escura no universo.

Bibliografia

- ¹ Sheth R., Mo H. and Tormen G., MNRAS 323, 1 (2001).
- ² Henry J.P., ApJ 609, 603 (2004).
- ³ Wang P., [astro-ph/0507195] (2005).
- ⁴ Marassi L. & Lima J. A. S., MNRAS, submetido (2007).
- ⁵ Bernui A., Tsallis C. and Villela T., [astro-ph/0512267] (2005).
- ⁶ Leubner I.H., AGUSM, P21D, 01L (2005).
- ⁷ Kronberger T., Leubner M.P. and Van Kampen E., A&A 453, 21K (2006).
- ⁸ Wuensche C.A., Ribeiro A.L.B., Ramos F.M., Rosa R.R., [astro-ph/0403472] (2004).
- ⁹ Robinson J., Gawiser E. and Silk J., ApJ 532, 1 (2000).
- ¹⁰ Seto N., ApJ 553, 488S (2001).
- ¹¹ Tsallis C., Chaos, Solitons and Fractals 6, 539 (1995).
- ¹² Alemany P.A. & Zanette D.H., PRE 49, R956 (1994).
- ¹³ Silva R., Alcaniz J. S. & Lima J. A. S., Physica A 356, 419 (2005).
- ¹⁴ Lima, J. A. S., Silva R. & Santos, J., PRE 61, 3260 (2000).
- ¹⁵ Lima J.A.S. & de Souza R.E., Physica A 350, 303 (2005).
- ¹⁶ Reed D.S. *et al.*, [astro-ph/0607150] (2006).
- ¹⁷ Cunha J. V., Marassi L., & Lima J. A. S., astro-ph/0611934 (2006).

- ¹⁸ Astier P. *et al.*, A&A 447, 31 (2006).
- ¹⁹ Liddle A.R. & Lyth D.H., Phys. Rep. 231, 1, [astro-ph/9303019] (1993).
- ²⁰ Weinberg S., “Gravitation and Cosmology”, John Wiley & Sons (1972).
- ²¹ Pal P.B., “Determination of cosmological parameters”, [hep-ph/9906447] (1999).
- ²² Burles S., Nollett K.M., Truran J.N., Turner M.S., PRL 82, 4176, [astro-ph/9901157] (1999).
- ²³ Olive K.A., Steigman G. and Walker T., [astro-ph/9905320] (1999).
- ²⁴ Dicke R.H., Peebles P.J.E., Roll P.G. and Wilkinson D.T., ApJ 142, 414 (1965).
- ²⁵ Peebles P.J.E., “Principles of Physical Cosmology”, Princeton U.P. (1993).
- ²⁶ Padmanabhan T., “Structure Formation in the Universe”, Cambridge U.P. (1993).
- ²⁷ Harrison E.R., PRD 1, 2726 (1970); Zel’dovich Ya. B., A&A 5, 84 (1970).
- ²⁸ IRAS Point Source Catalog:
http://simbad3.u-strasbg.fr/cgi-bin/cdsbib?1988IRASP.C.....0J
- ²⁹ Steinhardt P.J., “Particle and Nuclear Astrophysics and Cosmology in the Next Millennium”, ed. by E.W. Kolb and R. Peccei, World Scientific, Singapore (1995).
- ³⁰ Freedman W.L., “Determination of cosmological parameters”, Nobel Symposium, [hep-ph/9905222] (1998).
- ³¹ Grogin N.A. & Narayan R., ApJ 464, 92, [astro-ph/9512156] (1996).
- ³² Birkinshaw M., Phys. Rep. 310, 97, [astro-ph/9808050] (1999).
- ³³ Davis M. & Huchra J., ApJ 254, 437 (1982); Kirshner R.D. *et al.*, Astron. J. 88, 1285 (1983).
- ³⁴ Copi C.J. & Schramm D.N., Comm. Nucl. Part. Phys. 22, 1, [astro-ph/9504026] (1996).
- ³⁵ Freeman K.C., ApJ 160, 811 (1970).
- ³⁶ Begeman K.G., Broeils A.H. and Sanders R.H., MNRAS 249, 523 (1991).

- ³⁷ Sarazin C.L., Rev. Mod. Phys. 58, 1 (1986).
- ³⁸ Ostriker J.P. & Steinhardt P.J., Nature 377, 600 (1995).
- ³⁹ Perlmutter S. *et al.*, The Supernova Cosmology Project, Bull. Am. Astron. Soc. 29, 1351, [astro-ph/9812473] (1997); ApJ 517, 565, [astro-ph/9812133] (1999).
- ⁴⁰ Reiss A. *et al.*, Astron. J. 116, 1009, [astro-ph/9805201] (1998).
- ⁴¹ Bernardis P. de *et al.*, [astro-ph/9911461] (1999); Melchiorri A. *et al.*, [astro-ph/9911445] (1999); Mauskopf P.D. *et al.*, [astro-ph/9911444] (1999).
- ⁴² Planck Home Page:
<http://www.ipac.caltech.edu/Planck/planck.shtml>
- ⁴³ Bond J.R. & Efstathiou G., ApJ 285, L45 (1984).
- ⁴⁴ Gawiser E., Silk J., Science 280, 1405, [astro-ph/9806197] (1998).
- ⁴⁵ Carroll S.M., Press W.H., and Turner E.L., Ann. Rev. Astron. Astrophys. 30, 499 (1992).
- ⁴⁶ Kolb E.W. & Turner M.S., "The Early Universe", Redwood City, California: Addison-Wesley (1990).
- ⁴⁷ Heath D.J., MNRAS 179, 351 (1977).
- ⁴⁸ Eisenstein D.J., [astro-ph/9709054] (1997).
- ⁴⁹ Peebles P.J., ApJ 284, 439 (1984).
- ⁵⁰ Efstathiou G., Sutherland W.J. and Maddox S.J., Nature 348, 705 (1990).
- ⁵¹ Smoot G.F. *et al.*, ApJ 396, L1 (1992).
- ⁵² Hu W. & White M., [astro-ph/9606140] (1996).
- ⁵³ Bond J.R., Jaffe A.H. and Knox L., PRD 57, 2117, [astro-ph/9708203] (1998).
- ⁵⁴ Bahcall N.A. & Fan X., Publ. Nat. Acad. Sci. 95, 5956, [astro-ph/9804082] (1998).
- ⁵⁵ Carlberg R.G. *et al.*, ApJ 462, 32 (1996).

- ⁵⁶ Bahcall N.A., Lubin L.M. and Dorman V., ApJ 447, L81, [astro-ph/9506041] (1995).
- ⁵⁷ White S.D.M., Navarro J.F., Evrard A.E. and Frenk C.S., Nature 366, 429 (1993).
- ⁵⁸ Fukugita M., Hogan C.J. and Peebles P.J., ApJ 503, 518, [astro-ph/9712020] (1998).
- ⁵⁹ Mohr J., Mathiesen B. and Evrard G., ApJ 517, 627, [astro-ph/9901281] (1999).
- ⁶⁰ Peacock J.A. & Dodds S.J., MNRAS 267, 1020, [astro-ph/9311057] (1994).
- ⁶¹ Liddle A.R., Lyth D.H., Viana P.T. and White M., MNRAS 282, 281, [astro-ph/9512102] (1996).
- ⁶² Caldwell R.R., [astro-ph/9908168] (1999).
- ⁶³ Ratra B. & Quillen A., MNRAS 259, 738 (1992).
- ⁶⁴ Perlmutter S., Turner M.S. and White M., PRL 83, 670, [astro-ph/9901052] (1999).
- ⁶⁵ Peebles P.J. & Ratra B., ApJ 325, L17 (1988).
- ⁶⁶ Ratra B. & Peebles P.J., PRD 37, 3406 (1988).
- ⁶⁷ Caldwell R.R., Dave R. and Steinhardt P.J., PRL 80, 1582, [astro-ph/9708069] (1998).
- ⁶⁸ Peebles P.J. & Vilenkin A., PRD 59, 063505, [astro-ph/9810509] (1999).
- ⁶⁹ Felder G., Kofman L. and Linde A., PRD 60, 103505, [hep-ph/9903350] (1999).
- ⁷⁰ Dekel A., Bertschinger E. and Faber S.M., ApJ 364, 349 (1990); Dekel A. *et al.*, ApJ 412, 1 (1993).
- ⁷¹ Hawking S.W., ApJ 145, 544 (1966); Olson D.W., PRD 14, 327 (1976).
- ⁷² Lyth D.H. & Mukherjee M., PRD 38, 485 (1988).
- ⁷³ Lyth D.H. & Stewart E.D., ApJ 361, 343 (1990).
- ⁷⁴ Dunsby P.K.S., Bruni M. and Ellis G.F.R., ApJ 395, 54 (1992).
- ⁷⁵ Lesche B., J. Stat. Phys. 27, 419 (1982).
- ⁷⁶ Tsallis C., J. Stat. Phys. 52, 479 (1988).

- ⁷⁷ Curado E.M.F. & Tsallis C., J. Phys. A 24, L69 (1991) [Corrigenda: 24, 3187 (1991) and 25, 1019 (1992)].
- ⁷⁸ <http://tsallis.cat.cbpf.br/biblio.htm>
- ⁷⁹ Tsallis C., Levy S.V.F., Souza A.M.C. and Maynard R., PRL 75, 3589 (1995) [Erratum: 77, 5442 (1996)]; Zanette D.H. & Alemany P.A., PRL 75, 366 (1995); Zanette D.H. & Alemany P.A., PRL 77, 2590 (1996); Prato D. & Tsallis C., PRE60, 2398 (2000).
- ⁸⁰ Bak P., “How Nature Works”, Springer-Verlag, New York (1996).
- ⁸¹ Tsallis C., Bemski G. and Mendes R.S., Phys. Lett. A 257, 93 (1999).
- ⁸² Tsallis C., Anjos J.C. and Borges E.P., Phys. Lett. A 310, 372 (2003).
- ⁸³ Borland L., PRL 89, 098701 (2002).
- ⁸⁴ Bediaga I., Curado E.M.F. and Miranda J., Physica A 286, 156 (2000).
- ⁸⁵ Rosso O.A., Martin M.T. and Plastino A., Physica A 313, 587 (2002).
- ⁸⁶ Montemurro M.A., Physica A 300, 567 (2001).
- ⁸⁷ Tsallis C. & Borges E.P., [cond-mat/0301521] (2003).
- ⁸⁸ Borges E.P., Eur. Phys. J. B 30, 593 (2002).
- ⁸⁹ Malacarne L.C., Mendes R.S. and Lenzi E.K., PRE 65, 017106 (2002).
- ⁹⁰ Abe S. & Suzuki N., PRE 67, 016106 (2003).
- ⁹¹ E. Fermi, “Thermodynamics”, Dover, New York (1956).
- ⁹² Tisza L., “Generalized Thermodynamics”, MIT Press, Cambridge, Massachusetts (1966).
- ⁹³ Landsberg P.T., “Thermodynamics and Statistical Mechanics”, Oxford university Press, Oxford, (1978) [also Dover, New York, 1990].
- ⁹⁴ Cohen E.G.D., Physica A 305, 19 (2002).
- ⁹⁵ Baranger M., Physica A 305, 27 (2002).

- ⁹⁶ Walton D.B. & Rafelski J., PRL 84, 31 (2000).
- ⁹⁷ Lima J.A.S., Silva R. and Plastino A.R., PRL 86, 2938 (2001).
- ⁹⁸ Lyra M.L. & Tsallis C., PRL 80, 53 (1998); Oliveira H.P., Soares I.D. and Tonini E.V., Physica A 295, 348 (2001); Borges E.P., Tsallis C., Ananos G.F.J. and Oliveira P.M.C., PRL 89, 254103 (2002).
- ⁹⁹ Weinstein Y., Lloyd S. and Tsallis C., PRL 89, 214101 (2002).
- ¹⁰⁰ Tsallis C., Lamberti P.W. and Prato D., Physica A 295, 158 (2001); Alcaraz F.C. & Tsallis C., Phys. Lett. A 301, 105 (2002).
- ¹⁰¹ Plastino A.R. & Plastino A., Physica A 222, 347 (1995); Plastino A.R., Casas M. and Plastino A., Physica A 280, 289 (2000).
- ¹⁰² Cabral B.J.C. & Tsallis C., PRE 66, 065101(R) (2002); Anteneodo C. & Vallejos R.O., PRE 65, 016210 (2002).
- ¹⁰³ Salinas S.R.A. & Tsallis C., Braz. J. Phys. 29, 1 (1999); Kaniadakis G., Lissia M. and Rapisarda A., Physica A 305, 1/2, Elsevier, Amsterdam (2002).
- ¹⁰⁴ Lavagno A., Kaniadakis G., Rego-Monteiro M., Quarati P. and Tsallis C., Astroph. Let. and Comm. 35, 449 (1998).
- ¹⁰⁵ Hamity V.H. & Barraco D.E., Physica A 282, 203 (2000); Hanyu C. & Habe A., ApJ 554, 1268 (2001); Tonini E.V., “Caos e universalidade em modelos cosmologicos com pontos criticos centro-sela”, Tese de Doutorado, CBPF, Rio de Janeiro (2002).
- ¹⁰⁶ Kaniadakis G., Lavagno A. & Quarati P., Phys. Lett. B 369, 308 (1996); Kaniadakis G., Lavagno A. and Quarati P., Astroph. and Space Sci. 258, 145 (1998).
- ¹⁰⁷ Plastino A.R. & Plastino A., Physics Lett. A 174, 384 (1993).
- ¹⁰⁸ Plastino A.R., “Nonextensive Statistical Mechanics and Its Applications”, eds. Abe S. & Okamoto Y., Springer, Berlin (2001).
- ¹⁰⁹ Aly J.J. & Perez J., PRE 60, 5185 (1999); Taruya A. & Sakagami M., Physica A 307, 185 (2002).

- ¹¹⁰ Binney J. & Tremaine S., “Galactic dynamics”, Princeton University Press, Princeton, (1987).
- ¹¹¹ Bahcall N.A. & Oh S.P., Ap. J. Lett. 462, L49 (1996).
- ¹¹² Landsberg P.T. & Vedral V., Phys. Lett. A 247, 211 (1998).
- ¹¹³ Rajagopal A.K. & Abe S., PRL 83, 1711 (1999).
- ¹¹⁴ Tsallis C., Mendes R.S. and Plastino A.R., Physica A 261, 534 (1998).
- ¹¹⁵ Tsallis C. & Brigatti E., [cond-mat/0305606] (2003).
- ¹¹⁶ Abramowitz M., Stegun I.A., “Handbook of Mathematical Functions”, Dover, NY (1972).
- ¹¹⁷ Balbi A. *et al.*, ApJ 545, L1 (2000).
- ¹¹⁸ Bardeen J.M., Bond J.R., Kaiser N. and Szalay A.S., ApJ 304, 15 (1986).
- ¹¹⁹ Basilakos S., ApJ 590, 636 (2003).
- ¹²⁰ Bennett C.L. *et al.*, ApJS 148, 1 (2003).
- ¹²¹ Bond J.R., Cole S., Efstathiou G., Kaiser N., ApJ 379, 440 (1991).
- ¹²² Borgani S., Rosati P., Tozzi P. and Norman C., ApJ 517, 40 (1999b).
- ¹²³ Burles S. & Tytler D., ApJ 499, 699 (1998).
- ¹²⁴ Butkov, “Física Matemática”, ed. LTC, Rio de Janeiro, RJ (1988).
- ¹²⁵ Caldwell R.R., Dave R., Steinhardt P.J., Astroph. & Space sci. 261, 303 (1998a).
- ¹²⁶ Caldwell R.R., Dave R., Steinhardt P.J., PRL 80, 8 (1998b).
- ¹²⁷ Cunha J.V., Marassi L. & Santos R.C., Int. J. Mod. Phys. D 000, 0000, [astro-ph/0608686] (2007).
- ¹²⁸ Finoguenov A., Reiprich T.H. and Boehringer H., A&A 368, 749 (2001).

- ¹²⁹ Giuricin G., Mardirossian F., Mezzetti M., Persic M. and Salucci P., [astro-ph/9308015] (1993).
- ¹³⁰ Governato F. *et al.*, MNRAS 307, 949 (1999).
- ¹³¹ Gunn J.E., Gott J.R., ApJ 176, 1 (1972).
- ¹³² Hannestad S., [astro-ph/0504017] (2005).
- ¹³³ Jaffe A.H. *et al.*, PRL 86, 3475 (2001).
- ¹³⁴ Jedamzik K., ApJ 448, 1 (1995).
- ¹³⁵ Jenkins A., Frenk C.S., White S.D.M., Colberg J.M., Cole S., Evrard A.E., Couchman H.M.P., Yoshida N., MNRAS 321, 372 (2001).
- ¹³⁶ Kitayama T. & Suto Y., ApJ 469, 480 (1996).
- ¹³⁷ Lee J. & Shandarin S.F., [astro-ph/9811004] (1999).
- ¹³⁸ Bezerra J.R., Silva R. and Lima J.A.S., Physica A 322, 256 (2003); Potiguar F.Q. & Costa U.M.S., Physica A 303, 457 (2002).
- ¹³⁹ Lima J.A.S. & Marassi L., Int. J. Mod. Phys. D 13, 1345 (2004).
- ¹⁴⁰ Lima J.A.S., Silva R. and Santos J., A&A 396, 309 (2002); Silva R. & Alcaniz. J.S., Phys. Lett. A 313, 393 (2003); Hansen S.H., New Astron. 10, 371 (2005); Hansen S.H. *et al.*, New Astron. 10, 379 (2005.); Jiulin D., Eur. Lett. 67, 893 (2004).
- ¹⁴¹ Lokas E.L., Bode P. and Hoffman Y., MNRAS 349, 595 (2004).
- ¹⁴² Longair M.S., “Galaxy Formation”, Springer-Verlag, Berlin (1998).
- ¹⁴³ Lucchin F. & Matarrese S., ApJ 330, 535 (1988).
- ¹⁴⁴ Ma C.P., Caldwell R.R., Bode P. and Wang L., ApJ 521, L1 (1999).
- ¹⁴⁵ Maor I. & Lahav O., [astro-ph/0505308] (2005).
- ¹⁴⁶ Marassi L. & Lima J.A.S., Int. J. Mod. Phys. D, em impressão (2007).
- ¹⁴⁷ Mather J.C. *et al.*, ApJ 420, 439 (1994).

- ¹⁴⁸ Menzel D.H., “Fundamental Formulas of Physics”, Dover Publications, NY (1960).
- ¹⁴⁹ Mould J.R. *et al.*, ApJ 529, 786 (2000).
- ¹⁵⁰ Nagashima M., ApJ 562, 7 (2001).
- ¹⁵¹ Peacock J.A. & Heavens A.F., MNRAS 243, 133 (1990).
- ¹⁵² Percival W.J., [astro-ph/0508156] (2005).
- ¹⁵³ Percival W.J., Miller L. and Peacock J.A., MNRAS 318, 273 (2000).
- ¹⁵⁴ Press W.H. & Schechter P., ApJ 187, 425 (1974).
- ¹⁵⁵ Ratra B. & Peebles P.J.E., ApJ 325, 17 (1988).
- ¹⁵⁶ Reiprich T.H. & Boehringer H., ApJ 567, 716 (2002).
- ¹⁵⁷ Schuecker P., Boehringer H., Arzner K. and Reiprich T.H., A&A 370, 715 (2001).
- ¹⁵⁸ Sheth R.K. & Tormen G., MNRAS 108, 119 (1999).
- ¹⁵⁹ Silva R., Plastino A.R. and Lima J.A.S., Phys. Lett. A 249, 401 (1998); Lima J.A.S., Silva R. and Plastino A.R., PRL 86, 2938 (2001).
- ¹⁶⁰ Silva R., Lima J.A.S. and Santos J., PRE 61, 3260 (2000).
- ¹⁶¹ Silveira V. & Waga I., PRD 64, 4890 (1994).
- ¹⁶² Sneddon I.N., “Special Functions of Mathematical Physics and Chemistry”, Longman Group Limited, London (1980).
- ¹⁶³ Spergel D.N., Verde L., Peiris H.V. *et al.*, ApJS 148, 175 (2003).
- ¹⁶⁴ Spergel D.N., Bean R., Doré O. *et al.*, [astro-ph/0603449] (2006).
- ¹⁶⁵ Sugiyama N., ApJS 100, 281 (1995).
- ¹⁶⁶ Teugels J. & Sundt B. (editors), Encyclopedia of Actuarial Science, Vol. 3, (2004).
- ¹⁶⁷ Wang L. & Steidhardt P.J., ApJ 508, 483 (1998).
- ¹⁶⁸ Wang L., Caldwell R.R., Ostriker J.P. and Steidhardt P.J., ApJ 530, 17 (2000).

- ¹⁶⁹ White M., [astro-ph/0207185] (2002).
- ¹⁷⁰ Yano T., Nagashima M. and Gouda N., ApJ 466, 1 (1996).
- ¹⁷¹ Allen S.W. *et al.*, MNRAS, 353, 457 (2004).
- ¹⁷² Cunha J.V., Alcaniz J.S. and Lima J.A.S., PRD 69, 083501 (2004).
- ¹⁷³ Dogiel V.A., A&A, 357, 66 (2000).
- ¹⁷⁴ Dogiel V.A., A&A, 359, 66 (2000).
- ¹⁷⁵ Durret F. *et al.*, A&A 390, 397 (2002).
- ¹⁷⁶ Enßlin T.A., Lieu R. and Biermann P.L., A&A 344, 409 (1999).
- ¹⁷⁷ Fusco-Femiano R., DalFiume D. *et al.*, ApJ 513, L21 (1999).
- ¹⁷⁸ Fusco-Femiano R., Orlandini M. *et al.*, ApJ 602, L73 (2004).
- ¹⁷⁹ Gradshteyn I.S. & Ryzhik I.M., “Table of Integrals, Series and Products”, Academic Press Inc., Orlando, Florida (1980).
- ¹⁸⁰ Hansen S.H., [astro-ph/0501393] (2005).
- ¹⁸¹ Hertel P., Thirring W., Ann. Phys. 52, 479 (1971).
- ¹⁸² Liang H., Dogiel V.A. and Birkinshaw M., MNRAS 337, 567 (2002).
- ¹⁸³ Rybicki G.B. & Lightman A.P., “Radiative Processes in Astrophysics”, ed. John Wiley & Sons, (1979).
- ¹⁸⁴ Novikov I.D. & Thorne K.S., “Black Holes”, Les Houches, Eds. C. DeWitt and B. DeWitt, Gordon and Breach, New York, (1973).
- ¹⁸⁵ Timokhin A.N. *et al.*, A&A 417, 391 (2004).
- ¹⁸⁶ Feix M. *et al.*, [cond-mat/0407245] (2004).
- ¹⁸⁷ Sirghi L., Aoki T. and Hatanaka Y., Surf. & Coat. Tech. 187, 358 (2004).

- ¹⁸⁸ Rohde D., Pecher P., Kersten H., Jacob W. and Hippler R., *Surf. & Coat. Tech.* 149, 206 (2002).
- ¹⁸⁹ Lima J.A.S., Bezerra J.R., Silva R., *Physica A* 289, 296 (2002).
- ¹⁹⁰ Bittencourt J.A., “Fundamentals of Plasma Physics”, 2nd Ed., co-Edition FAPESP, Brazil, (1995).
- ¹⁹¹ Lima J.A.S. and Trodden M., *PRD* 53, 4280 (1996); Cunha J.V., Lima J.A.S. and Pires N., *A&A* 390, 809 (2002); Cunha J.V. & Santos R.C., *IJMPD* 13, 1321 (2004); Alcaniz J.S. & Lima J.A.S., *PRD* 72, 063516 (2005).
- ¹⁹² Cooray A.R. & Huterer D., *ApJ* 513, L95 (1999).
- ¹⁹³ Maor I., Brustein R. and Steinhardt P.J., *PRL* 86, 6 (2001).
- ¹⁹⁴ Weller J. & Albrecht A., *PRD* 65, 103512 (2002).
- ¹⁹⁵ Linder E.V., *PRL* 90, 091301 (2003).
- ¹⁹⁶ Padmanabhan T. & Choudhury T.R., *MNRAS* 344, 823 (2003).
- ¹⁹⁷ Pen U., *New Astronomy* 2, 309 (1997).
- ¹⁹⁸ Sasaki S., *Pub. Astron. Soc. Japan* 48, L19 (2002).
- ¹⁹⁹ Lima J.A.S., Cunha J.V. and Alcaniz J.S., *PRD* 68, 023510 (2003).
- ²⁰⁰ Allen S.W., Schmidt R.W. and Fabian A.C., *MNRAS* 334, L11 (2002).
- ²⁰¹ Freedman W. *et al.*, *ApJ* 553, 47 (2001).
- ²⁰² Kirkman D. *et al.*, *ApJS* 149, 1 (2003).
- ²⁰³ Riess A.G. *et al.*, *ApJ* 607, 665 (2004).
- ²⁰⁴ Jain D. & Dev A., [astro-ph/0509212] (2005).
- ²⁰⁵ Silk J. & White S.D.M., *ApJ* 226, L103 (1978).
- ²⁰⁶ Birkinshaw M., *MNRAS* 187, 847 (1979).

- ²⁰⁷ Reese E.D. *et al.*, ApJ 581, 53 (2002).
- ²⁰⁸ Reese E.D., “Measuring and Modeling the Universe”, ed. Freedman W.L., CUP, [astro-ph/0306073] (2004).
- ²⁰⁹ De Filippis E., Sereno M., Bautz M. W. and Longo G., ApJ 625, 108 (2005).
- ²¹⁰ Sereno M., De Filippis E., Longo G., Bautz M.W., ApJ 645, 170 (2006).
- ²¹¹ Fox D.C. & Pen U.L., ApJ 574, 38 (2002).
- ²¹² Jones M.E. *et al.*, MNRAS 357, 518 (2005).
- ²¹³ Bonamente M. *et al.*, ApJ 647, 25 (2006).
- ²¹⁴ Freedman W.L., Phys. Rep. 333, 13 (2000).
- ²¹⁵ Peacock J.A., “Cosmological Physics”, Cambridge Univ. Press, Cambridge (1999).
- ²¹⁶ Hu W., “ASP Conf. Ser. 339: Observing Dark Energy”, ed. Wolf S.C. & Lauer T.R., (2005).
- ²¹⁷ Eisenstein D.J. *et al.*, ApJ 633, 560 (2005).
- ²¹⁸ Lima J.A.S., Cunha J.V. and Alcaniz J.S., [astro-ph/0608469] (2006).
- ²¹⁹ Alcaniz J.S., PRD 69, [astro-ph/083521] (2004).
- ²²⁰ Mason B.S. *et al.*, ApJ 555, L11 (2001).
- ²²¹ Ebeling H. *et al.*, MNRAS 281, 799 (1996).
- ²²² Cunha J.V., Lima J.A.S. and Pires N., A&A 390, 809 (2002).
- ²²³ Cunha J.V. & Santos R.C., Int. J. Mod. Phys. D, 13, 1321 (2004).
- ²²⁴ Alcaniz J.S., Lima J.A.S. and Cunha J.V., MNRAS, 340, L39 (2003).
- ²²⁵ Sandage A., Tamman G.A., Saha A., Reindl B., Machetto F.D. and Panagia N., [astro-ph/0603647] (2006).
- ²²⁶ Peebles P.J.E. & Ratra B., Rev. Mod. Phys. 75, 559 (2003).

²²⁷ Lima J.A.S., Braz. J. Phys. 34, 194 (2004).

²²⁸ Sunyaev R.A. & Zel'dovich Ya.b., Comments Astrophys. Space Phys. 4, 173 (1972).